1-1-2012

Performance-Driven Behavioral Battery Modeling for Large Format Batteries

Jianwei Li

PERFORMANCE-DRIVEN BEHAVIORAL BATTERY MODELING FOR LARGE FORMAT BATTERIES

By

Jianwei Li

A Dissertation
Submitted to the Faculty of
Mississippi State University
in Partial Fulfillment of the Requirements
for the Degree of Doctor of Philosophy
in Electrical Engineering
in the Department of Electrical and Computer Engineering

Mississippi State, Mississippi

May 2012

PERFORMANCE-DRIVEN BEHAVIORAL BATTERY MODELING FOR LARGE FORMAT BATTERIES

By

Jianwei Li

Approved:

Michael S. Mazzola Professor of Electrical and Computer Engineering (Dissertation Director)	Nicolas H. Younan Professor of Electrical and Computer Engineering (Committee Member)
G. Marshall Molen Professor of Electrical and Computer Engineering (Committee Member)	Ming Xin Assistant Professor of Aerospace Engineering (Committee Member)
James E. Fowler Professor of Electrical and Computer Engineering (Graduate Program Coordinator)	Sarah A. Rajala Dean of the Bagley College of Engineering

Name: Jianwei Li

Date of Degree: May 11, 2012

Institution: Mississippi State University

Major Field: Electrical Engineering

Major Professor: Michael S. Mazzola

Title of Study: PERFORMANCE-DRIVEN BEHAVIORAL BATTERY MODELING FOR LARGE FORMAT BATTERIES

Pages in Study: 99

Candidate for Degree of Doctor of Philosophy

A behavioral battery modeling approach aimed at large format batteries is the topic of this dissertation. Drawing from the development of cell - level electrical analogue battery models, the comprehensive modeling approach described here shows how to scale a high fidelity battery cell model to a computationally fast battery model of large format batteries for system level design and simulation. The accurate behavioral battery model is performance - driven and tailored for stringent system simulation requirements. A novel bandwidth - based parameter extraction algorithm and advanced State of Charge (SOC) - Open Circuit Voltage (OCV) profile identification method are presented. While a real-world battery system is non-linear and time varying, a truncated representation of the system is provided by a commonly studied non-physical "electrical analogue" battery model. However, the limited bandwidth characteristic of the electrical analogue battery model is often overlooked. The reported algorithm starts by assessing a desired battery application, followed by modeling the battery according to the application bandwidth, and then estimating the model parameters using the sequential quadratic programming method. This approach recognizes and makes use of the limited bandwidth

of the battery model by reconciling the bandwidth of the application into the bandwidth of the electrical analogue battery model.

The model will help in vehicle concept development, and provide an analytical tool during the process of selecting the most appropriate battery during system design but before a prototype system is built. Another application is to represent the plant in realtime model-based battery management and control systems embedded in actual application controllers.

This modeling approach is independent of the battery chemistry and therefore it is applicable to lithium-ion, nickel-metal-hydride (NiMH), and lead-acid batteries, among others.

DEDICATION

The author would like to dedicate this dissertation to his parents and his loving wife, for their unconditional love and continued support.

ACKNOWLEDGEMENTS

The author would like to express his upmost gratitude to Dr. Michael Mazzola, his major professor, who has provided unending source of knowledge, support and guidance.

The author would also like to thank Dr. Nicolas Younan, Dr. Marshall Molen, and Dr. Ming Xin for their invaluable suggestions, discussions and efforts serving on his committee. In addition, the author would like to extend the gratitude to Jim Gafford and Chris Parker for their advice and experiments support.

Finally, the author acknowledges the support from the Center for Advanced Vehicular Systems at Mississippi State University.

TABLE OF CONTENTS

Page

LIST OF TABLES

LIST OF FIGURES

LIST OF SYMBOLS

SOC	State of Charge
OCV	Open Circuit Voltage
NiMH	Nickel-Metal-Hydride
ICE	Internal Combustion Engine
EV	Electric Vehicle
HEV	Hybrid Electric Vehicle
PHEV	Plug-in Hybrid electric Vehicle
FCV	Fuel Cell Vehicle
ESS	Energy Storage System
BMS	Battery Management System
I-V	Current - Voltage
SQP	Sequential Quadratic Programming
GA	Generic Algorithm
NLS	Nonlinear Least Square
MSE	Mean Square Error
RMSE	Root Mean Square Error
SOP	State of Power
MSU	Mississippi State University

SVD	Singular Value Decomposition
GHQF	Gauss-Hermite Quadrature Filter
EKF	Extended Kalman filter
UKF	Unscented Kalman filter
PDF	Probability Density Function
GHQ	Gauss-Hermite Quadrature
UT	Unscented Transformation
I	Current
V	Voltage
V_{ocv}	Battery Open Circuit Voltage
V_t	Battery Terminal Voltage
V_{t-mea}	Measured Battery Terminal Voltage
V_{t-sim}	Estimated Battery Terminal Voltage
C	Battery Capacity
R_i	Resistor
R_s	Series Resistor
C_i	Capacitor
τ	Time Constant
a_i	Polynomial Equation Coefficients
m	Battery Weight
C_p	Battery Heat Capacity

$T(t)$	Battery Temperature
T_a	Ambient Temperature
h_c	Battery Heat Transfer Coefficients
A_s	Battery Surface Area
f_{low}	Low Frequency Bound
f_{high}	High Frequency Bound
λ_m	Lagrange Multiplier
h_m	Equality Constraint
d^k	Search Direction Vector
B^k	Positive Definite Matrix
A_i	Amplitude of Exponential Term
A_0	Constant Number of Exponential Term
λ_i	Decay Constant of Exponential Term
$\mathbf{v}_k$	Process Noise
$\mathbf{Q}_k$	Process Noise Covariance
$\triangle t$	Sampling Interval
$\mathbf{n}_k$	Measurement Noise
$\mathbf{R}_k$	Measurement Noise Covariance
$\mathbf{x}_k$	State Vector
$\mathbf{y}_k$	Output Vector

$\mathbf{P}_k$	Covariance
$\mathbf{F}_k$	Jacobian Matrix of $\boldsymbol{f}$
$\mathbf{H}_k$	Jacobian Matrix of $\boldsymbol{h}$
$\mathbf{K}_k$	Kalman Gain
N_p	Total Number of Points
W_i	Point Weight
ξ_i	Transformed Point
γ_i	Quadrature Point
$\mathbf{e}_i$	Unit Vector
κ	Tuning Parameter
$\boldsymbol{\varepsilon}$	Eigenvalue

CHAPTER I

INTRODUCTION

1.1 Background & motivation

Due to concerns for energy and environment [1-3], such as the limited resource of petroleum and global warming, a groundbreaking change has arisen in the automotive industry towards higher fuel economy, lower emission and enhanced power performance [4-8]. In 2007, the transportation sector consumed 71% of US oil consumption. The share used by cars, pickups and SUVs was 61% of the transportation sector [9]. By making the internal combustion engine (ICE) operate in a more efficient region and taking advantage of regenerative braking, hybrid electric vehicles (HEVs) are more fuel efficient and environmental friendly [4, 5]. Plug-in hybrid electric vehicles (PHEVs) and fuel cell vehicles (FCVs) can make use of renewable energy sources such as wind and solar energy to either store the renewable energy in the battery pack, or make hydrogen by the renewable energy and then produce electricity from the fuel cell [4, 5, 7, 10]. Therefore, it is imperative to have more electric, hybrid and fuel cell vehicles to alleviate the energy and environmental problems [4-6, 10].

Since the recent re-inception of hybrid electric vehicles in 1999, more than 2 million HEVs have been sold in the US [11]. However, challenges for designing higher performance lower cost HEVs, PHEVs and FCVs exists [5, 8]. One of the major challenges is designing a high power, high energy, long life cycle and low weight energy storage system (ESS) [6-8, 12, 13] to provide on-board energy to the vehicle's

powertrain. As one of the most promising and widely used components for an ESS, batteries are playing an important role in designing an advanced ESS [5-7, 12, 14-18]. To reduce the need to build expensive prototypes, high fidelity component models are necessary for system level design before making the prototype. Therefore, the need for an accurate battery model that is applicable to large format batteries arises among ESS and powertrain designers. They need a fast yet accurate battery model which can be easily integrated into circuit and system simulation environments such as Matlab/Simulink and Cadence/Pspice for system level design and simulation [6, 18-20].

1.2 Literature review

From the usage aspect, battery models can be used in two ways: on-line and off-line. An on-line battery model is used when instantaneous measurements of battery current and terminal voltage are fed into the model to estimate the internal state variables—most importantly, the battery state of charge (SOC). Accurate estimation of SOC and other parameters can be achieved by using filter technology [21-25]. These kinds of battery models are common in on-line estimation systems. The emphasis of these models is the filter included in the model, but not the model itself, although the filter does rely on the battery models to some extent. On the other hand, an off-line battery model is used without new environment inputs, focusing on predicting battery behavior—terminal voltage and SOC. The accuracy of these models greatly depends on carefully identified model parameters. These kinds of models are mostly used for system level design, such as selecting the most appropriate battery modules in simulation before physically building a prototype system. In this work, the primary focus is the off-line battery model. The on-line application of the same battery model is also investigated in the last chapter.

For off-line battery models, there are basically two main kinds of models found in the literature: physical models which are mainly electrochemical battery models, and behavior models, including mathematical models and electrical analogue battery models. There are direct relations between the battery physical parameters and the parameters in the electrochemical models [26-31], which usually involve a number of coupled partial differential equations. These models are complicated and comprehensive, which yield better accuracy than any other type of battery models. They are mostly used by battery designers for battery structure and material design. However, the electrochemical models are extremely slow in simulation, which make them unsuitable for system level design and simulation [32-35]. In the behavior models, there may not be a direct relationship between the battery physical parameters and the model parameters. The mathematical battery models typically come from empirical or stochastic equations [36, 37]. These models are simple and fast in simulation, but they are generally inaccurate compared with other types of battery models [32, 34]. In some circumstances they are acceptable for low power battery applications with slow dynamics, or when simulation accuracy is not strictly enforced. Nonetheless, these models are less acceptable for high power high dynamic large format batteries, such as the battery pack in EVs/HEVs/PHEVs, because fidelity may rapidly degrade under the heavy dynamic loading imposed on such batteries.

The electrical analogue battery models [32-35, 38-54] use electric circuit elements such as voltage sources, current sources, resisters, capacitors and inductors to represent a real battery, although the circuit elements do not physically exist. With several time constants associated with the model, it is actually a truncated representation of a non-linear system. The complexity of the electrical analogue battery models lies between the electrochemical models and the mathematical models [32, 34]. Since these models are

built based on electric circuit elements, they are inherently suitable for circuit simulation software, such as Matlab/Simulink and Cadence/Pspice, and could be easily implemented into larger system simulation.

Various electrical analogue battery models have been built and reported in the literature, however, the accuracy of most of the models fall short of the needs of high fidelity system level modeling [40, 42, 44], or the procedure to extract the model parameters is too difficult [35], or the modeling requires some information about the physical parameters that are not available to the general user [41]. What's more important is that all battery model developers have largely concentrated on modeling a single battery cell instead of a large format battery. A battery modeling procedure intended for large format batteries yielding an appropriate fidelity behavioral battery model is not available in the literature.

1.3 Detailed review of related work

1.3.1 Chen, M. et al: Accurate Electrical Battery Model Capable of Predicting Runtime and I-V Performance. IEEE Transactions on Energy Conversion, 2006.

In this paper [32], a comprehensive electrical analogue battery model was proposed for low power battery cells (Fig. 1.1). It accounts for battery cycling and self-discharging effect, nonlinear Open Circuit Voltage (OCV) and transient Current - Voltage (I-V) characteristics. The focus of this paper was to provide an accurate electrical analogue battery model of a single battery cell for circuit simulation. The main contribution of this paper is that it proposed the topology of the behavioral electrical analogue battery model based on previous Thevenin, impedance, and runtime based models. It employed a series resistor to be responsible for the instantaneous voltage drop,

and two RC networks for short and long time transient responses. The proposed model was experimentally verified on a polymer li-ion battery and a nickel-metal-hydride (NiMH) battery with accurate results. In the performance tests, maximum terminal voltage error was 15 mV - 30 mV for three set of performance tests on the 3.7 V, 850 mAh, TCL PL - 383562 polymer li-ion battery. The SOC - OCV profile was extracted based on the algorithm in [55]. The parameters were extracted using the method in [56].

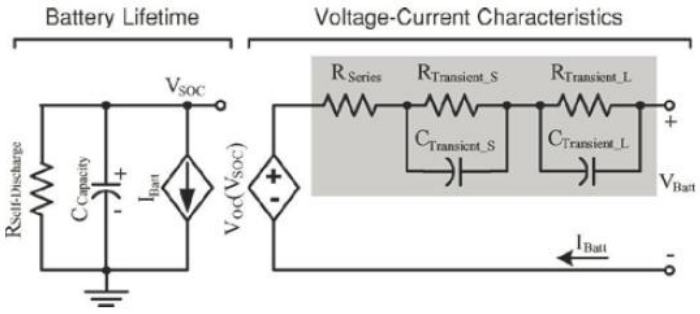

Figure 1.1 The battery model in [32]

Figure 1.2 shows the estimated parameters for R_{series}, $R_{Transient\_S}$, and $C_{Transient\_S}$. Although the parameters were assumed to be current and SOC dependent, results showed that they were close to constant during 20% - 100% SOC.

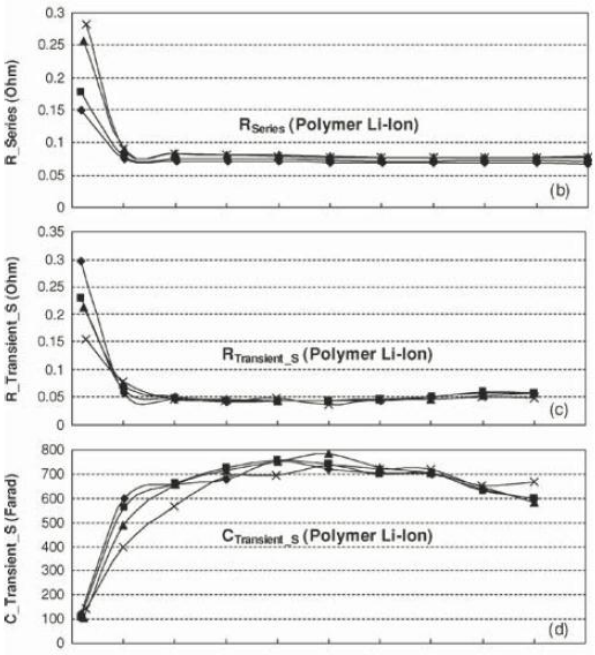

Figure 1.2 Extracted parameters in [32]

However, the limited bandwidth nature of the model was not acknowledged in this paper. As a result, the modeling procedure was unaware of the application environment. The model was built for a specific battery and considered accurate for all applications with the modeled battery. Another drawback of this paper is that the SOC - OCV profile extraction needs to be improved, as will be discussed in Section 1.3.3.

1.3.2 Schweighofer, B., K.M. Raab, and G. Brasseur, Modeling of high power automotive batteries by the use of an automated test system. IEEE Transactions on Instrumentation and Measurement, 2003.

Aimed at modeling a high power single battery cell, this paper [56] adopted the same 2-RC electrical analogue battery model in Fig. 1.3 as in [32]. The focus of this paper was the automated test system and the parameter extraction based on the test data. The highlight of the paper is the programmable battery test system (Fig. 1.4) that is

capable of delivering up to 50 A of charging current and sinking up to 500 A of discharging current with a maximum continuous power dissipation of 400 W.

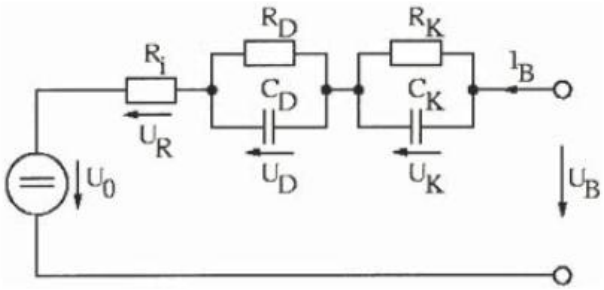

Figure 1.3 The battery model in [56]

There was no extraction of the SOC - OCV profile since the proposed procedure was intended for extracting the component parameters for a constant SOC. The component parameters were calculated based on Fig. 1.5 with (1.1):

$$u(t) = U_R + \hat{U}_D \cdot (1 - e^{-(t/\tau_D)}) \tag{1.1}$$

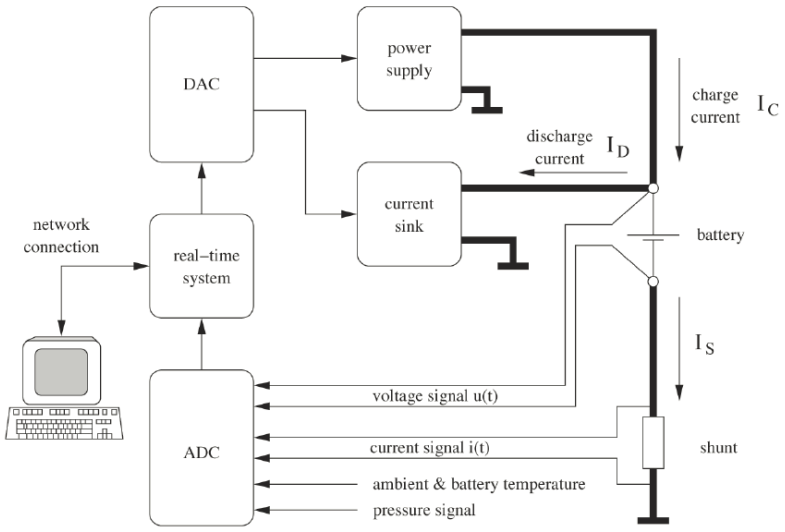

Figure 1.4 The automated test system in [56]

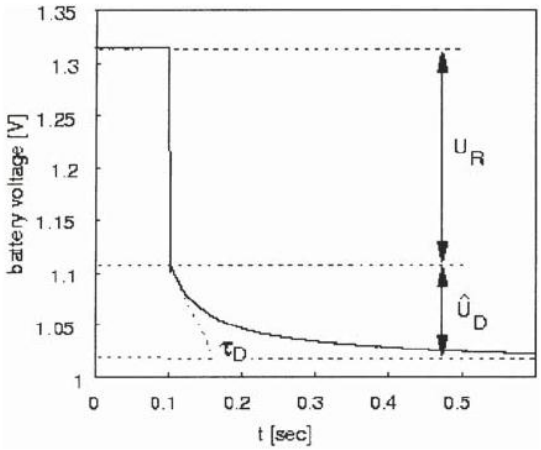

Figure 1.5 Voltage response to a discharge pulse [56]

The proposed method could reasonably extract the parameters for the series resistor and the first RC network only when the boundaries for U_R and U_D can be easily identified (Fig. 1.5). However, this is not the case. The boundary for U_R varies with system sampling rate, which is part of the limited bandwidth nature of the electrical analogue battery model. The choosing of the lower boundary for U_D is more arbitrary, because the open circuit voltage can only be reached after at least 24 hours after charging or discharging [55]. For the parameters of the second RC network, the claim "By analyzing the remaining part of the current pulse, the values for R_K and C_K are calculated in a similar way" was vague and of questionable validity.

The proposed method was verified on a 1.25 V, 9 Ah NiMH battery cell with results shown in Fig. 1.6. A large discrepency can be observed between the measured data and the model output. The error came from both the inaccurate model parameters and the assumption of constant SOC. The way the parameters were extracted in this work is inaccurate and needs improvement. This parameter estimation method was also used by [32].

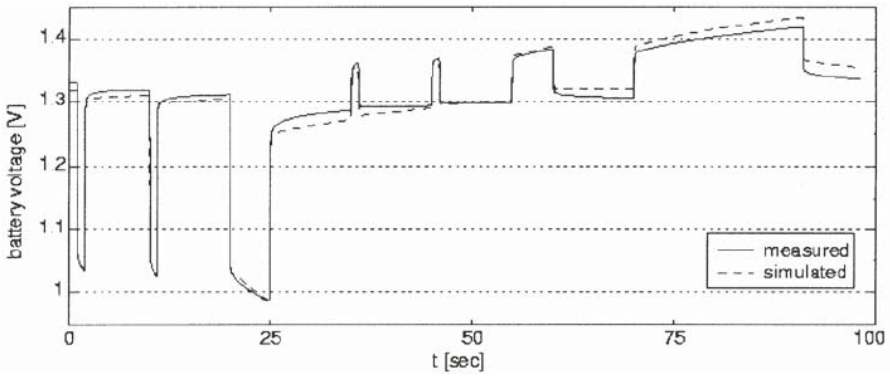

Figure 1.6 Voltage response to discharge and charge pulses [56]

1.3.3 Abu-Sharkh, S. and D. Doerffel, Rapid test and non-linear model characterisation of solid-state lithium-ion batteries. Journal of Power Sources, 2004.

In this paper [55], a rapid test procedure was proposed aimed at characterizing lithium-ion battery cells. A great contribution of this paper is the fast battery test procedure to extract the SOC - OCV profile of a battery cell. A 2-RC network electrical analogue battery model was used as Fig. 1.7. Instead of spending 20 days on extracting the SOC - OCV profile in the traditional way, one can get this profile in 24 hours with the proposed pulse charging and discharging test on a battery cell.

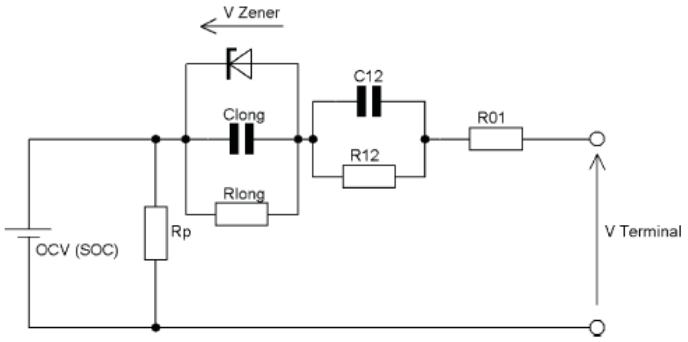

Figure 1.7 Equivalent circuit model during discharge in [55]

As illustrated in Fig. 1.8, the battery cell was pulse charged and discharged in a cycle with a 1-minute rest period at the end of each pulse. By connecting the lowest

voltage points during battery charging and the highest voltage points during discharging, the SOC - OCV profile was obtained by making an average of the two dotted lines (Fig 1.8).

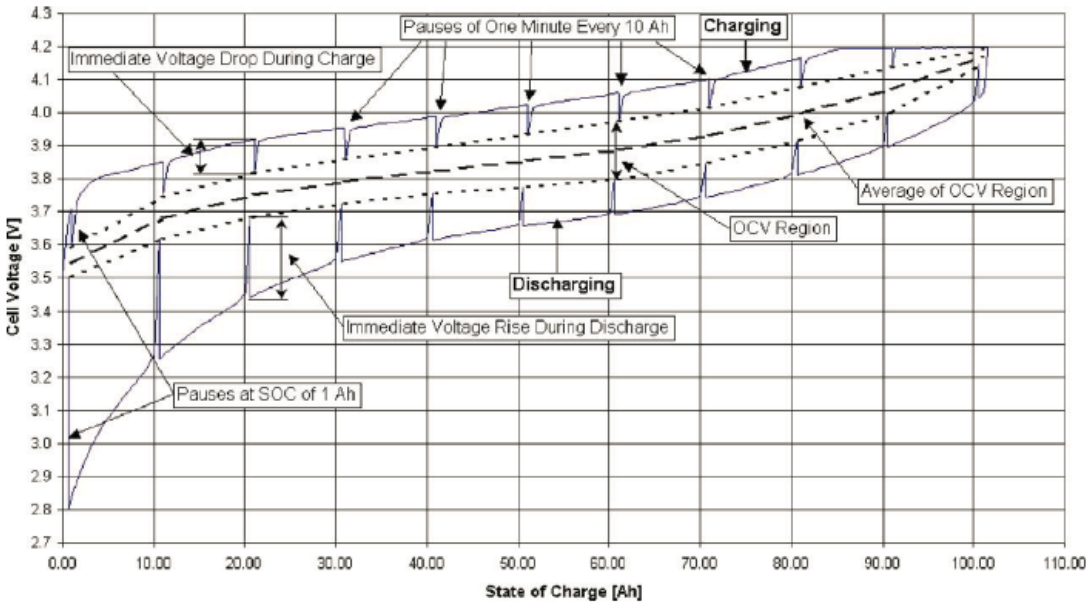

Figure 1.8 Voltage vs. SOC during the rapid test [55]

The SOC - OCV profile from the rapid test procedure had been compared with the one from the traditional method, which was considered more accurate (Fig. 1.9). A high energy lithium-ion battery cell with a capacity of 100 Ah was tested on a Digatron universal battery tester. Discrepancies were observed and acknowledged, but the errors were considered acceptable and thus no further action was taken. However, the parameter extraction for the circuit components was incomplete and further tests were suggested in the paper.

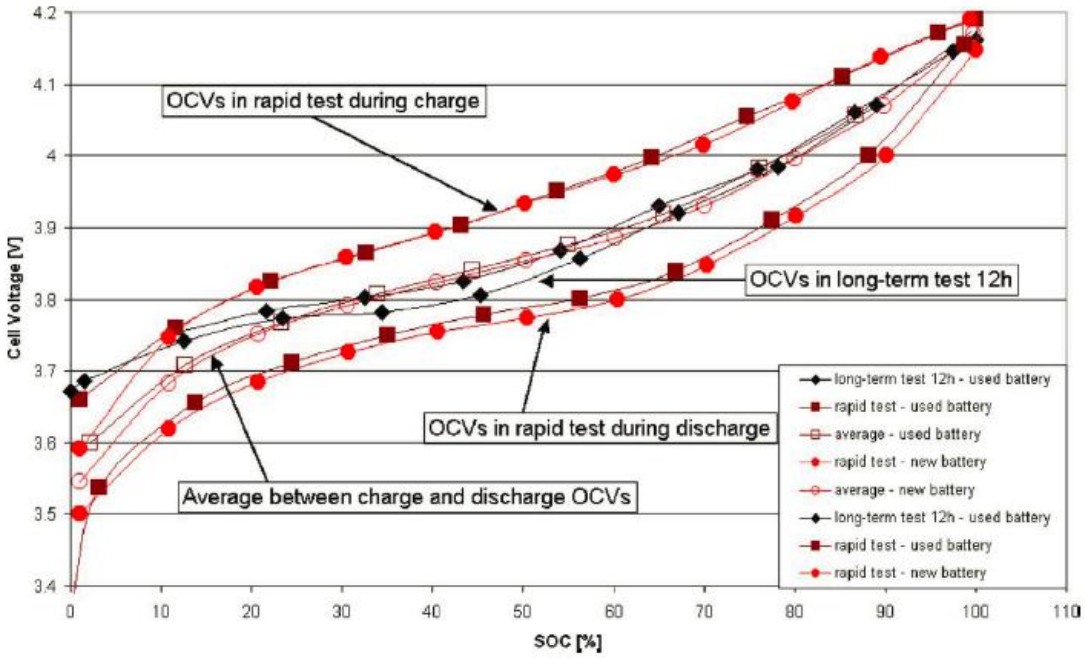

Figure 1.9 Comparison of OCV obtained from different tests [55]

1.3.4 Hussein, A.A.-h., N. Kutkut, and I. Batarseh. A Hysteresis Model for a Lithium Battery Cell with Improved Transient Response. in Applied Power Electronics Conference and Exposition (APEC). 2011.

A two-RC network equivalent electrical analogue battery model (Fig. 1.10) was proposed in this paper [44] intended for a battery cell.

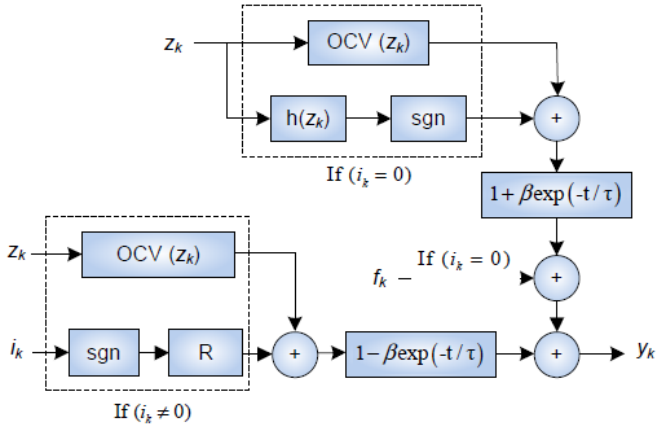

Figure 1.10 The improved hysteresis model in [44]

Terminal voltage was calculated from the discrete time expression:

$$y_k = (OCV(z_k) + (\text{sgn})(Ri_k))(1 - \beta \exp(\frac{-t}{\tau})) \text{ when } i_k \neq 0 \quad (1.2)$$

$$y_k = (OCV(z_k) + (\text{sgn})h(z_k))(1 + \beta \exp(\frac{-t}{\tau})) + f_k \text{ when } i_k = 0 \quad (1.3)$$

$$f_k = (\text{sgn})\frac{\varepsilon_v}{T_{\max}} t,\ 0<t \le T_{\max},\ |f_k| \le \varepsilon_v \quad (1.4)$$

where R is the equivalent internal resistance of the cell, sgn is an operator which is negative for discharging and positive for charging, k is a time index, z_k is the SOC of the cell, i_k is the cell's current and y_k is the output voltage of the cell model, all at time k. Coefficient β is used to improve transient dynamic responses, and f_k is an additive correction linear function. The function of $h(z_k)$ reflects the hysteresis effect.

Although the author did not point out the two-exponential or two-RC network characteristic of the model, it actually does consist of two exponential moments: one is reflected by the $1 \pm \beta \exp(-t/\tau)$ term, and the other one is reflected by the f_k term, which is the first order Taylor expansion of an exponential term.

The major drawback of the proposed model is that the transient response was poor, because an exponential term in the model was approximated by a first order Taylor expansion, which greatly reduced the available model accuracy. Another limitation is that the time constant was calculated from Fig. 1.11 by:

$$\exp(\frac{-t_1}{\tau}) \le 0.5\% \Rightarrow \tau = \frac{-t_1}{\ln(0.005)} = \frac{t_1}{5.3} \quad (1.5)$$

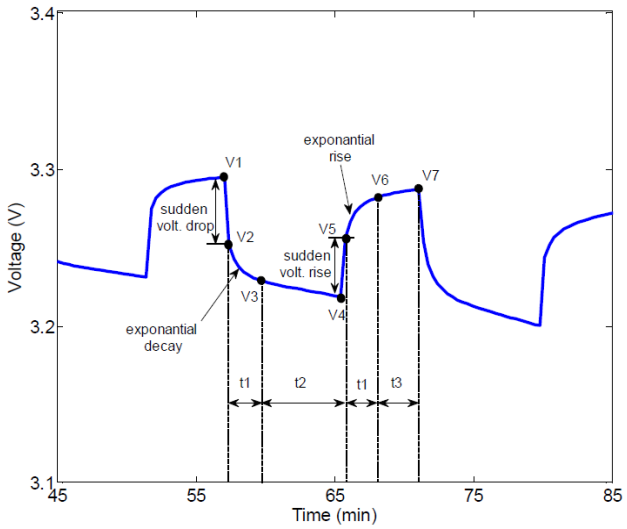

Figure 1.11 Cell's dynamics during discharge [44]

t1: transient on/off time; t2: steady-state on time; and t3: steady-state off time [44]

However, the choice of V_5 and V_6 to calculate τ was arbitrary, as a result of being aware of the limited bandwidth nature of the model. Other drawbacks of the model include the inaccurate way that the SOC - OCV profile is extracted, using only one exponential when $i_k \neq 0$, and the coefficient β was obtained by manual curve fitting. As a result of the above drawbacks, the battery cell model was rather inaccurate compared to other similar models when verified on a 1.1 Ah lithium-ion phosphate battery cell (Fig. 1.12) in the authors' own report.

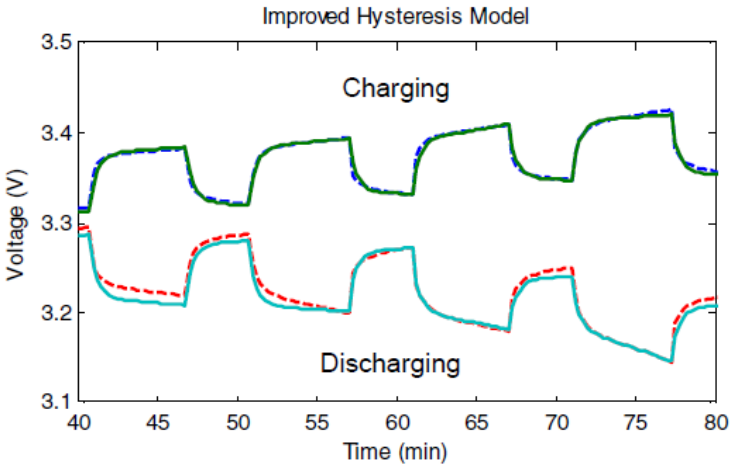

Figure 1.12 Battery voltage response during charge and discharge [44]

1.3.5 Zhang, J., et al. An enhanced circuit-based model for single-cell battery. in Applied Power Electronics Conference and Exposition (APEC). 2010.

In this paper [42], an electrical circuit battery cell model based on [32] was proposed (Fig. 1.13). The major difference between the new model and the original model was the introduction of the variable capacitor representing battery capacity on the left part of the model. The variable capacitor was introduced to take care of the so-called battery remaining capacity "recovery effect", which is basically the nonlinear variation in battery available capacity with charge or discharge current.

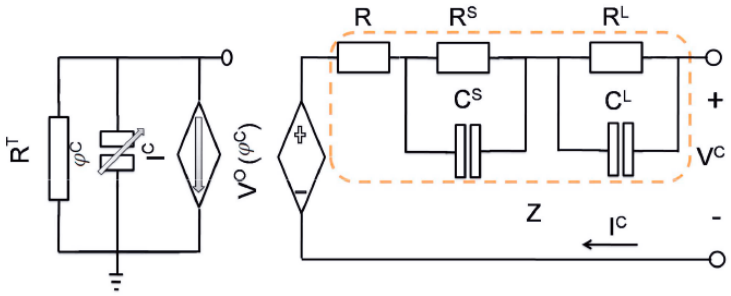

Figure 1.13 The reported model in [42]

In the proposed model, battery SOC was calculated as:

$$\alpha^A(I^C,\beta,L,t_s,t_e) = I^C F(L,t_s,t_e,\beta) \tag{1.6}$$

$$F(L,t_s,t_e,\beta) = t_s - t_e + 2\sum_{m=1}^{\infty}\frac{e^{-\beta^2 m^2(L-t_s)} - e^{-\beta^2 m^2(L-t_e)}}{\beta^2 m^2} \tag{1.7}$$

$$SOC = 1 - \frac{\alpha^A}{c^f} \tag{1.8}$$

where α^A is the accumulated capacity during time period [t_s, t_e]; c^f is the full capacity; function $F(L,t_s,t_e,\beta)$ is related to the recovery effect.

In the reported work, no detailed parameter extraction procedure was provided. Although the proposed model incorporating the recovery effect was intended to improve the model dynamic response, when it was verified on a 3.7 V, 2.6 Ah lithium-ion battery cell, 20 mV max voltage estimation error was observed (Fig. 1.14), which was close to the error reported in [32]. Therefore, the proposed method to improve the dynamic response of the original model is unsuccessful.

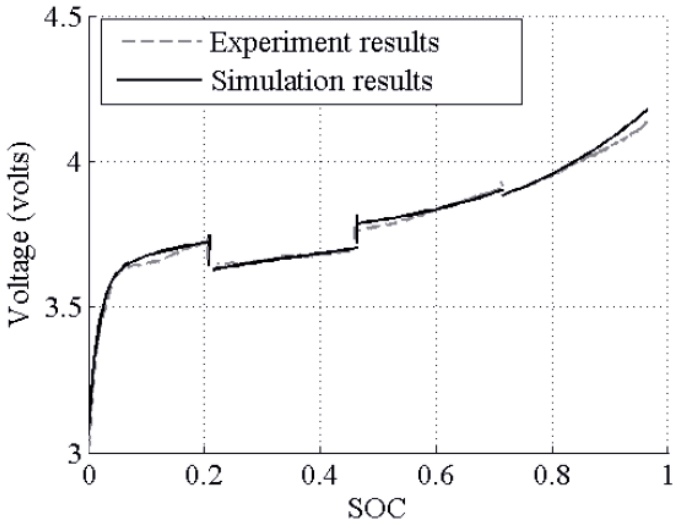

Figure 1.14 Battery model validation at variable loads [42]

1.4 Contributions

The proposed modeling procedure aims at modeling a large format battery - a battery module as a whole instead of a single cell. In this case the cell balancing, cell discrepancy and scaling issues are already captured in the modeling process. Thus the module-based battery model is readily integrated into larger systems for system level design and simulation, i.e., selecting the most appropriate battery modules for an ESS. A real battery system is non-linear and time varying. In the proposed research, a truncated representation of the system is reflected by a common non-physical behavioral battery model. The battery modeling procedure that is the subject of this research starts with a desired battery application environment, followed by modeling the battery according to the application bandwidth, and then estimating the model parameters using Sequential Quadratic Programming (SQP). This approach recognizes and makes use of the limited bandwidth of the battery model by reconciling the approximation with the limited bandwidth required by the simulation. The uniqueness of the proposed work is that it is aimed at large format batteries - a battery module instead of single battery cells, which embraces more engineering significance because battery modules are the ones that are widely available in the market and could be readily put together to build larger battery systems, i.e. the energy storage system in EV/HEV/PHEV. The battery model, which is represented by electrical circuit components, can be easily integrated into simulation environments such as Matlab/Simulink and Cadence/Pspice.

The major contributions of the proposed work are summarized as:

1. A high fidelity electrical analogue battery model was selected for large format batteries

2. A novel performance-driven, application-aware modeling technique was proposed for large format battery modeling
3. A novel bandwidth-based parameter extraction algorithm for the battery model was established
4. A method of rapid extraction of high accuracy SOC - OCV profile was established
5. The robustness of the characterized model was verified
6. Scalability of the battery model to battery packs and to higher order of approximations was examined

1.5 Dissertation Organization

This dissertation is organized as follows. Chapter II introduces the electrical analogue battery model for large format batteries. Chapter III describes the proposed bandwidth-based parameter estimation algorithm. Chapter IV explains the rapid extraction of accurate battery SOC - OCV profile. Chapter V shows the experimental apparatus and results of the proposed large format battery modeling technique on Ultralife 14.4 V, 6.8 Ah lithium-ion battery modules. The robustness of the constructed battery model from one battery module was tested on four battery modules of the same kind. Chapter VI describes the scaling of the electrical analogue battery model to the battery pack on Mississippi State University EcoCAR - a 360 V, 21.3 kWh battery pack assembled from modules made by A123, Inc. Chapter VII shows the scaling of battery model from 2-RC networks to 3-RC networks. Chapter VIII discusses the capability of the electrical analogue battery model to be used on-line for battery SOC estimation after

the model parameters are extracted based on the proposed modeling method. Chapter IX concludes this dissertation.

CHAPTER II

THE ELECTRICAL ANALOGUE BATTERY MODEL

2.1 Overview

A well-recognized electrical analogue battery model [32, 42, 44, 55, 56] for lithium-ion batteries is drawn as Fig. 2.1. It includes two parts: The left part is the state of charge estimator, which estimates battery SOC based on coulomb-counting; the right part - electric circuit part is the circuit representation of the electro-chemical battery system which could be directly integrated into circuit simulation software such as Matlab/Simulink and Cadence/Pspice. The bridge of these two parts is the SOC - OCV mapping - a unique relationship between battery charge level and internal voltage potential.

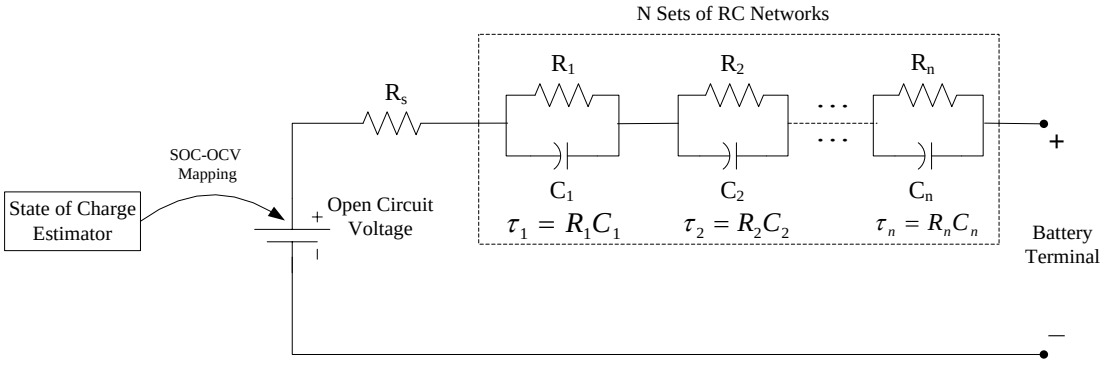

Figure 2.1 The electrical analogue battery model

2.2 State of charge estimation

In the battery model, battery terminal voltage is a reflection of the battery open circuit voltage, internal resistance, and transient effects caused by charging or discharging current. By measuring battery terminal current, the SOC could be estimated by coulomb-counting method from (2.1) if the initial SOC is known. If the initial SOC is not known but the battery has been left rest for a long time (more than 24 hours), initial SOC can be estimated from the SOC - OCV mapping in a reverse direction by measuring the initial battery terminal voltage (the battery terminal voltage is supposed to reach OCV after 24 hours [55]). Otherwise recursive estimation algorithms should be adopted to get an initial estimate of the SOC [23, 57, 58]. Once the battery SOC is known, battery open circuit voltage can be found from the SOC - OCV mapping.

$$SOC = SOC(0) - \frac{\int_0^t i(t)dt}{C} \tag{2.1}$$

2.3 Circuit representation of the real-world battery

On the circuit part of the model (the right part), instant voltage change is reflected by the voltage on R_s. The N sets of RC networks are employed to represent the dynamic responses of the electro-chemical process caused by charging or discharging current with time constants $\tau_1, \tau_2, \ldots, \tau_n$. The RC networks are truncated exponential representations of a non-linear system, which is a common engineering problem that widely exists in many areas [59, 60]. Although electric circuit components are used in this model, the model does not physically represent batteries, but a behavior representation of them.

The term “electrical analogue battery model” is introduced here as to emphasize the fact that although electric circuit components are used in the battery model, they do not physically (analog) represent the real-world battery, but a behavioral (analogue)

representation. Otherwise, people may interpret the term "electrical battery model" as "electrical analog battery model".

2.4 Limited bandwidth nature of the model

Since networks are used in the circuit part of the battery model, the electrical characteristics of the RC networks are embodied in the battery model. One important characteristic of the RC networks is that they have limited bandwidth. Taking the first RC network as an example, the natural response of the RC network is:

$$V_1(t) = V_1(0)e^{-\frac{t}{R_1C_1}} \tag{2.2}$$

The voltage across the RC network will decrease to 5% of the original voltage in $3\tau_1$ (where $\tau_1 = R_1C_1$). Thus transient responses longer than several times τ will not be adequately approximated by this RC network. In general, the bandwidth of the electrical analogue battery model is limited to $[1/\tau_{\max}, 1/\tau_{\min}]$.

Another bandwidth limiting factor of the model is the sampling frequency. For example, if the sampling frequency of the battery test is 1 Hz, then battery dynamics faster than 0.5 Hz will not be accurately modeled. In other words, the battery model built on a particular sampling frequency is not supposed to be used in a simulation with shorter computational time steps because of the possibility of aliasing.

The limited bandwidth nature is of vital importance to this behavioral electrical analogue battery model because an accurate model will turn out to be inaccurate if used in an environment that is different from the environment that the model was built for.

Since a real-world battery is a continuous nonlinear system which involves complex reactions between anode and cathode, if exponential terms are used to approximate the battery behavior, there should be no natural exponential moments as a

result of the nonlinearity. The commonly used electrical analogue battery model (Fig. 2.1), which is used in many papers to model batteries in different formats and different chemistries, is actually a truncated multi-term exponential approximation. Thus there are no natural time constants in these models. A decision should be made to the time constants of the battery model based on users' preferences. This part of the electrical analogue battery model is ignored in most scenarios. Instead, much work has been done seeking the natural moments for the exponential terms [40, 61, 62], where the model parameters including the time constants that define the bandwidth of the battery model were estimated as giving the "best fit" of an arbitrary load stimulus for a battery test. Large modeling errors were reported in these papers compared to those of the reported work here. The authors' research reveals that when the bandwidth of the model is determined based on the bandwidth of the battery application, the highest fidelity can be achieved for the electrical analogue battery model. In short, the bandwidth of the battery model is chosen as the bandwidth of the actual battery application in the proposed work.

2.5 Thermal prediction of the battery model

Battery temperature can be calculated dynamically based on the thermal energy balance [33] as:

$$m \cdot C_p \cdot \frac{dT(t)}{dt} = i(t)^2 \cdot R - h_c \cdot A_s \cdot [T(t) - T_a] \qquad (2.3)$$

Where

m : Battery mass (kg);

C_p : Battery heat capacity (J/kg/K);

$T(t)$: Battery temperature ( );

$i(t)$: Battery current (A);

R : Battery internal resistance ( );

h_c : Battery heat transfer coefficients (W/ /K);

A_s : Battery surface area ( );

T_a : Ambient temperature.

The heat power terms include resistive heating and heat exchange to the ambient. Other possible heat generations have been ignored as a compromise for high speed simulation.

In Fig. 2.2, the thermal equation is implemented into Matlab/Simulink block to give the battery temperature estimation.

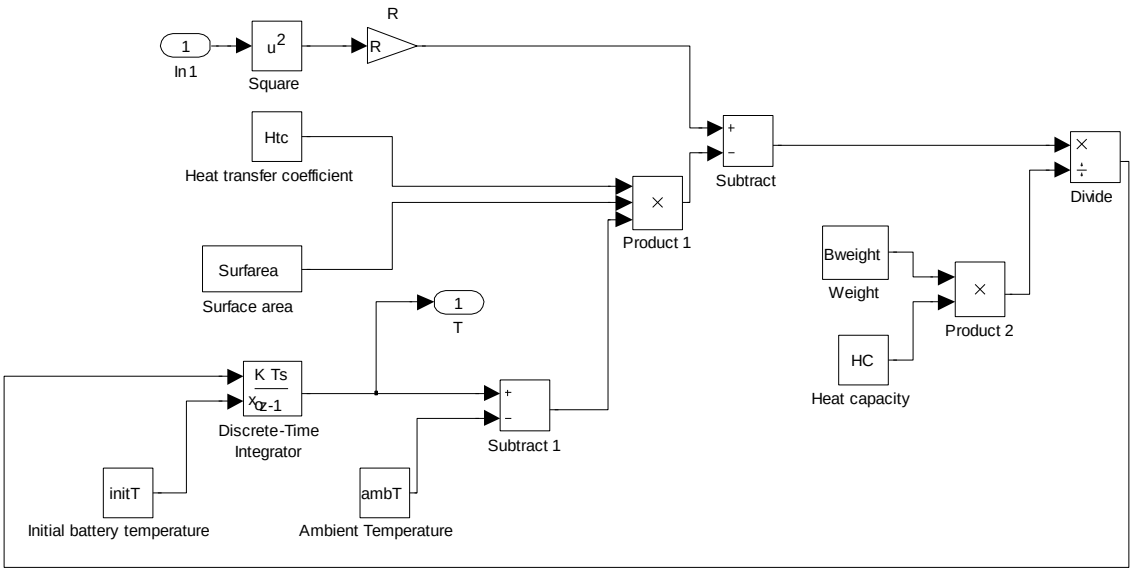

Figure 2.2 Battery temperature estimation in Matlab/Simulink

2.6 Battery temperature effects on usable capacity

There is a non-linear relation between battery usable capacity and battery temperature. Within a limited range, the higher the battery temperature, the larger the battery usable capacity will be. When we implement this relation into the calculation of

SOC of batteries by adding a temperature factor coefficient [33], the calculation of SOC can be changed instantaneously as the temperature changes. Fig. 2.3 shows the temperature factor – temperature relation.

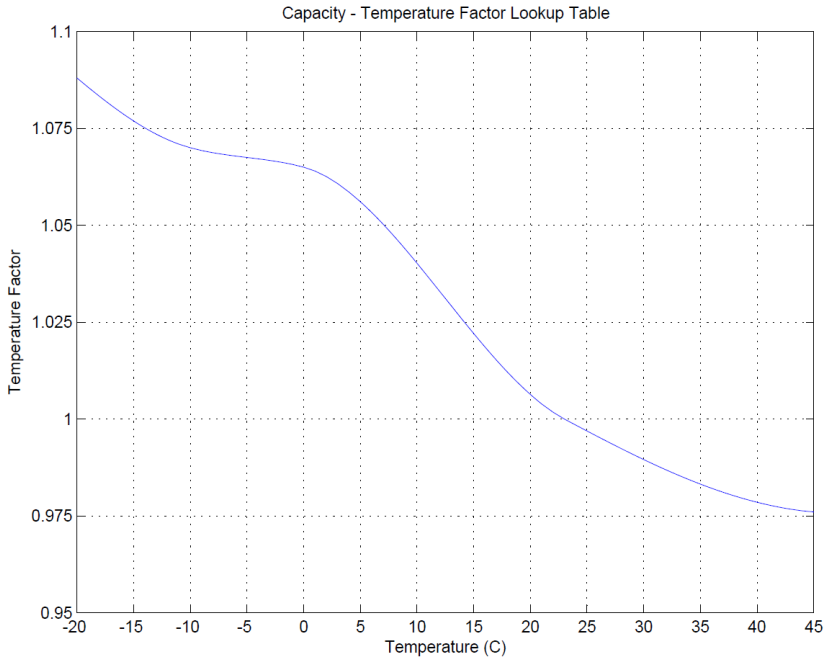

Figure 2.3 Temperature factor - temperature relation

Although the battery model is capable of predicting battery temperature as described in Section 2.5, and the battery capacity dependency on temperature is investigated in Section 2.6, these two parts were not included in the electrical analogue battery model for parameter estimation and experimental tests in the following parts of this dissertation. For the experimental battery tests discussed in this dissertation, the tested battery modules and the battery pack were well-cooled, with very limited temperature fluctuation noticed.

Besides the temperature effects, the electrical analogue battery model is also capable of working with battery aging effects by introducing aging-related coefficients to

the model parameters. The aging effects [63-67] on the battery model are beyond the scope of this dissertation and thus not discussed here.

2.7 A typical battery transient response

A typical battery transient response during a discharge pulse is shown in Fig. 2.4, which includes 5 parts: (1) instantaneous voltage drop after discharging current is applied to the battery, which is reflected by the voltage change on R_s; (2) transient period dominated by τ_1 and τ_2; (a two RC network electrical analogue battery model is assumed in this case); (3) transient period dominated by τ_2 ($\tau_1 < \tau_2$), because τ_1 vanished after a short period; (4) instantaneous voltage rise after discharging current is turned off, which is reflected by the voltage change on R_s; (5) transient period dominated by τ_1 and τ_2 during the rest period.

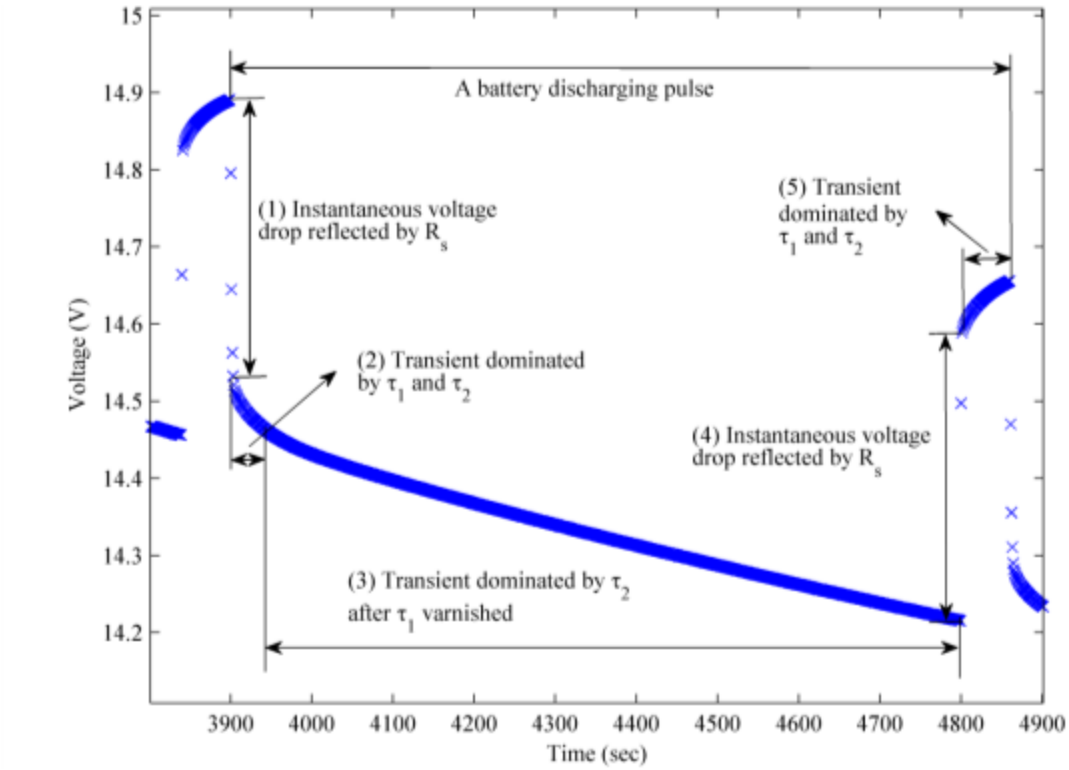

Figure 2.4 Battery transient response during discharge

Although we recognize the effects of each circuit parameter on approximating battery dynamic responses, all the data points in the behavior battery test are taken as a whole while using SQP for parameter estimation.

CHAPTER III

PARAMETER ESTIMATION

3.1 Overview

The proposed work flow of the large format battery modeling is summarized as Fig. 3.1. The parameter estimation algorithm should be designed to accommodate the limited bandwidth characteristic of the electrical analogue battery model [68]. It is necessary to investigate the battery application prior to constructing the model. The bandwidth of the battery application will determine the bandwidth of the battery model, which will in turn fix the time constants of the RC networks. Two battery tests should be conducted for the modeling purpose, one is for the SOC - OCV profile extraction, and the other one is for the circuit parameters estimation. After the battery tests, the SOC - OCV profile and circuit parameter can be obtained based on the proposed approach. The last step is model verification, where the completed battery model will be tested with different loads. The steps are discussed in detail next, with the SOC - OCV profile extraction discussed in Chapter IV.

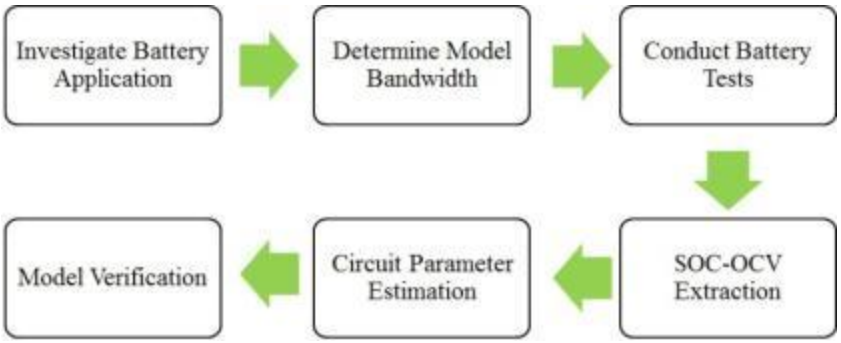

Figure 3.1 The proposed battery modeling workflow

3.2 Model bandwidth and the number of RC networks

If the bandwidth of battery application is $[f_{low}, f_{high}]$, then the smallest and the largest time constants of the RC networks in the battery model should be selected as $\tau_{\min} = 1/f_{high}$ and $\tau_{\max} = 1/f_{low}$. The number of RC networks with time constants between $[\tau_{\min}, \tau_{\max}]$ should be determined based on the fidelity requirement of the model. If a simple model with the least computational burden is desired, the number of RC networks can be two. If fidelity of the model is the first concern, the number of RC networks can be larger than two (e.g., 3 or 4 or N).

3.3 Circuit parameter estimation

3.3.1 Behavior battery test

To estimate the circuit component parameters, a behavior battery test with frequencies close to $[f_{low}, f_{high}]$ should be conducted for parameter estimation. This test data can also be taken as measurements on the actual battery in an application over a period of time in service. The choice of load stimulus is arbitrary as far as it has sufficient frequency components within the model bandwidth to adequately excite the battery.

The term “behavior test” as defined here is when the measured battery terminal current and terminal voltage are known to the battery model for the purpose of parameter

estimation. Later, the term "performance test" will be introduced when only the measured terminal current is known to the battery model. The measured terminal voltage is kept unknown to the battery model to judge the model accuracy by comparing the measured terminal voltage with the model output voltage. Thus, a performance test tracks the open-loop accuracy of the battery model.

3.3.2 Mathematical description of the model

A two-RC network representation of the battery model is the current level of approximation commonly found in similar advanced work and was thus also selected for this work as illustrated in Fig. 3.2. In Chapter VII it will be shown that this modeling approach can be extended beyond order two using the methods reported in this work. The mathematical equations for the two-RC network are derived as (3.1) and (3.2):

$$\begin{bmatrix} \dot{V}_{c1} \\ \dot{V}_{c2} \\ \dot{SOC} \end{bmatrix} = \begin{bmatrix} -\frac{1}{R_1 C_1} & 0 & 0 \\ 0 & -\frac{1}{R_2 C_2} & 0 \\ 0 & 0 & 0 \end{bmatrix} \begin{bmatrix} V_{c1} \\ V_{c2} \\ SOC \end{bmatrix} + \begin{bmatrix} \frac{1}{C_1} \\ \frac{1}{C_2} \\ \frac{1}{C} \end{bmatrix} i_t \tag{3.1}$$

$$V_t = V_{ocv}(SOC) + R_s i_t + V_{c1} + V_{c2} \tag{3.2}$$

where V_{c1}, V_{c2}, SOC are capacitor C_1, C_2 voltages and battery SOC, respectively. The parameters which need to be estimated are R_s, R_1, C_1, R_2, and C_2. Battery capacity C in (3.1) is assumed to be a constant. Battery open circuit voltage $V_{ocv}(SOC)$ is an eighth-order polynomial equation in SOC representing the SOC - OCV mapping.

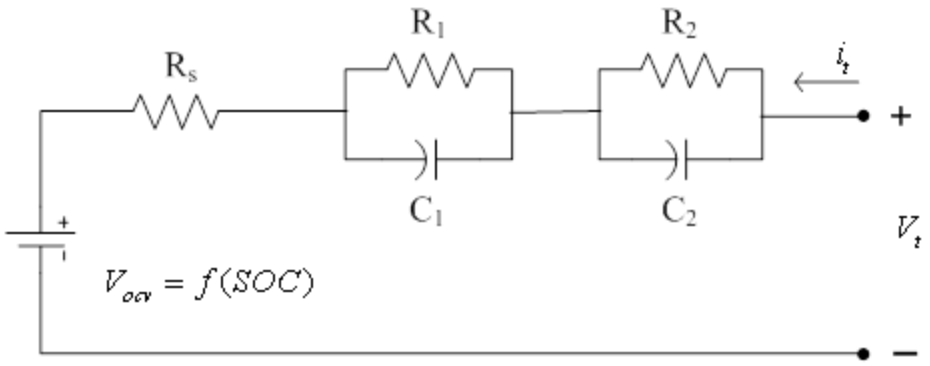

Figure 3.2 The battery model with two RC networks

3.3.3 Sequential Quadratic Programming

Sequential Quadratic Programming (SQP) is used for parameter estimation. The objective function is formed as the error between the measured battery terminal voltage from the behavior test and the model terminal voltage output with the behavior battery test current as load stimulus. And then SQP is used to minimize the objective function by varying the circuit parameters R_s, R_1, C_1, R_2, and C_2.

Define:

$$Z = [R_s \; R_1 \; C_1 \; R_2 \; C_2]^T \tag{3.3}$$

The minimization problem is summarized as:

Minimize:

$$f(Z) = \sum_{i=1}^{n} (V^i{}_{t-mea} - V^i{}_{t-sim})^2 \tag{3.4}$$

Subject to:

$$\begin{aligned} h_1(Z) &= R_1 C_1 - \tau_1 = 0 \\ h_2(Z) &= R_2 C_2 - \tau_2 = 0 \\ R_s, R_1, C_1, R_2, C_2 &> 0 \end{aligned} \tag{3.5}$$

where $V^i{}_{t-mea}$ and $V^i{}_{t-sim}$ are the measured battery terminal voltage and estimated battery terminal voltage, respectively.

The Lagrange function is formed as

$$L(Z) = f(Z) + \sum_{m=1}^{2} \lambda_m h_m(Z) \tag{3.6}$$

where λ_m representing the Lagrange multiplier associated with equality constraint h_m.

Let $d^k = \Delta Z^k$ be a 5-dimentional search direction vector, and then the quadratic programming sub-problem at a specific design point is formulated [69, 70] as,

Minimize:

$$Q(d^k, Z^k) = \nabla f(Z^k)^T d^k + 0.5(d^k)^T B^k d^k \tag{3.7}$$

Subject to:

$$h_m(Z^k) + \nabla h_m(Z^k)^T d^k = 0 \quad m = 1,2 \tag{3.8}$$

where B^k is a positive definite matrix used to approximate the Hessian of the Lagrange function $L(Z)$.

This is a typical SQP problem that could be solved using the standard SQP algorithm [69, 70]. The optimum solution to this SQP problem is the optimum Z, which represents the optimum circuit parameters.

The main advantage of the proposed algorithm over other parameter estimation algorithms is that during the parameter estimation process, the time constants of the RC networks are kept constant, because they are the preferred approximations that fit the bandwidth of the battery application. This reduction in the number of degrees of freedom removes a source of poor conditioning on the estimation process, which was found to improve the selectivity of the remaining parameter estimations.

CHAPTER IV

SOC - OCV EXTRACTION

4.1 Overview

An accurate SOC - OCV profile is a key factor for achieving a high fidelity electrical analogue battery model. A two-step process has been established to get the best estimate of the SOC - OCV profile in a short period. The traditional way of obtaining the battery SOC - OCV profile is inefficient and time-consuming. As the battery transients are supposed to vanish after a 24 hour period, to get multiple points on the SOC - OCV profile, several weeks are needed to complete the test. A rapid test procedure [55] has been developed to accelerate the process, however, as the author pointed out, the accuracy of the extracted SOC - OCV profile needs to be improved for use with higher fidelity models.

The proposed algorithm of extracting the SOC - OCV profile includes two steps: the rapid test procedure was used to develop an initial estimate of the battery SOC - OCV profile, and then four points on the SOC - OCV profile were tested with longer rest periods to get an improved measurement of the true OCV at those points, which was further used to correct the initial estimate of the SOC - OCV profile from the rapid test. In this work, the proposed algorithm has been proven to be an accurate and efficient way to extract the SOC - OCV profile.

4.2 Initial extraction of the SOC - OCV profile

A battery pulse charging/discharging cycle is required for the SOC - OCV profile extraction. As illustrated in Fig. 4.1, the battery was pulse discharged from full SOC to about 10% SOC and then pulse charged back to full to extract the SOC - OCV profile [55]. The SOC test range of [10%, 100%] was selected to embrace the normal battery operating ranges without the risk of causing irreversible changes to battery physical structures by overly deep discharging. The pulse length was chosen to discharge or charge the battery by 10% SOC, while allowing the battery to rest for 1 min between each pulse to catch the battery dynamics during relaxation. The battery was allowed to rest for 24 hours between discharging and charging.

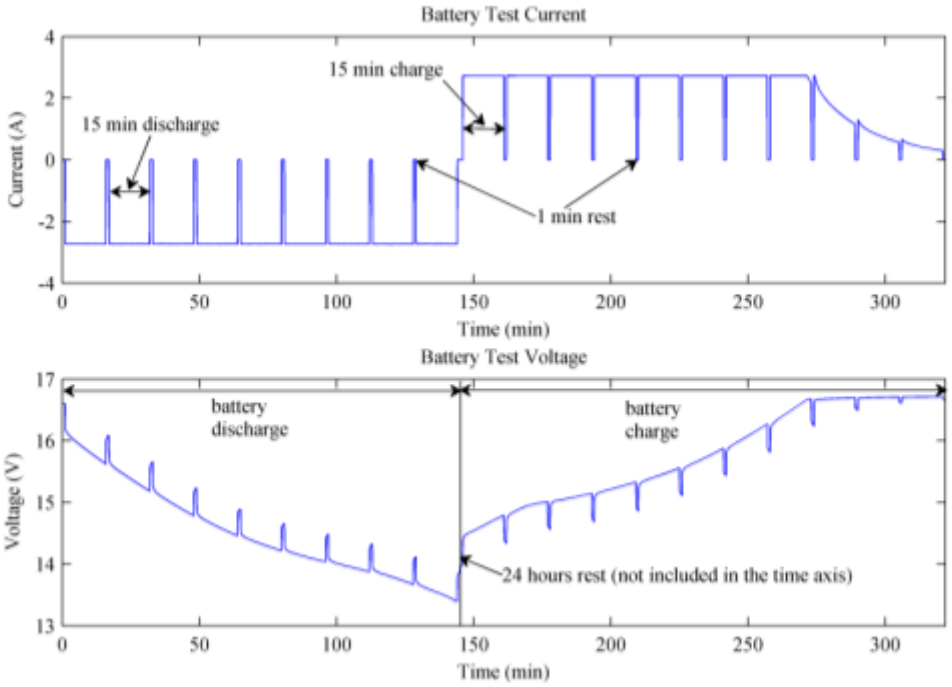

Figure 4.1 Behavior battery test for SOC - OCV profile extraction

Figure 4.2 shows the initial extraction of the SOC - OCV profile based on the cycle charge/discharge test. The ending points of the rest periods from the charging test

were connected with the green dotted lines, and the ending points of the rest periods from the discharging test were connected with the blue dotted lines. An average of the green line and the blue line was shown as the red line to represent the initial extraction of the SOC - OCV profile.

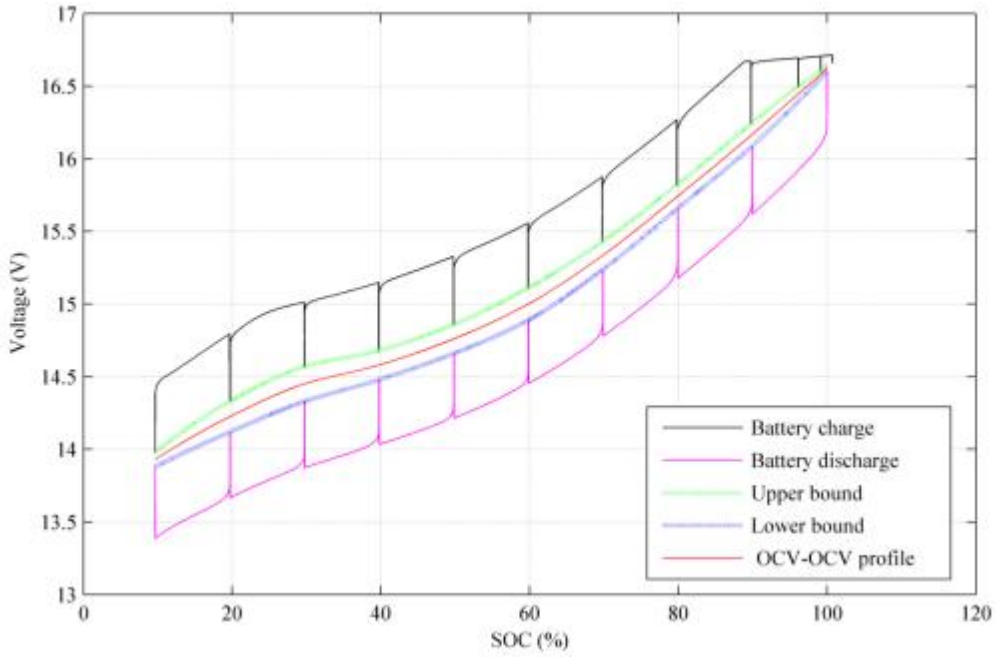

Figure 4.2 Initial extraction of the SOC - OCV profile

4.3 Correction of the SOC - OCV profile

A major improvement compared with the method in [55] is that after the initial SOC - OCV extraction, this profile was further corrected with another pulse discharging/charging with several long rest periods (24 hours) during the test cycle (in the behavior tests the rest period was 1min). By letting the battery rest for 24 hours, we were seeking to get the true battery open circuit voltage, as all the battery transients were supposed to vanish within 24 hours [55].

Figure 4.3 shows the correction of the SOC - OCV profile based on a new test profile with four longer rest periods. Four points were chosen to correct the SOC - OCV profile at about 25%, 50%, 75% and 100% of SOC. The battery module was allowed to rest for 24 hours after each pulse charge/discharge. This test started with discharging (battery was charged to full and leftover for 24 hours before discharge) and ended with charging back to full state of charge. The same criteria was adopted to charge the battery to full both before the test and at the end of the test, however, the final SOC went beyond 100% by 1% based on the coulomb-counting for two reasons: 1) The battery was not fully reversible, especially in the high SOC range, which made the coulomb-counting method of calculating the SOC inaccurate. 2) There were measurements noises that had not been taken into account.

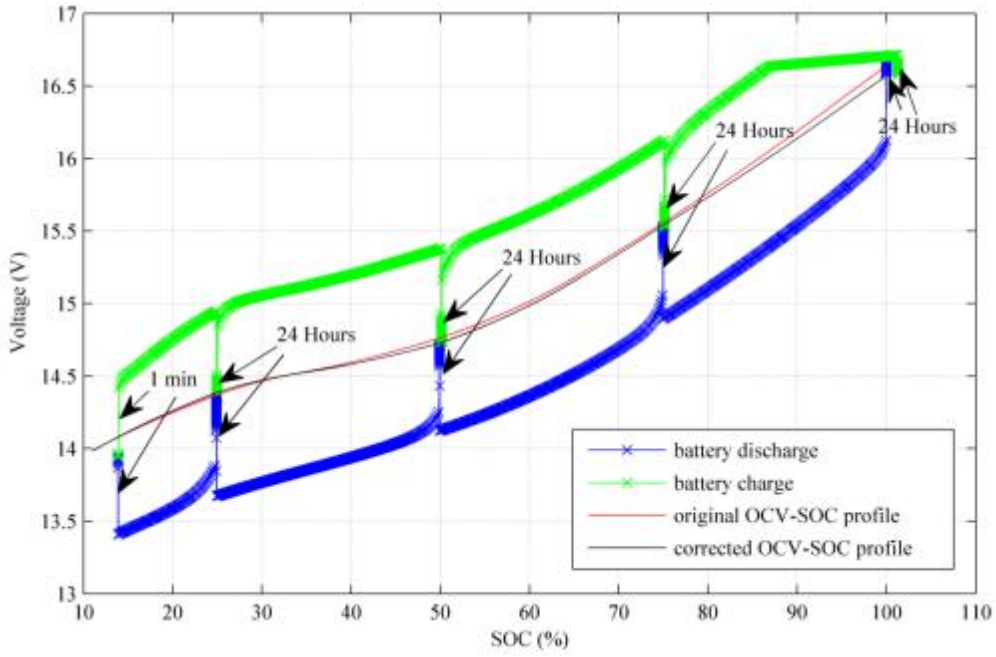

Figure 4.3 Correction of the extracted SOC - OCV profile

The battery terminal voltage was supposed to reach the open circuit voltage after 24 hours [55], and hence reach the red line in Fig. 4.3 if the red line could accurately represent the battery OCV. As we notice from Fig. 4.3, the ending points of the rest periods failed to lie exactly on the red line, and thus the SOC - OCV profile extracted from the three behavior tests should be corrected accordingly, which was represented as the black curve in the figure. The point at about 14% SOC was not used to correct the SOC - OCV profile because the rest periods at that point were only two minutes altogether.

CHAPTER V

EXPERIMENTAL APPARATUS AND RESULTS

5.1 Experimental apparatus

The battery experimental apparatus is shown in Fig. 5.1 with a corresponding block diagram illustrated in Fig. 5.2. The power source is a Sorensen SGI 60-V/500-A programmable power supply. The load is a Sorensen M540071-01 SLM 60-V/60-A 300-W DC Electronic Load. The shunt is a 5-mΩ resistor rated for 10 A. The current is calculated from the shunt voltage divided by the shunt resistance; the battery voltage is measured from the battery terminals. The data logger is an Agilent 34970A Data Acquisition/ Data Switch Unit. The battery in Fig. 5.1 is an Ultralife UBBL10 lithium-ion battery module. The battery voltage and current are measured at the battery terminals.

Figure 5.1 Experimental apparatus

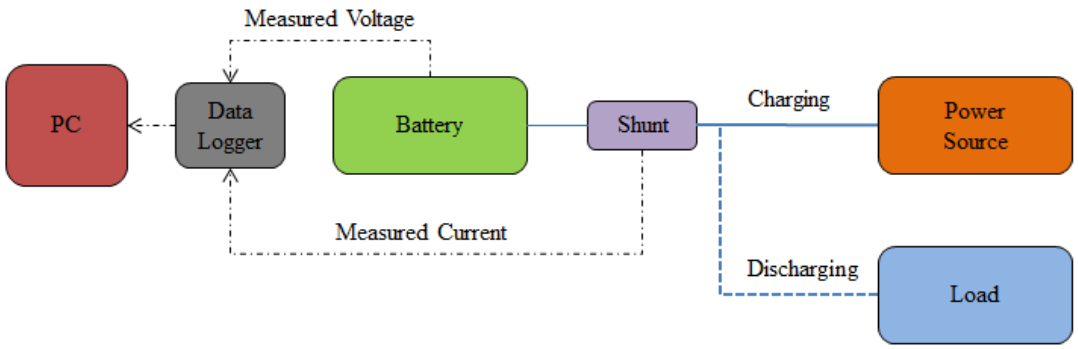

Figure 5.2 Block diagram of the experimental apparatus

The resolution of the data logger is 6.5 points. For the Ultralife UBBL10 lithium-ion battery (nominal voltage: 14.4 V) test, the voltage measurement accuracy is calculated [71] as 0.888 mV; the current measurement accuracy through the shunt is calculated [71] as 0.79 mA.

5.2 The Ultralife UBBL10 lithium-ion battery module

The proposed approach was experimentally verified on 6.8 Ah Ultralife UBBL10 lithium-ion battery modules as shown in Fig. 5.3. It has two sections, which can be configured in series or parallel form. In this test one section is used with a nominal voltage of 14.4 V [72]. The voltage range for each section is 10 V – 16.5 V. In each section, there are 3 battery cells in parallel and four cells in series. So altogether there are 12 cells in each section. The battery cell is Panasonic CGR18650 cells with a nominal voltage of 3.6 V and a standard capacity of 2450 mAh [73]. The cathode is made with lithium cobalt oxide; the anode is made with carbon [74]. A smart circuit was built in the battery module for cell-equilibration and protection. The battery module came with a SOC indicator on top of the battery module, which was not used by the author. The configuration and material information of the battery module is provided here to the reader for reference only, as the detailed electro-chemical reactions is beyond the scope

of this dissertation. The proposed modeling approach focuses on the battery external characteristics at the system level.

Figure 5.3 The lithium-ion battery module

In this chapter, four Ultralife UBBL10 lithium-ion battery modules of the same age were used for tests, numbered as #1, #2, #3, and #4. These four batteries were in the same condition - they had been left on the shelf for 2.5 years with good maintenance. The battery model was built on #1 based on behavior tests, and then the completed model was verified on #1, #2, #3, and #4 with same performance tests. All the tests were conducted in room temperature. Results verified that the battery model built on battery module #1 was accurate when tested with performance tests, and it was robust enough to be used to represent other battery modules of the same kind. It was also shown that the module to module variation is less than the cell to cell variation, as a result of cell averaging.

5.3 Parameter extraction

Battery module #1 among the four modules was used for parameter extraction in this part.

5.3.1 Model bandwidth and number of RC networks

Since the 2-RC representation of the battery is the current complexity level commonly used in other works, the number of RC networks is chosen as two for comparison purposes with this work. For illustration purposes, the time constants of the 2-RC network are pre-determined as $\tau_1 = 60\ s$ and $\tau_2 = 2100\ s$, which are assumed to have been determined to accommodate the bandwidth of the battery application. A detailed spectral analysis of battery application for time constants determination can be found in Chapter VI for the A123 battery pack used in a PHEV.

5.3.2 SOC - OCV profile extraction

The battery SOC - OCV profile was extracted from the battery experimental test as discussed in Chapter IV. The result is an 8th degree polynomial equation correlating battery SOC and OCV as:

$$V_{ocv} = a_8 SOC^8 + a_7 SOC^7 + a_6 SOC^6 + a_5 SOC^5 + a_4 SOC^4 + a_3 SOC^3 + a_2 SOC^2 + a_1 SOC + a_0 \quad (5.1)$$

The coefficients for the polynomial equation are shown in Table 5.1.

Table 5.1 Equation coefficients for SOC - OCV profile

a_8	98.2484
a_7	-466.09
a_6	960.925
a_5	-1111.5
a_4	761.716
a_3	-291.93
a_2	50.7016
a_1	1.14153
a_0	13.3044

5.3.3 Circuit parameter estimation

A behavior battery test was conducted on battery #1 for circuit parameter identification, as shown in Fig. 5.4. As the name "behavior" indicates, the battery test was designed to sufficiently excite the battery with different working conditions, which includes five parts. In part one, the tested battery was discharged from full SOC to 70% SOC with 3 A constant current for 40 min. This allows the pulse charging/discharging tests range between 50% - 70% SOC, which represents the desired battery normal operating range. This desired SOC operating range should be accommodated to specific application. In part two, the battery was pulse discharged and charged with 1 A, 1.5 A, 2 A and 2.5 A currents. The length of the pulse was 12 min and the rest period was 1 min. The length of the pulse should be chosen based on the bandwidth of the application. Rest periods of 1 min were used to characterize the battery natural behavior while there was no external current excitation. In this part, the battery was discharged from 70% to 50% SOC and then charged back to 70% SOC. In part three, interleaving pulse discharging and charging current were used with 5 min pulse length without rest periods. The currents used were 1 A, 1.5 A, 2 A and 2.5 A. This part represents faster dynamics than the dynamics in part two. The pulse length should also be altered to accommodate the actual

battery application bandwidth. In part four, gradually increasing current from 1 A to 3 A and constant 3 A current were used to charge the battery, until the terminal voltage reached the voltage limit of 16.6 V, which is defined in the datasheet. This step represents a different battery usage condition than part two & three. After battery terminal voltage reaches this voltage, the battery charging went to voltage controlled mode. In part five, the battery was charged with controlled voltage of 16.6 V, until the current tapers to 300 mA, which is the full SOC defined in the datasheet. This represents the voltage controlled operating mode of the battery application.

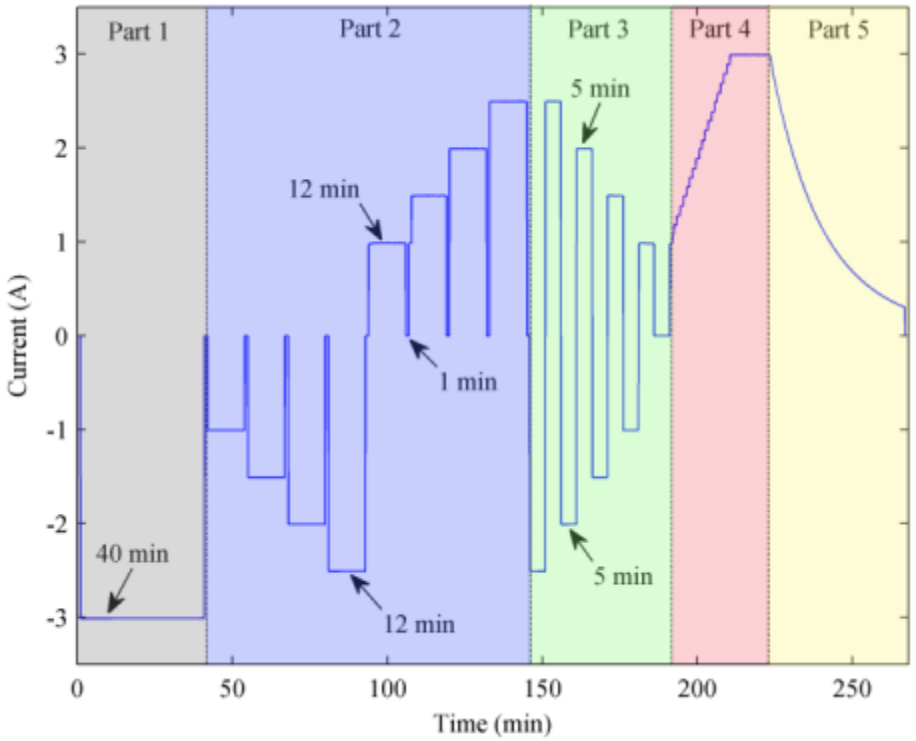

Figure 5.4 Behavior test current

With the proposed parameter estimation algorithm, the parameters were estimated as shown in Table 5.2. The nature of the battery model explains why the capacitor values are too large to be practical. Although physical components are used the electrical analog

circuit, these components have no physical values because the battery model itself is not a physical based model, but a behavior based model. With the estimated parameters, the model output voltage was compared with the measured battery terminal voltage, as shown in Fig. 5.5. Although the battery terminal voltage estimation is accurate with the completed battery model, this comparison will not be taken as model verification, as the measured terminal voltage was known to the battery model during the parameter estimation process. An independent performance battery test is used in next step for model verification. As common criteria for battery model accuracy, the rated error was calculated as the max error over battery nominal voltage, which was 0.41% in this case.

Table 5.2 Estimated circuit parameters

R_S (Ω)	R_1 (Ω)	C_1 (F)	R_2 (Ω)	C_2 (F)
0.1472	0.0338	1777.8	0.0446	47101

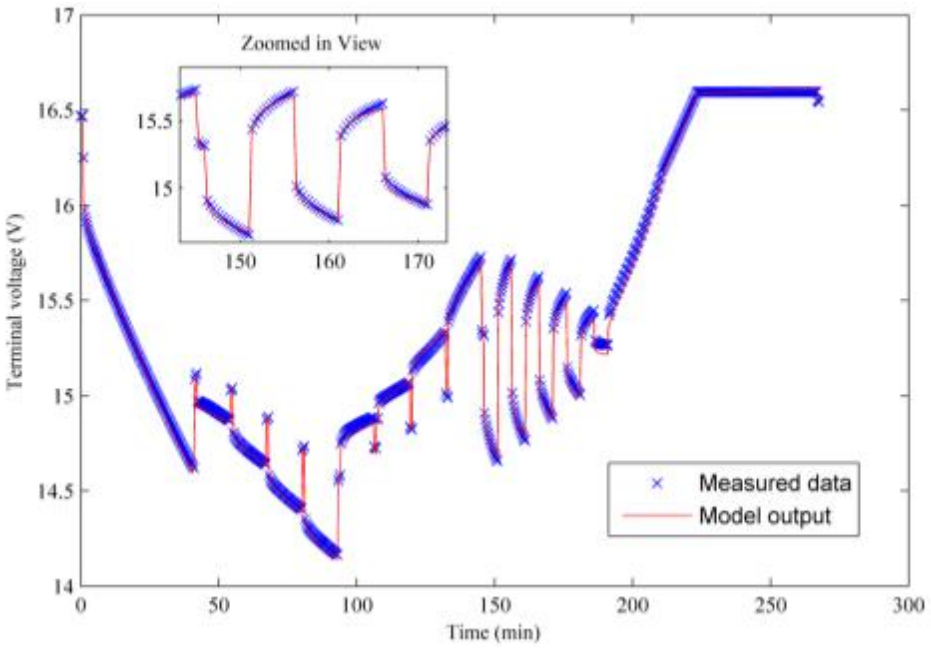

Figure 5.5 Terminal voltage estimation results

5.4 Model verification and robustness tests

To verify the robustness of the battery model with identified parameters on battery #1 with a different test profile, as well as on other battery modules from the same batch, a performance test stimulus was designed as shown in Fig. 5.6. The performance test current includes five current rates: 1 A, 1.5 A, 2 A, 2.5 A and 3 A, with pulse lengths of 5 min and 16 min. This performance test current has similar bandwidth with the behavior test current, which is the key to conserve the accuracy from the behavior test to the performance test. In reality, the performance test profile, which usually is the actual working environment for the batteries comes first, and then behavior battery test is designed to sufficiently excite the battery in the bandwidth similar to the working environment. The current in Fig. 5.6 is actually the measured current from battery #1 during the performance test.

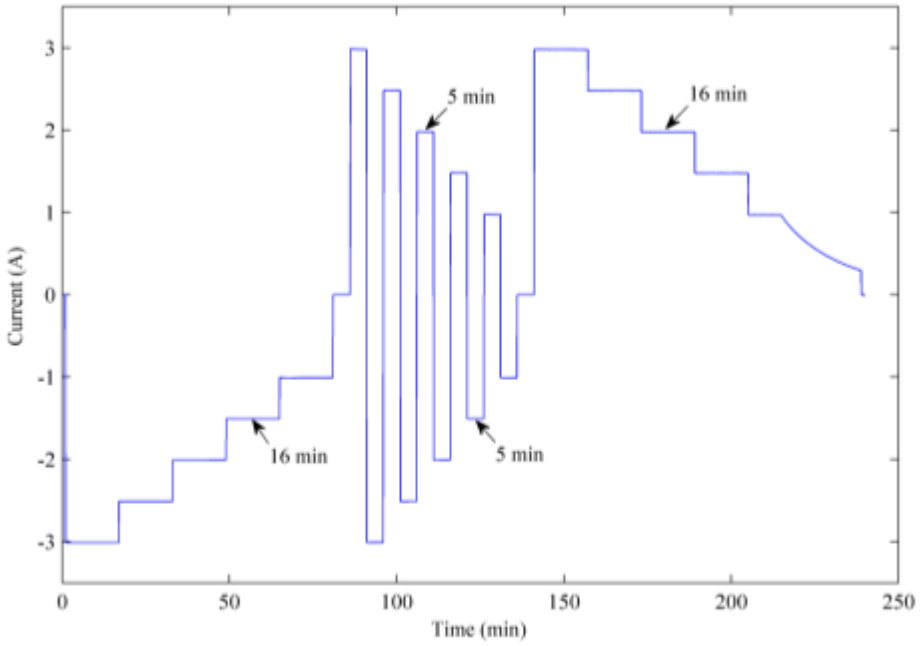

Figure 5.6 Performance test current

Figure 5.7 includes all the test currents on battery #1, #2, #3 and #4. In most parts, the current from the four batteries overlapped on each other. Although it was intended to control the test stimulus to have exactly the same current, there were minor differences in the current because of the manual switch of the circuit. The current variations at the end of the performance test, while charging the batteries to the full state of charge, reflect the battery module variations. Figure 5.8 shows the measured battery terminal voltage during the battery performance test with a max voltage difference of 0.17 V (1.2% rated) among the four battery modules.

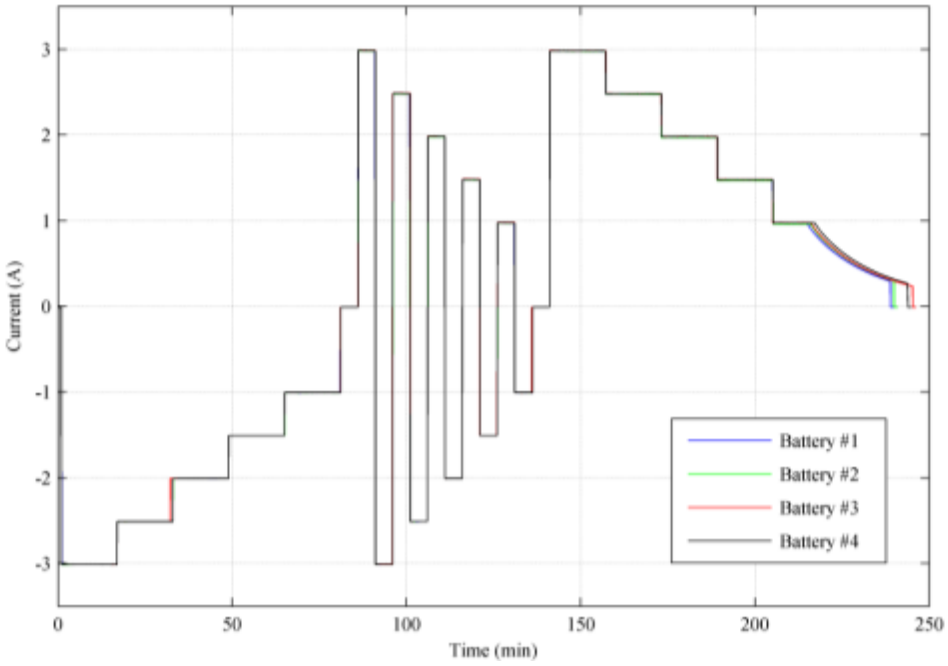

Figure 5.7 Compare four current profiles

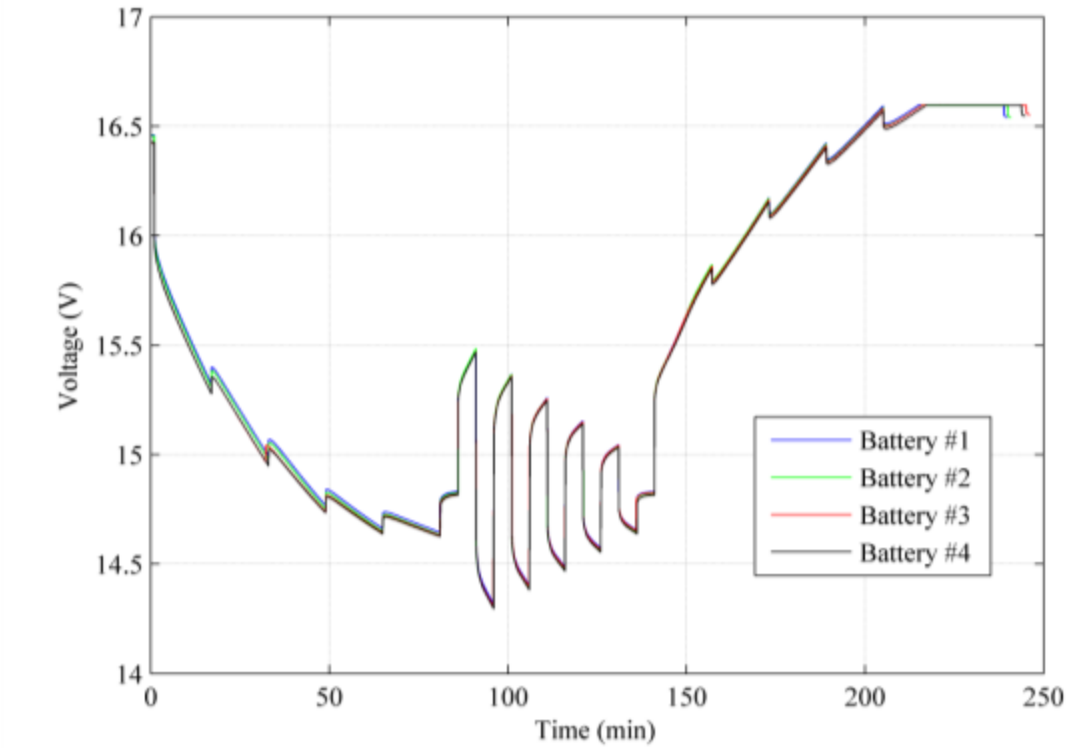

Figure 5.8 Compare four voltage profiles

As an example of the open loop battery terminal voltage estimation results, Fig. 5.9 shows the results from battery #1. The terminal voltage estimation results from battery #2, #3, and #4 are not plotted here, because they are very similar to Fig. 5.9.

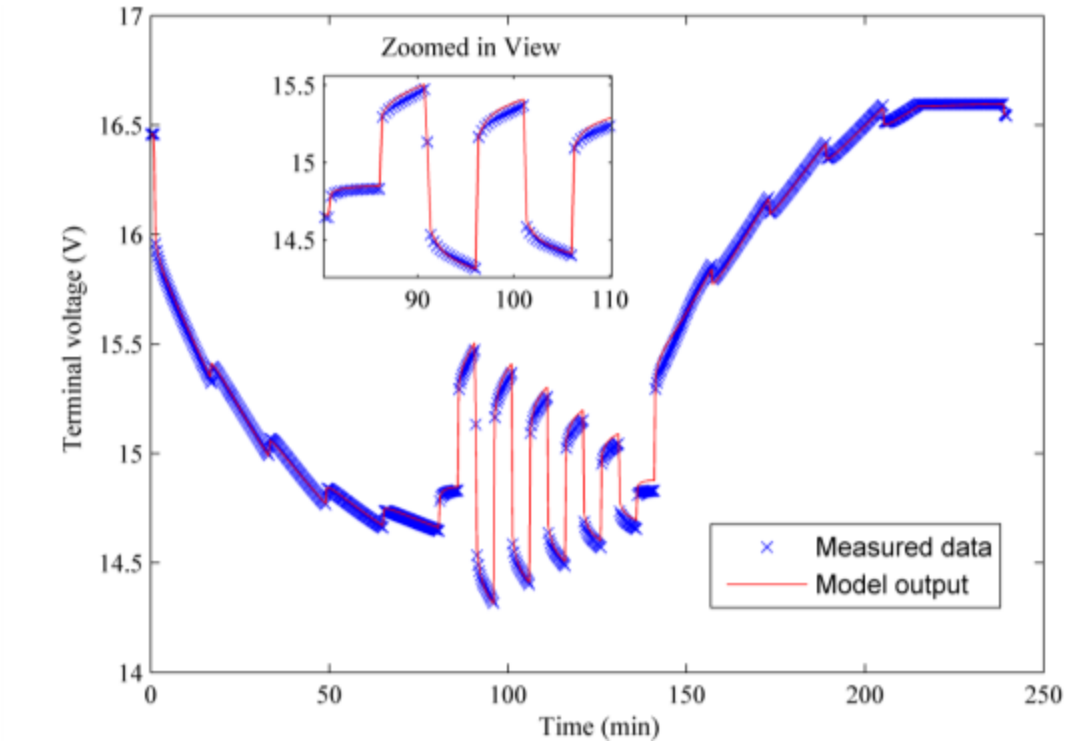

Figure 5.9 Terminal voltage estimation results

The statistical errors from open loop battery terminal voltage estimation from the electrical analogue battery model with the identified parameters are shown in Table 5.3. Battery #1 is the one that was used for parameter identification based on the behavior test. The rated error on battery #1 is 0.44%, while the rated errors on battery #2, #3 and #4 are 0.42%, 0.37% and 0.36%, respectively. The statistical errors indicate that the model accuracy (0.41% error from behavior test) was conserved when the battery model with identified parameters was used with a different test profile, or even on other batteries from the same batch. Please note that when the same battery model was used for all four batteries with the parameters extracted from a single battery module, the terminal voltage estimation error (0.36% - 0.44%) does not contradict the measured terminal voltage difference among the four batteries (rated as 1.2%), because there were slight differences among the manually switched current stimuli (Fig. 5.7).

Table 5.3 Model verification results of the four battery modules

UBBL10 Battery #	1	2	3	4
MSE (1E-4 V^2)	5.040	6.748	4.464	5.243
Mean Error (mV)	-8.269	-12.15	-5.131	-5.075
Max error (mV)	63.9	60.0	53.7	52.4
Rated error (%)	0.44	0.42	0.37	0.36

5.5 Discussion

From the model verification, we can conclude that the proposed battery modeling approach can be successfully applied to module-level batteries. The completed electrical analogue battery model proved to be highly accurate (less than 0.44% error) for four battery modules of the same kind when verified with performance battery tests.

CHAPTER VI

SCALING THE BATTERY MODEL TO A123 BATTERY PACK

6.1 Overview

In this chapter, the proposed battery modeling approach was applied to a battery pack – an A123 21.3 kWh, 360 V lithium-ion battery pack installed on the Mississippi State University (MSU) EcoCAR (PHEV). A complete model of the A123 battery pack, illustrating the modeling process, is explained in this section as an example of a real-world application of the proposed battery modeling approach. Three sets of battery data were acquired for the modeling purpose. One set of data came from a pulse discharge/charge cycle on the battery pack (off-vehicle) for the purpose of battery pack SOC - OCV profile extraction. The other two sets of data were acquired when the battery pack was operated on-vehicle during vehicle drive cycle tests. One of them was used for model circuit parameter estimation; the other one was used for battery pack model verification.

In contrast to the common approach of congregating hundreds of battery cell models in series and parallel for the battery pack representation, a simple battery model was used to represent the whole battery pack without the loss of model accuracy. The modeling process involves only the external characteristics of the battery pack; thus detailed knowledge of the physical construction of the battery pack or the physical parameters of the battery cells are not required for the modeling work. This simple yet accurate modeling approach is achieved by imposing the bandwidth of the battery

application into the bandwidth of the battery pack model. The reported work enables a new level of fast dynamic battery pack simulation with high fidelity.

6.2 Introduction to battery pack modeling

An accurate battery pack model is of significant importance for electric-drive vehicle drivetrain design and simulation. It was common in the past to see simple resistance battery models being used in vehicle simulations or energy storage system simulations [75, 76], which in practice would involve fast dynamics in an actual vehicle powertrain. In contrast to the view that vehicle system level simulation does not require high accuracy of the battery model [36], a high fidelity battery pack model is critical for the vehicle simulation because the drivetrain power management, the motor/generator control, AC/DC & DC/DC converter design and control [77], the battery pack state of power (SOP) management, etc. are highly dependent on the accurate prediction of the battery power and battery SOC. Difficulty in achieving this accuracy results from the fast dynamics of the battery current when the battery pack is used in a real-world electric drive vehicle, e.g., EV, HEV, and PHEV. As a result, these simple models were not capable of predicting the dynamic responses of the battery pack, which could invalidate the whole simulation.

Battery packs usually consist of hundreds of battery cells connected in series and parallel, including some battery packs that are made up of several battery modules, and each battery module includes several battery cells in series, parallel, or series-parallel configuration. Much battery modeling work has been reported at the battery cell level [32, 33, 42, 44, 55, 56], with little work reported in the literature discussing the battery models at the battery pack level, leaving the cell model to pack model integration work to

the system level designer or power electronics designers who do not have the expertise in batteries. Going from battery cell model to battery pack model is not simply congregating cell models to make a pack model, because in this way not only will it tremendously introduce unnecessary computational power requirement to the system, but also some phenomena that can only be observed in the battery pack level are ignored [78]. Significant fidelity loss will occur if not enough attention is paid to the battery pack behavior, as opposed to cell-level modeling only. Thus it is inevitably necessary to investigate the construction of battery pack model separately with the cell model.

6.3 Review of battery pack modeling approaches

Currently, there are three approaches for battery pack modeling available in the literature. The first approach is the method of congregating cell models in series and parallel to represent the battery pack model [34, 79]. This approach requires a minimal level of analytical effort going from the cell model to pack model, as the only required information to generate a model is the cell configuration of the battery pack. However, serious fidelity loss may be found in the battery pack model, as a result of ignoring the effects due to cell discrepancy, thermal unbalancing in the battery pack, etc. In reality, not all battery cells found in battery packs are directly available to the actual system designers for battery cell modeling.

The second approach is to scale the cell model to a battery pack model with one simplified model representing the battery pack [80-82]. In this case, the cell discrepancy issues and the phenomena only related to the battery pack are investigated and included in the pack model which requires much less computational power than the first approach. Compared with the first approach, the second approach is comprehensive and fast in

simulation; therefore, it is more suitable for system level design and simulation. Nonetheless, the investigation of cell discrepancy and thermal distribution in a battery pack requires extensive time and effort, and often the battery cells are not directly available to the designers.

The third approach is building a battery pack model directly on a well-built battery pack with a single battery model [61, 62, 83]. In this case, the battery cells characteristics and thermal influences on cells are naturally included into the battery pack models, as a result of cumulative effects of cell averaging; and at the same time the battery model will be fast in simulation requiring the least computational power. Another advantage of this battery pack level procedure is that non-idealities that are known to exist in battery packs, such as weak cells and interconnection impedances, is captured self-consistently at the time the battery pack model is built. This approach does not require cell-level details or pack configurations, and some modeling algorithms at this level are even independent of battery chemistry. For commercially available battery packs, the third approach may be the only possible approach, as in this case the battery tests can only be conducted at the battery pack level. Two prerequisites for the third approach are that the battery cells must be well balanced with advanced cell balancing algorithms, and the battery pack should be cooled with effective cooling methods so that the battery pack does not encounter a tremendous temperature increase to ensure the safety of the battery pack. In other words, only when a well-designed battery system is available can one confidently model the battery pack as a single battery model. The issue of battery cells discrepancy has been discussed in a number of papers and communications [80, 84]. A two-step screening process has been proposed in [80] to

ensure a stable configuration of a battery pack, and many cell equalization approaches and been proposed [75] as well.

Comparing the three battery pack modeling approach discussed above, the third approach which builds a battery pack model directly on a battery pack seems to be the most promising one for system level designers. However, large modeling errors up to 3.1% for this battery pack modeling technique even with moderate real-world test environment have been reported in [61, 62, 83]. Obviously, this method has room for improvements in terms of high fidelity system level simulations. An advanced direct battery pack modeling approach is the subject of this chapter.

6.4 The A123 lithium-ion battery pack

The A123 lithium-ion battery pack representing the cutting-edge lithium-ion battery technology is shown in Fig. 6.1, where the battery pack is sitting at the back of the MSU EcoCAR (PHEV). This battery pack includes five A123 battery modules (Fig. 6.2 left) connected in series. In each battery module, there are 22 prismatic battery cells (Fig. 6.2 right) in series and 3 in parallel [85]. So altogether there are 66 battery cells in each battery module. Each battery cell has a capacity of 20 Ah and a nominal voltage of 3.2 V. A well-designed battery control module is included in the battery module to ensure a safety operation of the battery pack. As stated earlier, the detailed configuration of the battery module is provided here to the reader for reference only. The proposed modeling approach focuses on the battery external characteristics at the system level.

Figure 6.1 A123 battery pack on vehicle

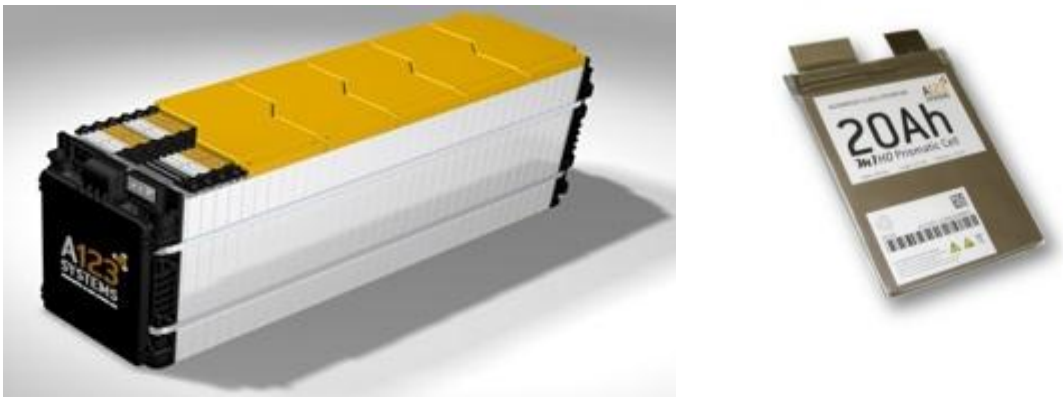

Figure 6.2 A123 battery module (left) and cell (right)

6.5 Parameter extraction

6.5.1 Model bandwidth and number of RC networks

The battery pack for parameter estimation came from a vehicle drive cycle test with the battery pack installed on the MSU EcoCAR. The speed profile of the drive cycle test is shown in Fig. 6.3. With the data of the battery pack acquired from the drive cycle

test, it is possible to analyze the frequency of the battery application by doing a Fourier analysis of the battery terminal current. The battery terminal current, terminal voltage and battery SOC during the on-vehicle battery test were shown in Fig. 6.4. A single-sided amplitude spectrum of battery terminal current is shown in Fig. 6.5 and 6.6. From the spectral analysis of the battery current stimulus, the major frequency components range can be identified as from 0.0008799 Hz to 0.02134 Hz.

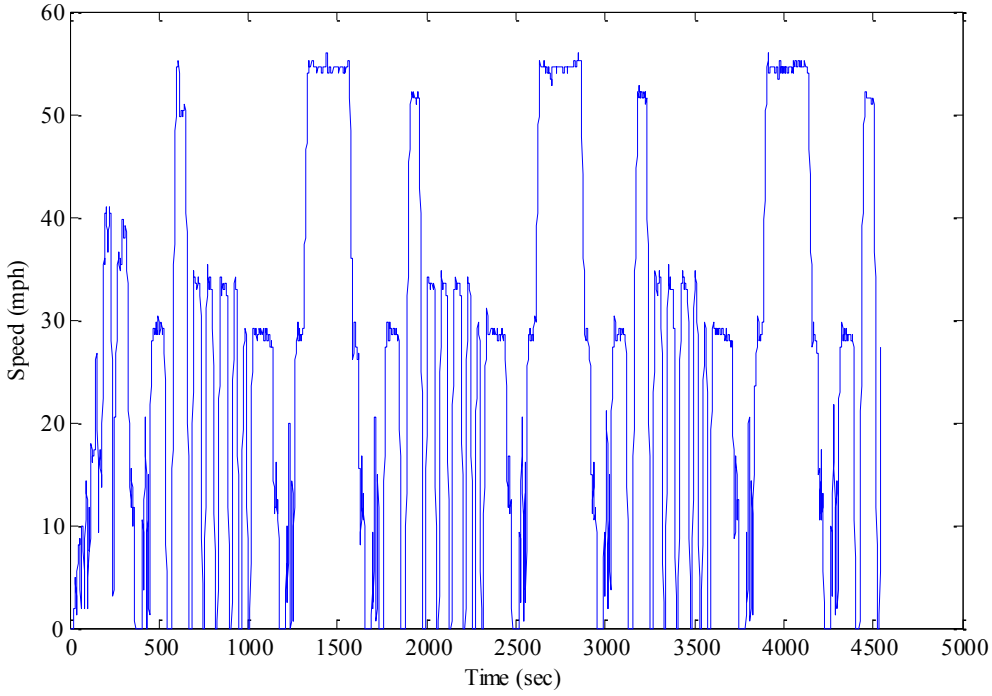

Figure 6.3 Vehicle drive cycle test speed profile

With the major frequency of the battery application identified, the bandwidth of the battery model should be in the same range. Thus the range for the time constants of the RC networks should be chosen as [1/0.02134 s, 1/0.0008799 s], which is [47 s, 1137 s]. The selected time constants determine the bandwidth of the model directly.

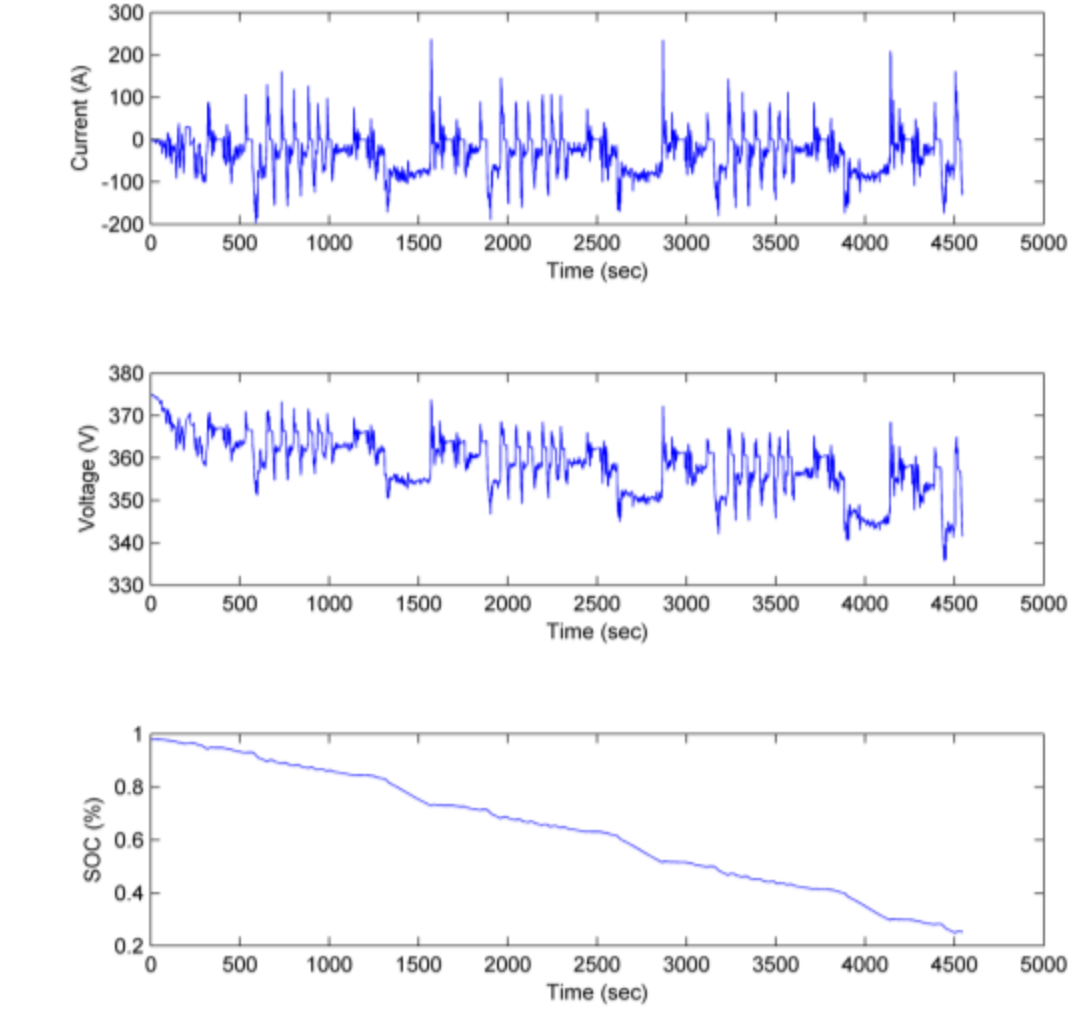

Figure 6.4 A123 battery pack behavior test profile

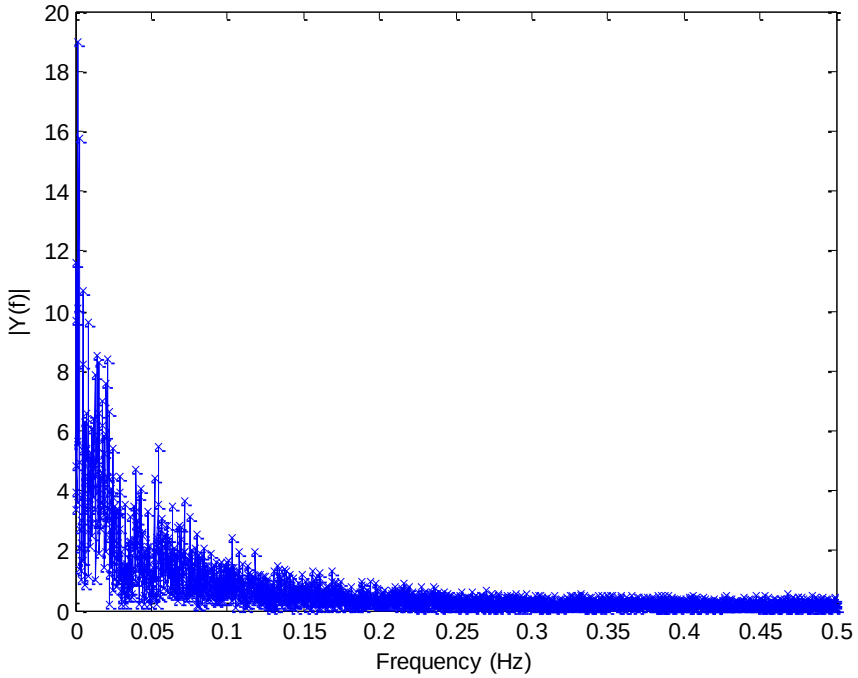

Figure 6.5 Spectral analysis of the battery current: overview

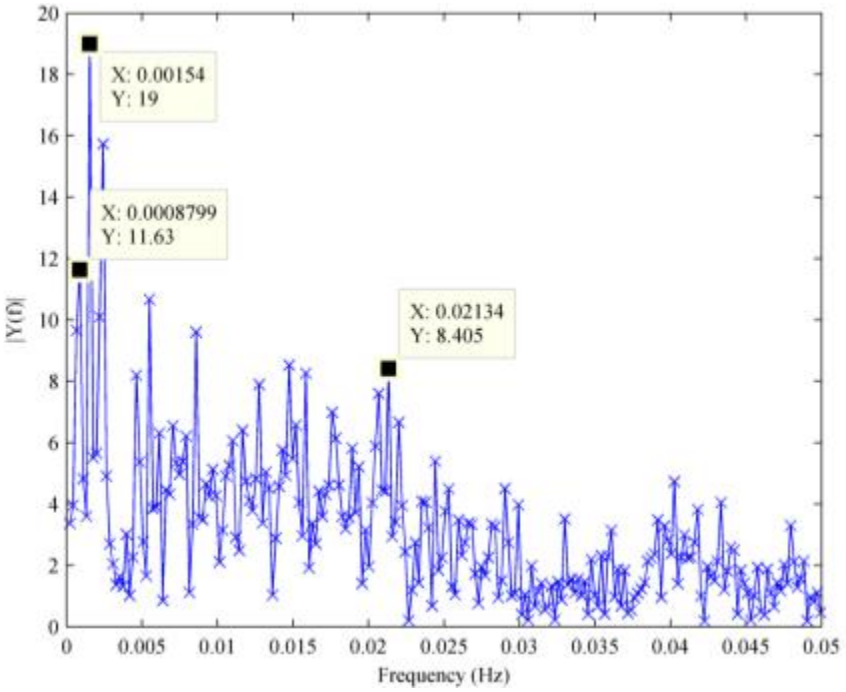

Figure 6.6 Spectral analysis of the battery current: close view

For simplicity and illustration purposes, the number of RC networks is chosen as two; however, this number should increase as the model fidelity requirement increase. In this case, the time constants of the RC networks in the battery model are determined as: $\tau_1 = 47\ s$ and $\tau_2 = 1137\ s$. For example, if a more accurate battery pack model is desired with three RC networks, the third time constant can be chosen as $\tau_3 = 1/0.00154\ s = 649.4\ s$, which locates between τ_1 and τ_2.

6.5.2 SOC - OCV profile extraction

To extract the SOC - OCV profile, an off-vehicle battery pack test has been performed in the laboratory as shown in Fig. 6.7. In this test, the battery pack was discharged from full SOC with pulse discharging, left to rest for 24 hours, and then charged back to full SOC with pulse charging. The discharging and charging pulse length was chosen as 15 min, which would charge/discharge the battery pack by about 10% SOC. At the end of each charging/discharging pulse, the battery was allowed to rest for 1 min for relaxation. With the SOC - OCV profile extraction method described in Chapter IV, the extracted profile was shown in Fig. 6.8. Because of the limited time and resources, no SOC - OCV profile correction step was conducted for the A123 battery pack, where the initially extracted profile was used as the final extracted SOC - OCV profile.

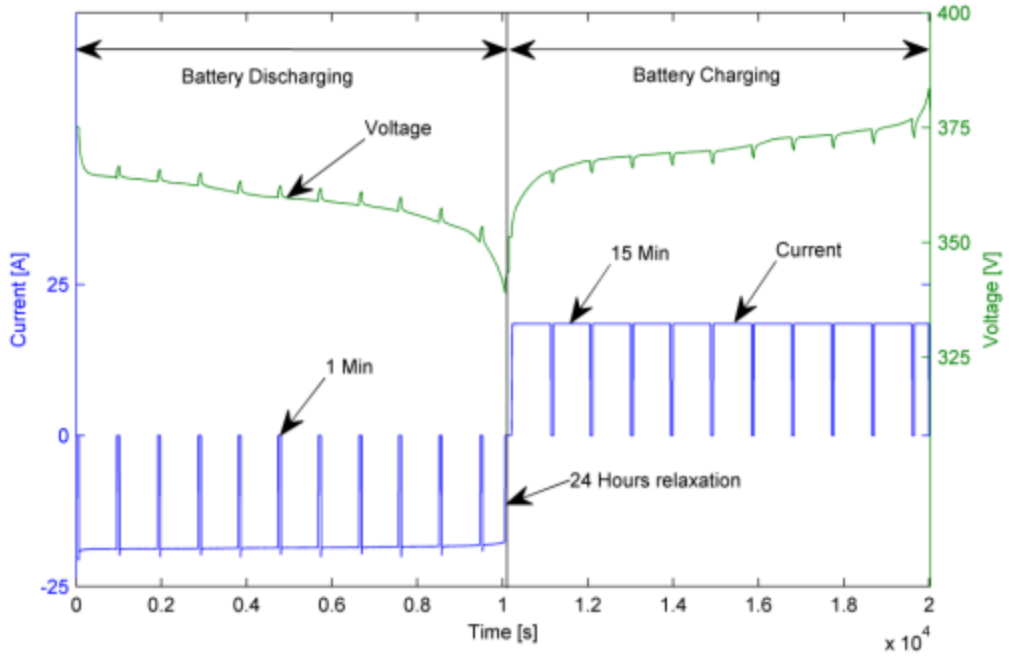

Figure 6.7 A123 battery test for SOC - OCV profile extraction

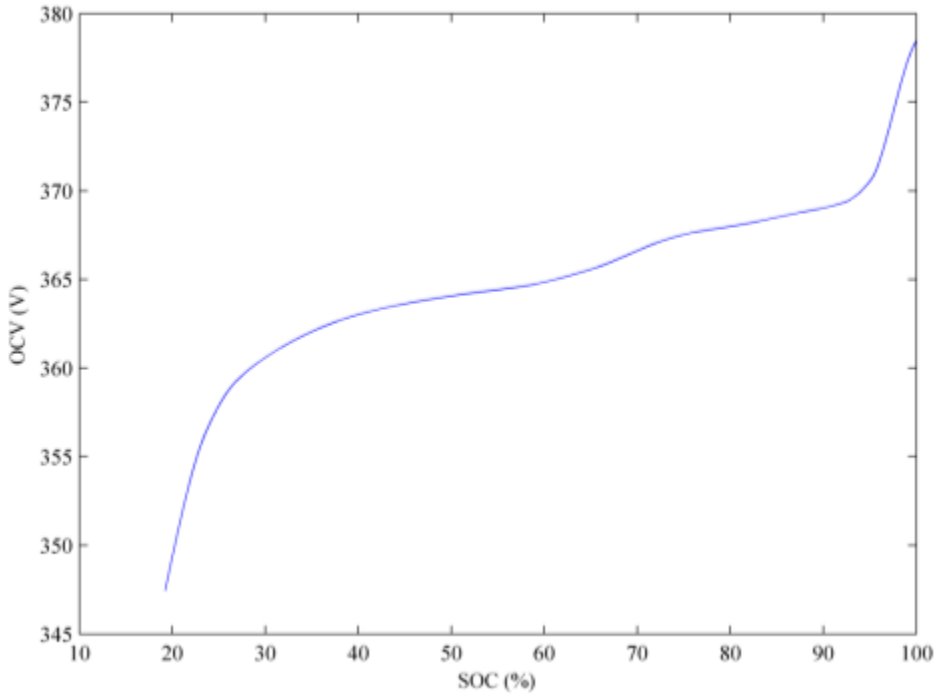

Figure 6.8 Extracted SOC - OCV profile for A123 battery pack

The extracted SOC - OCV profile was made into a lookup table as part of the battery pack simulation model in Matlab/Simulink. In terms of the polynomial representation, the coefficients for the 8th degree polynomial equation are summarized in Table 6.1.

Table 6.1 Coefficients for the polynomial equation

a_8	-1.68E+04
a_7	1.03E+05
a_6	-2.53E+05
a_5	3.37E+05
a_4	-2.66E+05
a_3	1.29E+05
a_2	-3.76E+04
a_1	6.10E+03
a_0	-6.58E+01

(Note: the coefficients are for SOC from 20% to 100%.)

6.5.3 Circuit parameter estimation

Table 6.2 Extracted circuit parameters

R_s (Ω)	R_1 (Ω)	C_1 (kF)	R_2 (Ω)	C_2 (kF)
0.0764	0.0776	0.6053	0.0779	14.5982

The on-vehicle battery pack test data used for bandwidth analysis was used for circuit parameters extraction. During this step, the time constants of the circuit parameters are pre-determined as [47 s, 1137 s]. The extracted parameters are shown in Table 6.2. Figure 6.9 shows the battery pack terminal voltage estimation results with the extracted parameters, with the errors shown in Fig. 6.10. The mean error for the terminal voltage estimation is 0.52 V.

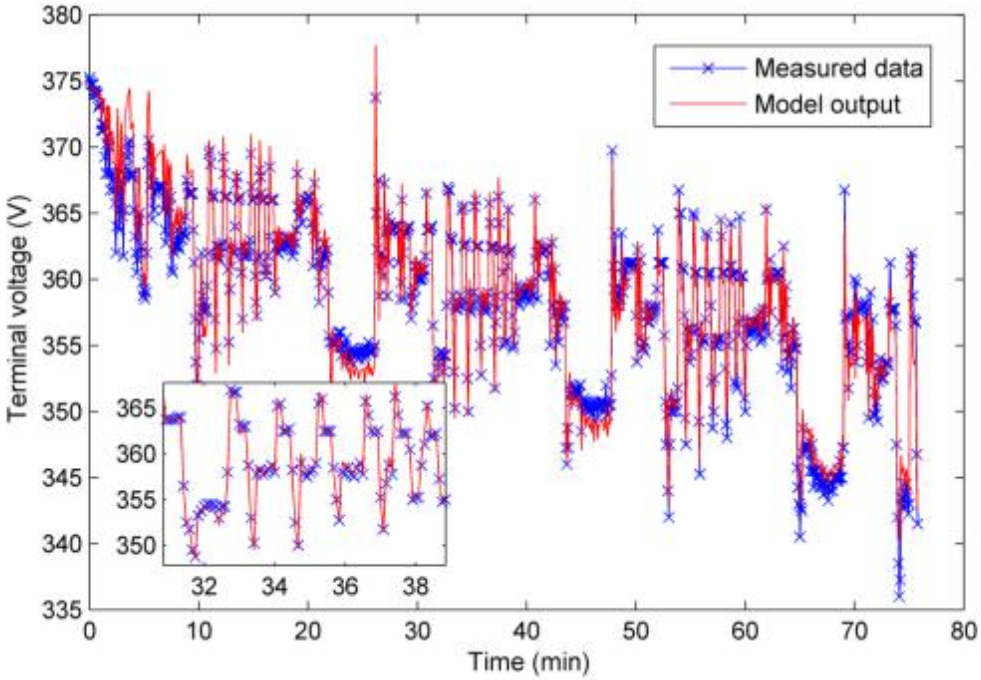

Figure 6.9 Terminal voltage estimation results during behavior test

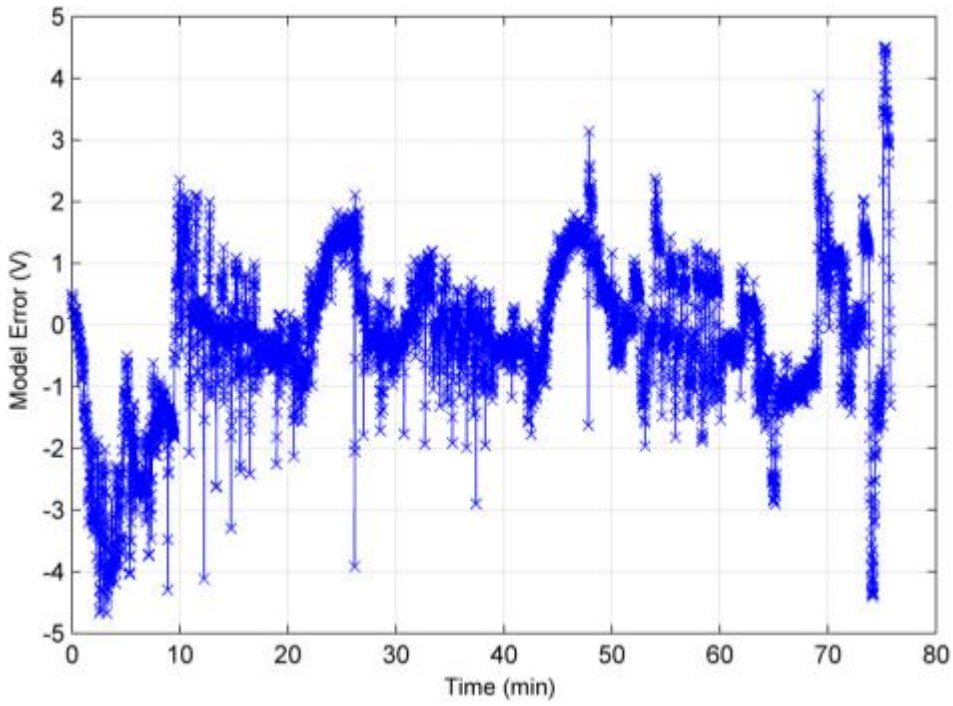

Figure 6.10 Terminal voltage estimation errors during behavior test

The completed electrical analogue battery model was implemented into Matlab/Simulink as shown in Fig. 6.11. This model was integrated into EcoCAR vehicle simulation program as the battery pack sub-system.

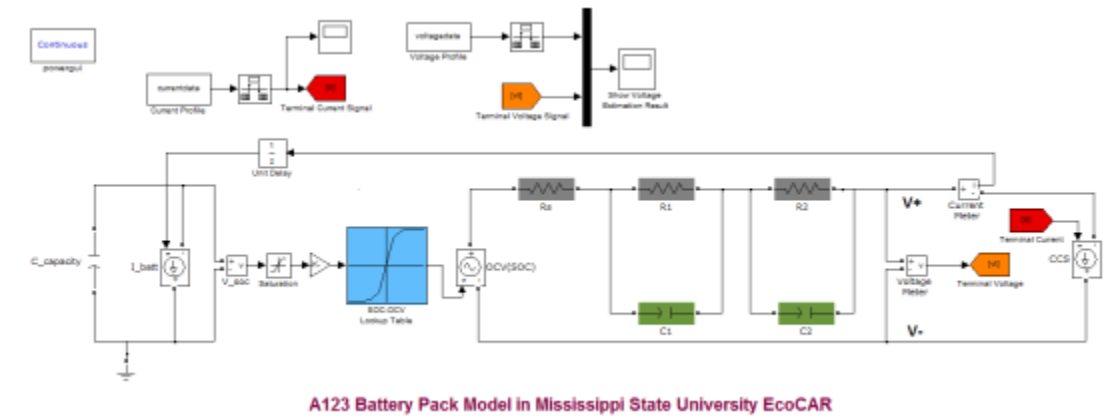

Figure 6.11 A123 battery pack model

6.6 Model verification

The completed battery pack model with the extracted SOC - OCV profile and circuit parameters was verified with a different battery on-vehicle test profile as shown in Fig. 6.12. The acquired battery pack data is shown in Fig. 6.13.

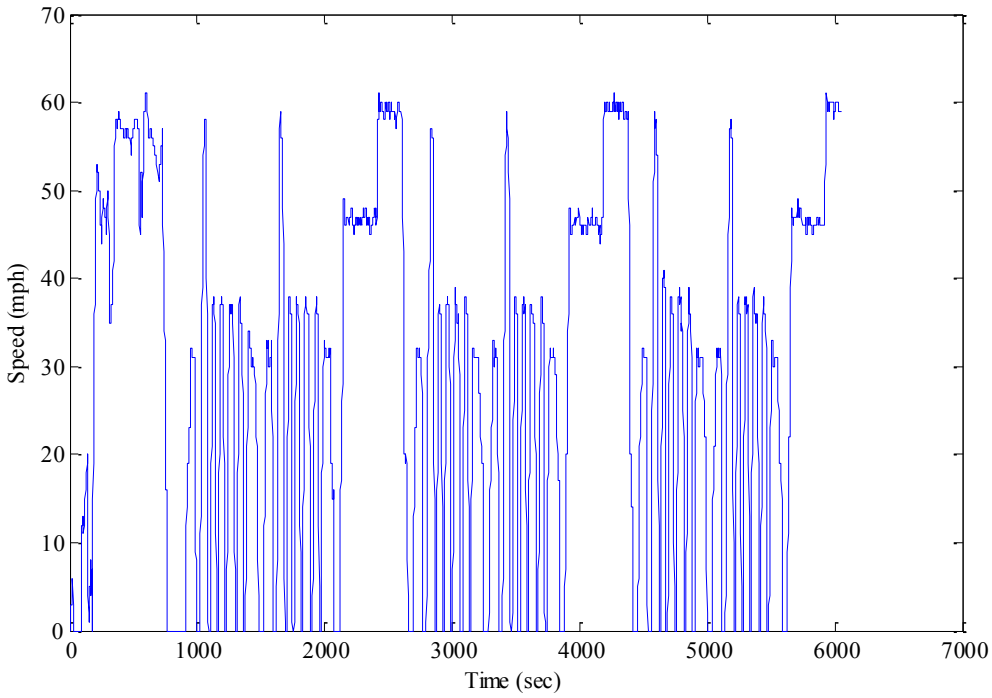

Figure 6.12 Vehicle drive cycle test speed

A spectral analysis of this test current stimulus shows that the new test current has similar bandwidth of [0.0004957 Hz, 0.01702 Hz] with the battery model ([0.0008799 Hz, 0.02134 Hz]). With the measured battery pack terminal current as the input to the battery pack model, the battery terminal voltage estimation results were plotted in Fig. 6.14, with the errors shown in Fig. 6.15. For the estimation results, the mean terminal voltage estimation error is 0.4112 V. 99.87% of the calculated errors were bounded within ±4 V, which was very accurate considering the battery nominal voltage of 360 V. The rated error can be calculated as 1.11% of the nominal battery pack voltage.

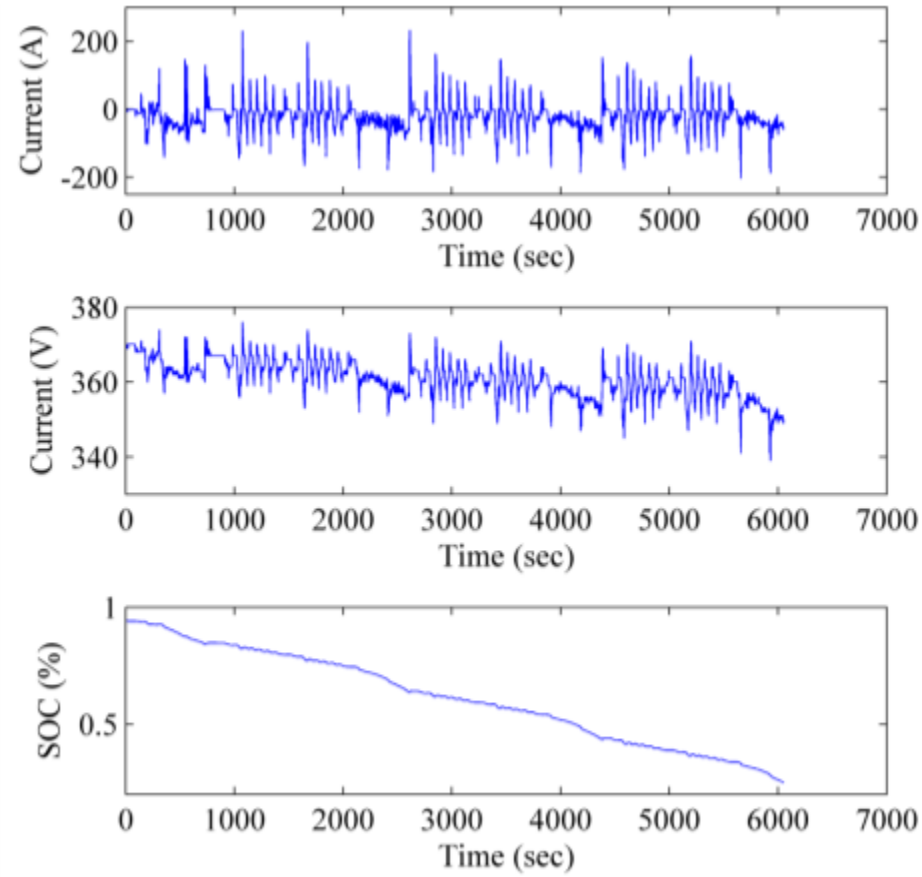

Figure 6.13 A123 battery pack performance test profile

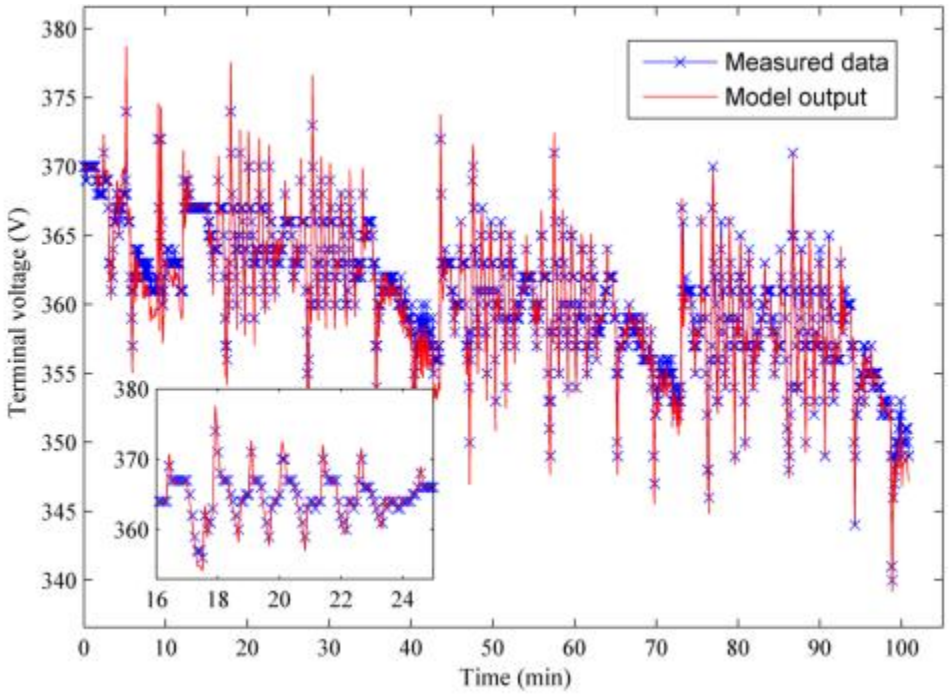

Figure 6.14 Terminal voltage estimation results during performance test

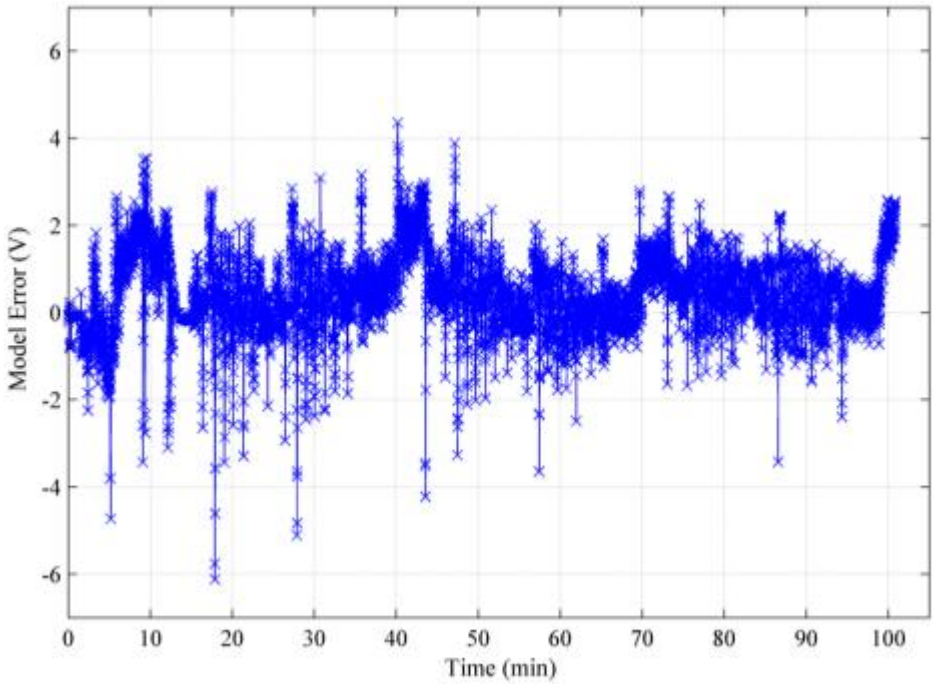

Figure 6.15 Terminal voltage estimation errors during performance test

6.7 Discussion

The application of the proposed battery modeling approach on an A123 battery pack systematically explained the way the proposed approach can be used in real-world automotive applications. We can conclude that the proposed battery modeling approach can be scaled to very large format battery packs, while maintaining the model accuracy at a very low level (less than 1.11% for a 360 V battery pack). We can also observe that even when constant model parameters (i.e., not battery current dependent or SOC dependent) were used in the electrical analogue battery model, high fidelity could be achieved for the model even when there were aggressive current dynamics (up to 237 A). Although some researchers have claimed that the parameters should be battery current dependent or SOC dependent [32-34, 61], the parameters in the electrical analogue battery model can be independent of current and SOC, as a result of behavior modeling of a real-world battery instead of a physical representation.

CHAPTER VII

SCALING THE BATTERY MODEL TO 3-RC MODEL

7.1 Overview

The electrical analogue battery model with 3-RC networks is shown in Fig. 7.1. Compared with the model with the 2-RC network (Fig. 3.2), the only difference is the extra RC network. In this chapter, a newer (compared to the ones used in Chapter V) UBBL10 lithium-ion battery was used for the experimental tests.

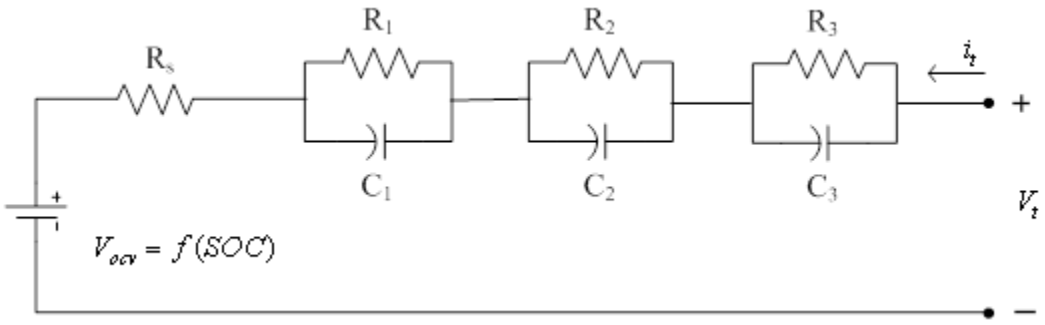

Figure 7.1 The electrical analogue battery model with 3 RC network

The battery SOC - OCV profile extraction was performed exactly as illustrated in chapter IV, but the circuit parameter estimation was done in two ways: the proposed bandwidth based method and the singular value decomposition (SVD) - Prony's method. The results from the two methods were compared. The major difference between the two methods is the way the time constants of the RC networks are defined.

7.2 Model characterization with the proposed method

7.2.1 Model bandwidth

As for the battery model with 2 RC networks the two time constants were pre-determined as 60 s and 2100 s, a third time constants close to the geometric mean of the two time constants was chosen as 350 s. So the time constants for the 3-RC model are: $\tau_1 = 60\ s;\ \tau_2 = 350\ s;\ \tau_3 = 2100\ s$.

7.2.2 SOC - OCV profile extraction

The battery SOC - OCV profile was extracted from battery experimental test as discussed in Chapter IV. The result is an 8th degree polynomial equation correlating battery SOC and OCV as shown in Table 7.1.

Table 7.1 Coefficients for the polynomial equation

a_8	-139.1
a_7	481.664
a_6	-555.94
a_5	123.455
a_4	230.917
a_3	-185.97
a_2	50.1971
a_1	-2.5346
a_0	13.872

7.2.3 Circuit parameter estimation

A fully scalable parameter estimation program has been coded based on the parameter estimation algorithm discussed in Chapter III. The program can be used to scale the battery model to any number of RC networks (the number is set to be 3 in this case). Besides SQP, generic algorithm (GA) has also been implemented into the program

for the parameter estimation. The SQP algorithm has been implemented in the program with parallel computing for fast computation of the parameters.

The behavior battery test current profile is shown in Fig. 7.2. With the time constants pre-determined, the circuit parameters were estimated as Table 7.2 with SQP, and Table 7.3 with GA.

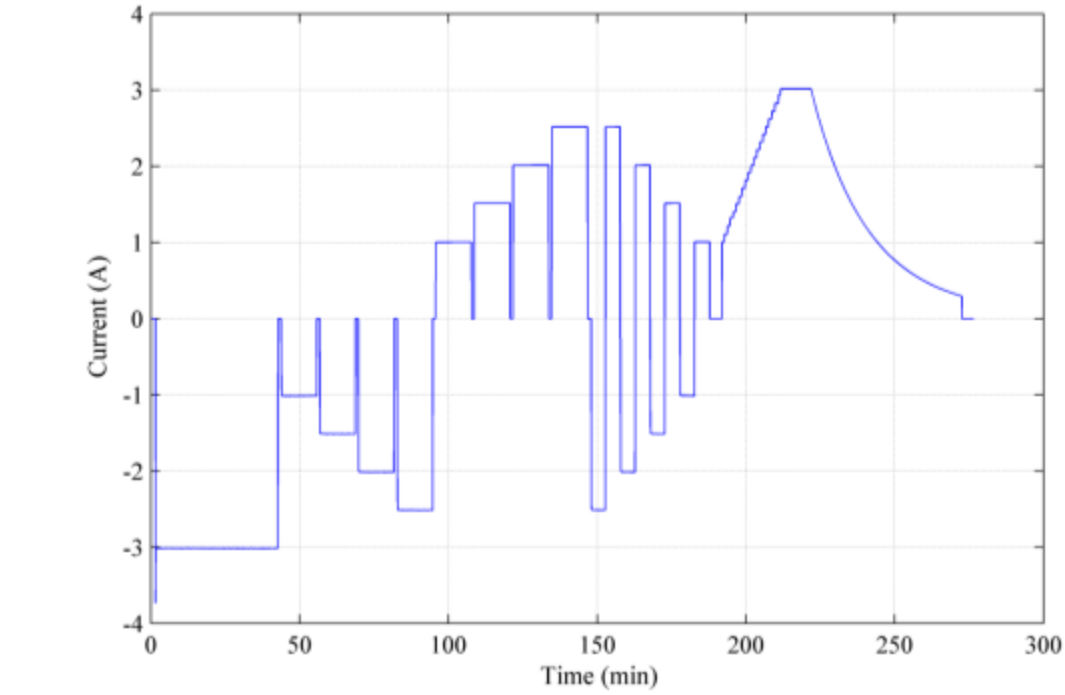

Figure 7.2 Battery behavior test for parameter estimation

Table 7.2 Circuit parameters estimated with SQP

R_s (Ω)	R_1 (Ω)	C_1 (kF)	R_2 (Ω)	C_2 (kF)	R_3 (Ω)	C_3 (kF)
0.1483	0.0216	2.7830	0.0165	21.2570	0.0309	68.0322

Table 7.3 Circuit parameters estimated with GA

R_s (Ω)	R_1 (Ω)	C_1 (kF)	R_2 (Ω)	C_2 (kF)	R_3 (Ω)	C_3 (kF)
0.1386	0.0385	1.5587	0.0014	253.5401	0.0430	48.8872

7.3 Model characterization with SVD-Prony's method

7.3.1 The SVD-Prony's method

With SVD-Prony's method [59, 60, 86-89], the nonlinear battery transient data was approximated by an exponential expression in the form of

$$f(x) \approx A_0 + A_1 e^{-\lambda_1 x} + A_2 e^{-\lambda_2 x} + \ldots + A_n e^{-\lambda_n x} \tag{7.1}$$

Equation (7.1) includes a constant A_0 (the baseline) and n number of exponential. The task of the exponential analysis is to determine the ideal number of the term of exponentials and further identify the parameters of the exponential terms. Although the nonlinear battery transient response cannot be exactly expressed by the exponential expression (7.1), the best reasonably fit of the data is searched. The data being used is a set of sampled data points of battery terminal voltage during the rest period after a pulse discharge. The battery OCV is constant during this period, thus A_0 is constant. Figure 7.3 shows the battery transient response data. The sampling frequency is 1 Hz.

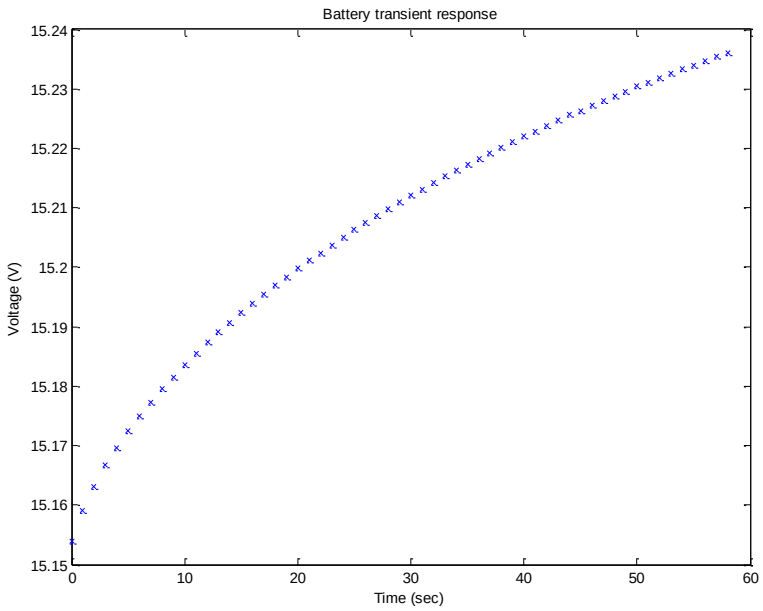

Figure 7.3 Battery transient response

7.3.1.1 Determine the number of exponential terms by SVD

The SVD algorithm described in [87] is very robust even with nonlinear data set. A criterion for the least acceptable singular value of a well-designed data matrix is defined and a recursive algorithm has been developed to identify the ideal number of exponential terms for either exponential data or non-exponential data. And this algorithm does not require subtraction of baseline. For detailed algorithm please refer to [87].

7.3.1.2 Identify the exponential parameters using nonlinear least square Prony's method

The original Prony's method for exponential analysis cannot handle multi-exponentials with the baseline included, which require the elimination of the baseline prior to applying the Prony's method. An assumption for subtracting the baseline is that the tail of the decay (for both mono-exponential and multi-exponential) can be approximated by a single exponential of the form:

$$f(t) = A_0 + A_1 \exp(-\lambda_1 t) \tag{7.2}$$

A three-point method [60] was adopted to extract the baseline based on (7.3):

$$\begin{aligned} Y_1 &= A_0 + A_1 \exp(-\lambda_1 t_0) \\ Y_2 &= A_0 + A_1 \exp[-\lambda_1 (t_0 + t_1)] \\ Y_3 &= A_0 + A_1 \exp[-\lambda_1 (t_0 + 2t_1)] \\ A_0 &= (Y_1 Y_3 - Y_2^{\,2}) / (Y_1 + Y_3 - 2Y_2) \end{aligned} \tag{7.3}$$

Since only three data points are needed for the extraction of A_0, the 3 points are chosen as the first point, the one in the middle, and the last data point from the battery test data.

The original Prony's method is a computationally efficient yet accurate way of identifying exponential moments in multi-exponential terms.

By taking $\mu_i = e^{-\lambda_i}$, equation (7.1) changed into the form of (7.4)

$$f(x) \approx A_0 + A_1\mu_1^{\,x} + A_2\mu_2^{\,x} + \ldots + A_n\mu_n^{\,x} \tag{7.4}$$

The data points need to be evenly spaced to be used by Prony's method. Let x= 0, 1, 2…N-1, where N is the number of sampled data points. Based on the N sampled data points, a set of equations could be formed into (7.5) [86]:

$$\begin{aligned} &A_1 + A_2 + \ldots + A_n = f_0 \\ &A_1\mu_1 + A_2\mu_2 + \ldots + A_n\mu_n = f_1 \\ &A_1\mu_1^{\,2} + A_2\mu_2^{\,2} + \ldots + A_n\mu_n^{\,2} = f_2 \\ &\bullet\ \bullet\ \bullet\ \bullet\ \bullet\ \bullet \\ &A_1\mu_1^{\,N-1} + A_2\mu_2^{\,N-1} + \ldots + A_n\mu_n^{\,N-1} = f_{N-1} \end{aligned} \tag{7.5}$$

The original Prony's method uses only 2*n (n is the number of exponential terms) data points to identify the parameters. A modified Prony's method [86] with nonlinear least square (NLS) algorithm was used to take advantage of more sampled data points. Now with the NLS Prony's method, all data points can be used for the identification of the exponential parameters.

7.3.2 SOC-OCV profile extraction

Since the SVD-Prony's method is only for the circuit parameter estimation, the SOC - OCV profile from Section 7.22 was used.

7.3.3 Circuit parameter estimation

The rate window from the battery behavior test is defined in Fig. 7.4, which includes two parts: a discharge pulse (part one) and a rest period (part two). Since in part one, the battery OCV was changing with discharge current, this part cannot be analyzed by SVD-Prony's method because of the time varying constant in (7.1) [60]. A time constant of 2100 s has been assigned to the RC network to take care of the long transient period in part one. Part two with constant OCV was analyzed by SVD-Prony's method, where two exponential terms has been identified for this part. The time constants for the

two RC networks (exponential terms) are identified as 2.1 s and 38.3 s. So the three time constants for the battery model are: $\tau_1 = 2.1\ s;\ \tau_2 = 38.3\ s;\ \tau_3 = 2100\ s$.

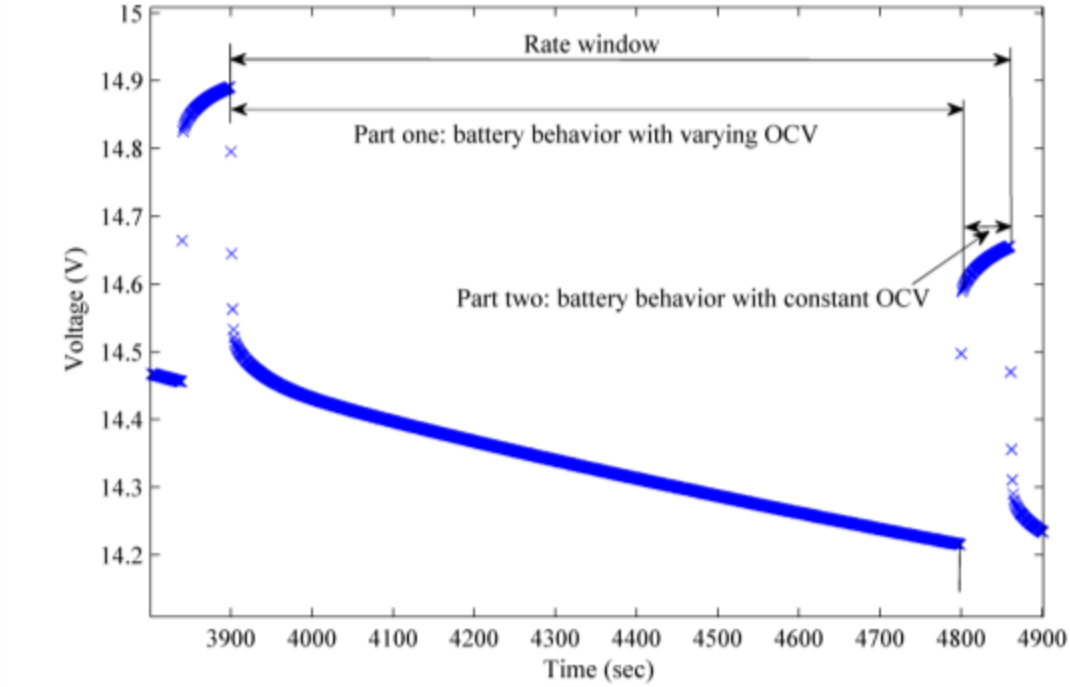

Figure 7.4 Rate window for parameter estimation

With the time constants defined above, the circuit parameters were estimated with SQP and GA based on the behavior battery test profile in Fig. 7.2. Table 7.4 shows the estimated parameters with SQP and Table 7.5 shows the estimated parameters with GA.

Table 7.4 Estimated parameters with SQP

R_s (Ω)	R_1 (Ω)	C_1 (kF)	R_2 (Ω)	C_2 (kF)	R_3 (Ω)	C_3 (kF)
0.1325	0.0076	0.2776	0.0371	1.0331	0.0440	47.6980

Table 7.5 Estimated parameters with GA

R_s (Ω)	R_1 (Ω)	C_1 (kF)	R_2 (Ω)	C_2 (kF)	R_3 (Ω)	C_3 (kF)
0.0735	0.0563	0.0373	0.0478	0.8011	0.0435	48.2830

7.4 Results comparison and discussion

A performance battery test was conducted to verify the battery models with the parameters in Table 7.2, 7.3, 7.4, and 7.5. The performance test current profile is shown in Fig. 7.5. The battery terminal voltage estimation results are compared with the measured battery terminal voltage, as shown in Fig. 7.6, 7.7, 7.8 and 7.9, respectively.

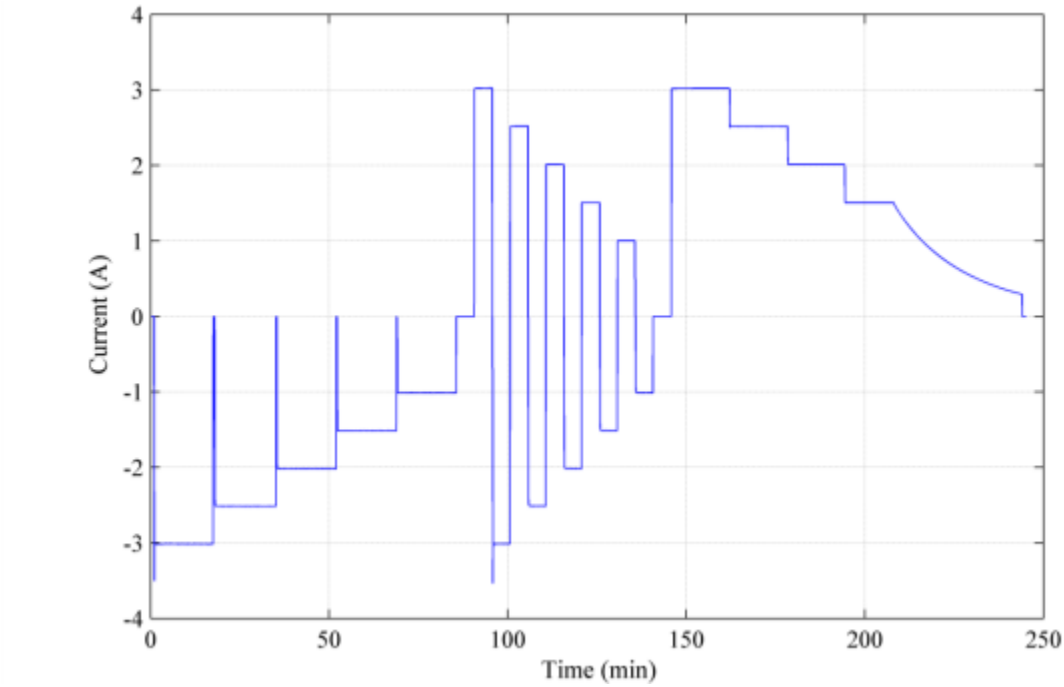

Figure 7.5 Performance test current

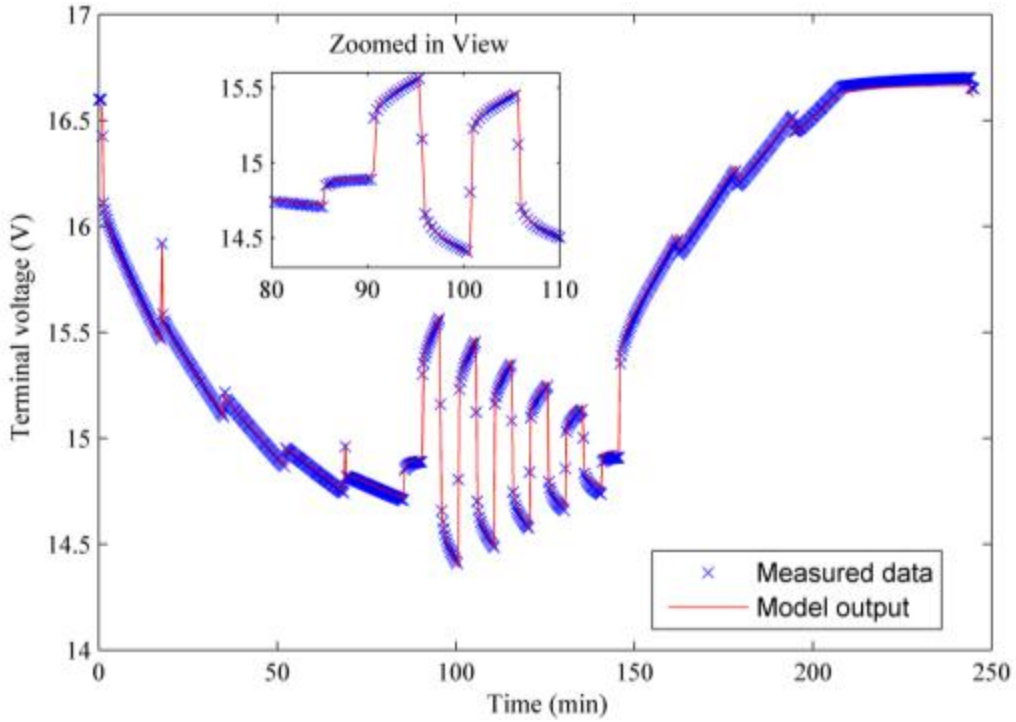

Figure 7.6 Terminal voltage estimation - proposed method with SQP

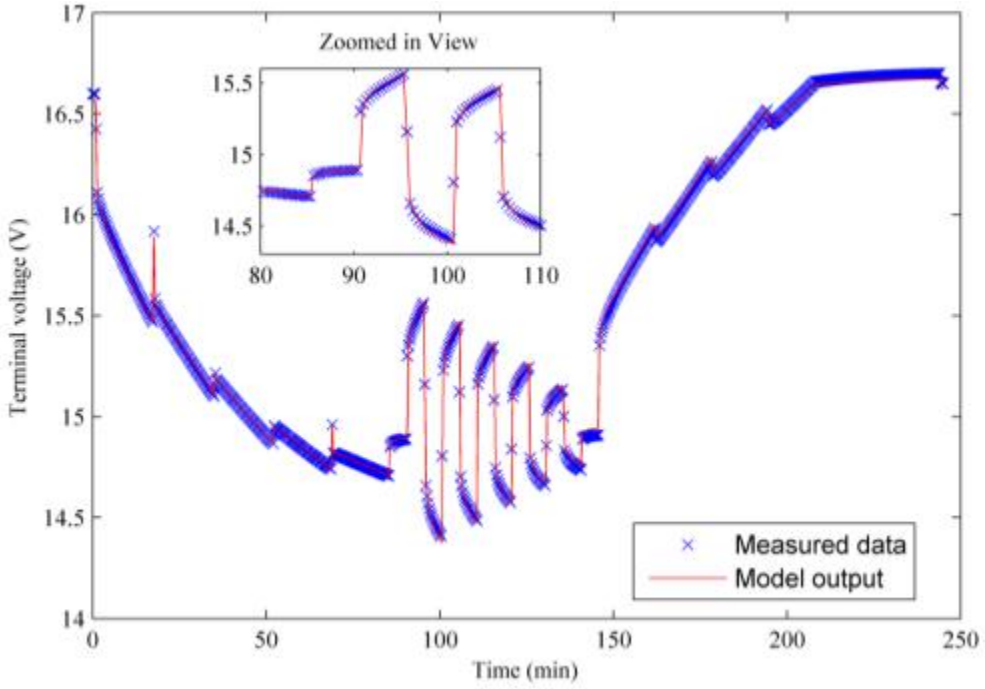

Figure 7.7 Terminal voltage estimation - proposed method with GA

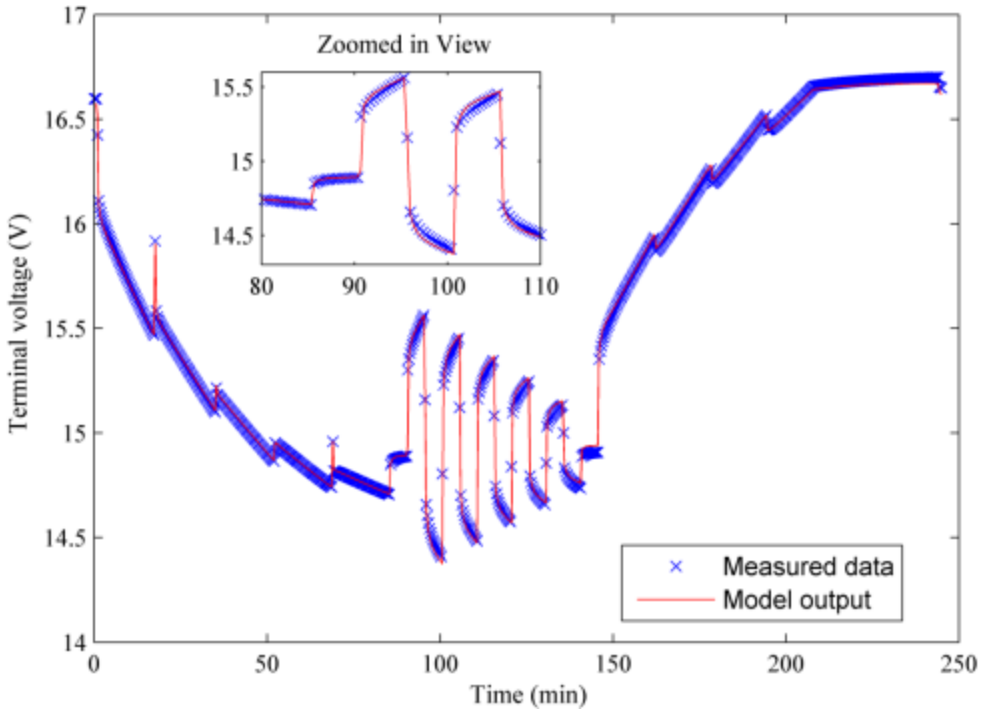

Figure 7.8 Terminal voltage estimation - SVD Prony with SQP

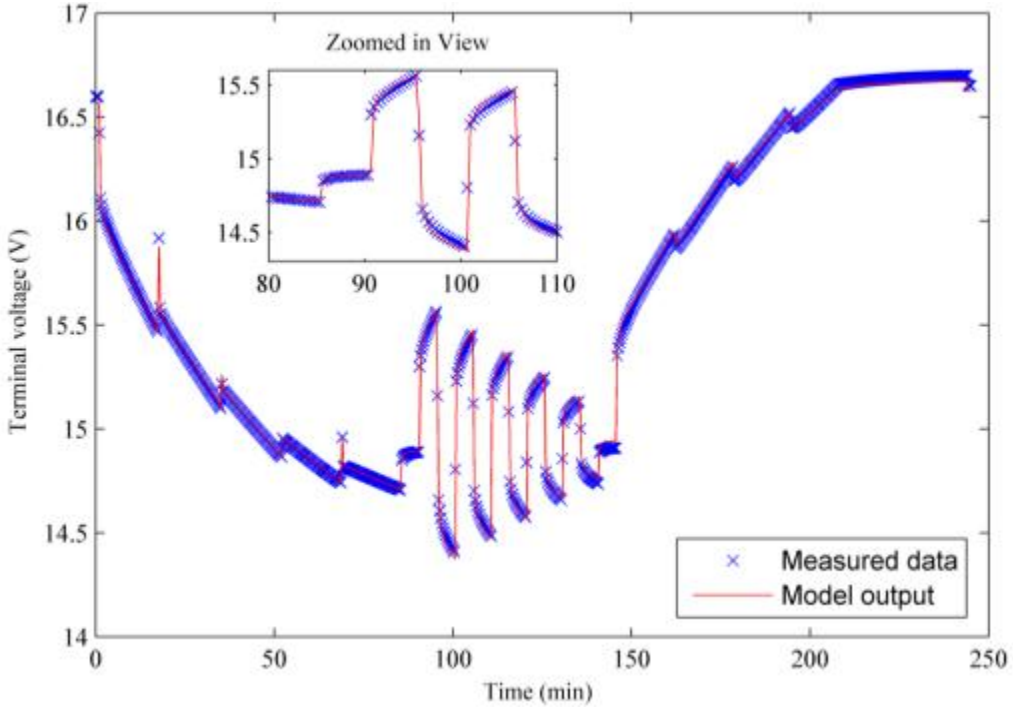

Figure 7.9 Terminal voltage estimation - SVD Prony with GA

The statistical errors of the battery model with four sets of parameters are summarized as Table 7.6.

Table 7.6 Statistical errors of the battery model with 3 RC network

Methods	SVD Prony		Proposed Method	
	GA	SQP	GA	SQP
Mean Square Error (1E-4V^2)	4.17	3.69	2.99	4.40
Mean Error (mV)	2.64	2.57	2.69	4.22
Max Error (mV)	47.01	50.50	34.10	54.10
Rated Error (%)	0.33	0.35	0.24	0.38

For the battery model with 3-RC, the proposed method with generic algorithm provides the best accuracy when tested with the performance battery test. The model accuracies with parameters estimated from other methods are at the same level. The extra accuracy with the "proposed method + GA" comes from the pre-determination of the battery model time constants, rather than seeking the natural time constants with the SVD Prony's method.

Comparing GA and SQP, GA is very slow in computation, which takes two - three days for parameter estimation, but it is not sensitive to the initial value of the parameters because GA does not take initial values. SQP on the other hand, is much faster than GA, which takes about 2 hours with parallel computing enabled (four computer cores), but is sensitive to the initial values of the parameters. In general, although slower, GA is more likely to find the global optimum for the parameter estimation problem than SQP.

As a conclusion, the electrical analogue battery model can be successfully scaled to 3-RC network model in two ways: the proposed method and the SVD Prony's method.

However, the SVD Prony's method cannot work independently, as it suffers from the baseline problem which had to be overcome by assigning the third RC time constant. Increased accuracy was observed for the 3-RC model over that of the 2-RC model as a result of the increased order of approximation.

CHAPTER VIII

ON-LINE BATTERY SOC ESTIMATION

8.1 Overview

In this chapter, the electrical analogue battery model was used on-line for battery SOC estimation with Gauss-Hermite quadrature filter (GHQF), extended Kalman filter (EKF), and unscented Kalman filter (UKF). The SOC estimation results from the three filters were compared. Results show the GHQF excels among the commonly used filters when used with the high fidelity electrical analogue battery model [90].

Battery SOC estimation is a key issue for a battery management system (BMS), especially with the rapid development and commercialization of HEVs and PHEVs [21, 24, 25, 57, 58]. Accurate SOC estimation is crucial to determine the optimal operation mode of the PHEV or HEV, so that the best overall performance can be achieved. Compared with the batteries in low power applications, i.e., laptops or cell phones, batteries in high power applications encounter faster dynamics and more cycles of charging/discharging until the battery SOC can be recalibrated [23, 58, 91]. Therefore, it is more difficult to get an accurate SOC estimation in high power applications.

An on-line SOC estimation model runs simultaneously with the actual physical battery system, taking measurements such as terminal voltage and current as inputs to estimate the internal state variable—SOC. In [57] it is claimed that an accurate battery model is not necessary, the inaccuracy of which can be compensated by the observer, however, the reported SOC estimation error is up to 3% in [57], which is only at the

acceptable level. In other reported works, filters built on more accurate battery models can give SOC estimation with less than 2% error [22, 23, 92]. Thus accurate battery models are still essential for a filter used as an observer to work with less error. In this work, the battery model that the filter is built upon is the high fidelity open loop electrical analogue battery model described in Chapter II.

Several SOC estimation algorithms are available in the literature, including [91] discharge test, coulomb-counting, measurement of electrolytes physical properties, open circuit voltage, internal resistance, Kalman filters, etc. Among the above approaches, coulomb-counting and Kalman filters are the most commonly used methods [57, 58, 91]. Coulomb-counting method is open loop based and easy to configure, but it has several drawbacks [23, 58, 91]. To begin, the initial battery SOC needs to be known or estimated. The error included in the initial SOC value will shift the whole SOC estimation results with a bias. Secondly, current loss is not taken into account and thus increases the model inaccuracy, because in reality not all measured current accumulates stored or discharged accessible chemical energy. Thirdly, battery capacity is assumed to be constant. However, actual battery capacity decreases as the battery becomes aged. Finally, there is measurement noise that is accumulated during battery operation. Based on the above drawbacks, a closed loop SOC estimation algorithm is necessary to compensate the open loop SOC estimation errors.

8.2 Mathematical description of the battery model

The electrical analogue battery model with 2 RC networks was redrawn here as Fig. 8.1.

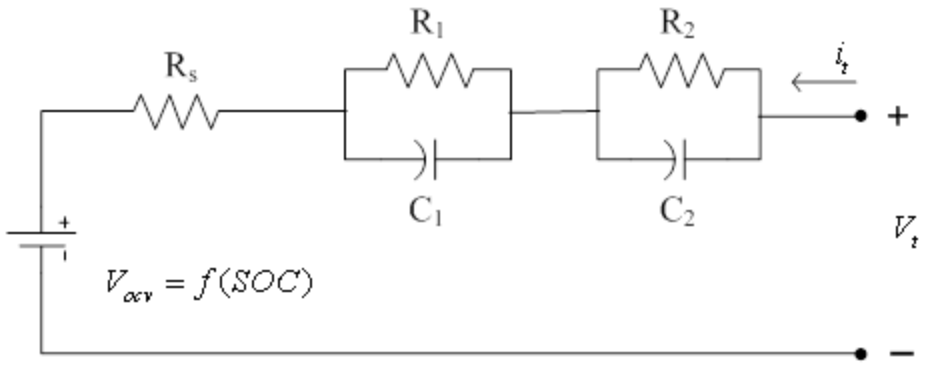

Figure 8.1 The electrical analogue battery model with 2 RC networks

Based on Kirchhoff's current law and voltage law, a discrete time mathematical description of the electrical analogue battery model is derived as (8.1) and (8.2).

$$\begin{bmatrix} V_{c1,k} \\ V_{c2,k} \\ SOC_k \end{bmatrix} = \begin{bmatrix} -\frac{\Delta t}{R_1 C_1} & 0 & 0 \\ 0 & -\frac{\Delta t}{R_2 C_2} & 0 \\ 0 & 0 & 0 \end{bmatrix} \begin{bmatrix} V_{c1,k-1} \\ V_{c2,k-1} \\ SOC_{k-1} \end{bmatrix} + \begin{bmatrix} \frac{1}{C_1} \\ \frac{1}{C_2} \\ \frac{1}{C} \end{bmatrix} i_{k-1}\Delta t + \mathbf{v}_{k-1} \tag{8.1}$$

where the state variables $V_{c1,k-1}$, $V_{c2,k-1}$, and SOC_k are capacitor C_1 voltage, capacitor C_2 voltage, and battery SOC, respectively. R_s, R_1, C_1, R_2, and C_2 are model parameters which need to be identified prior to using this model. Constant C represents battery capacity. Input i_{k-1} is the current at time instant $k-1$. Parameter $\mathbf{v}_{k-1}$ is white Gaussian noise with zero mean value and covariance $\mathbf{Q}$. The sampling interval is Δt.

$$V_k = V_{ocv,k}(SOC_k) + R_s i_{k-1} + V_{c1,k} + V_{c2,k} + \mathbf{n}_k \tag{8.2}$$

where $\mathbf{n}_k$ is the measurement noise which is assumed to be white Gaussian noise with zero mean value and covariance $\mathbf{R}$.

The mapping of OCV on SOC is reflected by (8.3), where $f(SOC)$ is an eighth order polynomial equation in SOC.

$$V_{ocv,k} = f(SOC_k) \tag{8.3}$$

8.3 A review of Gaussian approximation filters

In this section, two kinds of Gaussian approximation filter: the extended Kalman filter and quadrature based Gaussian approximation filters are briefly reviewed. Consider a class of nonlinear discrete-time dynamical systems and the measurement equation described by:

$$\mathbf{x}_k = \boldsymbol{f}(\mathbf{x}_{k-1}) + \mathbf{v}_{k-1} \tag{8.4}$$
$$\mathbf{y}_k = \boldsymbol{h}(\mathbf{x}_k) + \mathbf{n}_k \tag{8.5}$$

where $\mathbf{x}_k \in \mathbf{R}^n$; $\mathbf{y}_k \in \mathbf{R}^m$, $\mathbf{v}_k$ and $\mathbf{n}_k$ are independent white Gaussian process noise and measurement noise with covariance $\mathbf{Q}_{k-1}$ and $\mathbf{R}_k$, respectively.

8.3.1 Extended Kalman filter

Given the initial estimate state $\hat{\mathbf{x}}_0$ and covariance $\mathbf{P}_0$, the estimation of states can be obtained by the famous EKF.

Prediction:

$$\hat{\mathbf{x}}_{k|k-1} = \boldsymbol{f}(\hat{\mathbf{x}}_{k-1|k-1}) \tag{8.6}$$
$$\mathbf{P}_{k|k-1} = \mathbf{F}_{k-1}\mathbf{P}_{k-1|k-1}\mathbf{F}_{k-1}^T + \mathbf{Q}_{k-1} \tag{8.7}$$

where $\mathbf{F}_{k-1}$ is the Jacobian matrix of $\boldsymbol{f}$ evaluated at $\hat{\mathbf{x}}_{k-1|k-1}$.

Update:

$$\mathbf{K}_k = \mathbf{P}_{k|k-1}\mathbf{H}_k^T\left(\mathbf{H}_k\mathbf{P}_{k|k-1}\mathbf{H}_k^T + \mathbf{R}_k\right) \tag{8.8}$$
$$\hat{\mathbf{x}}_{k|k} = \hat{\mathbf{x}}_{k|k-1} + \mathbf{K}_k(\mathbf{y}_k - \boldsymbol{h}(\hat{\mathbf{x}}_{k|k-1})) \tag{8.9}$$
$$\mathbf{P}_{k|k} = \left(\mathbf{I} - \mathbf{K}_k\mathbf{H}_k\right)\mathbf{P}_{k|k-1} \tag{8.10}$$

where $\mathbf{H}_k$ and $\mathbf{K}_k$ are the Jacobian matrix of $\boldsymbol{h}$ evaluated at $\hat{\mathbf{x}}_{k|k-1}$ and the Kalman gain at time k, respectively.

8.3.2 Quadrature based Gaussian approximation filters

Assuming that the probability density function (PDF) of the states is Gaussian, the Gaussian approximation filters can be obtained as follows [93-95]. Note that only the mean and covariance need to be calculated.

Prediction:

$$\hat{\mathbf{x}}_{k|k-1} = \sum_{i=1}^{N_p} W_i \boldsymbol{f}(\boldsymbol{\xi}_i) \tag{8.11}$$

$$\mathbf{P}_{k|k-1} = \sum_{i=1}^{N_p} W_i \left(\boldsymbol{f}\left(\boldsymbol{\xi}_i\right) - \hat{\mathbf{x}}_{k|k-1} \right)\left(\boldsymbol{f}\left(\boldsymbol{\xi}_i\right) - \hat{\mathbf{x}}_{k|k-1} \right)^T + \mathbf{Q}_{k-1} \tag{8.12}$$

where N_p is the total number of points, W_i is the point weight, and $\boldsymbol{\xi}_i$ is the transformed point obtained from the covariance decomposition, i.e.

$$\mathbf{P}_{k-1|k-1} = \mathbf{S}\mathbf{S}^T \tag{8.13}$$

$$\boldsymbol{\xi}_i = \mathbf{S}\boldsymbol{\gamma}_i + \hat{\mathbf{x}}_{k-1|k-1} \tag{8.14}$$

where $\boldsymbol{\gamma}_i$ is the quadrature point for $N(\mathbf{x};\ \mathbf{0};\ \mathbf{I}_n)$ with n as the state dimension.

Update:

$$\hat{\mathbf{x}}_{k|k} = \hat{\mathbf{x}}_{k|k-1} + \mathbf{L}_k \left(\mathbf{y}_k - \mathbf{z}_k \right) \tag{8.15}$$

$$\mathbf{P}_{k|k} = \mathbf{P}_{k|k-1} - \mathbf{L}_k \mathbf{P}_{xz}^T \tag{8.16}$$

where

$$\mathbf{L}_k = \mathbf{P}_{xz} \left(\mathbf{R}_k + \mathbf{P}_{zz} \right)^{-1} \tag{8.17}$$

$$\mathbf{z}_k = \sum_{i=1}^{N_p} W_i \boldsymbol{h}\left(\tilde{\boldsymbol{\xi}}_i \right) \tag{8.18}$$

$$\mathbf{P}_{xz} = \sum_{i=1}^{N_p} W_i \left(\tilde{\boldsymbol{\xi}}_i - \hat{\mathbf{x}}_{k|k-1} \right)\left(\boldsymbol{h}\left(\tilde{\boldsymbol{\xi}}_i \right) - \mathbf{z}_k \right)^T \tag{8.19}$$

$$\mathbf{P}_{zz} = \sum_{i=1}^{N_p} W_i \left(\boldsymbol{h}\left(\tilde{\boldsymbol{\xi}}_i \right) - \mathbf{z}_k \right)\left(\boldsymbol{h}\left(\tilde{\boldsymbol{\xi}}_i \right) - \mathbf{z}_k \right)^T \tag{8.20}$$

where $\tilde{\boldsymbol{\xi}}_i$ is the transformed point obtained from the decomposition of the predicted covariance, i.e.

$$\mathbf{P}_{k|k-1} = \tilde{\mathbf{S}}\tilde{\mathbf{S}}^T \tag{8.21}$$

$$\tilde{\boldsymbol{\xi}}_i = \tilde{\mathbf{S}}\boldsymbol{\gamma}_i + \hat{\mathbf{x}}_{k|k-1} \tag{8.22}$$

Note that $\boldsymbol{\gamma}_i$ and W_i can be chosen according to the Gauss-Hermite quadrature (GHQ) rule [93, 94], the Unscented Transformation (UT) [95].

For convenience, the points and weights for UT are given as follows.

For the UT with $2n+1$ points [95], $\boldsymbol{\gamma}_i$ and W_i are given by

$$\begin{cases} \boldsymbol{\gamma}_1 = [0,0,\cdots 0,0]^T; & W_1 = \dfrac{2\kappa}{2(n+\kappa)} \\ \boldsymbol{\gamma}_i = \sqrt{n+\kappa}\,\mathbf{e}_{i-1}; & W_i = \dfrac{1}{2(n+\kappa)}, \quad 2 \le i \le n+1 \\ \boldsymbol{\gamma}_i = -\sqrt{n+\kappa}\,\mathbf{e}_{i-n-1}; & W_i = \dfrac{1}{2(n+\kappa)}, \quad n+2 \le i \le 2n+1 \end{cases} \tag{8.23}$$

where $\mathbf{e}_{i-1}$ is the unit vector in $\mathbf{R}^n$ with the (i-1)th element being 1 and κ is a tuning parameter with the suggested optimal value $\kappa = 3-n$ for Gaussian distributions [95]. It is exact for all polynomials of the form $x_1^{i_1} x_2^{i_2} \cdots x_n^{i_n}$ with $1 \le i_1 + \cdots + i_n \le 3$ [94].

For the univariate GHQ rule with m quadrature points, $\boldsymbol{\gamma}_i$ and W_i can be calculated as follows [93]. If $m=1$, then $\boldsymbol{\gamma}_1 = 0$ and $W_1 = 1$. If $m>1$, first construct a symmetric tri-diagonal matrix J with zero diagonal elements and $J_{i,i+1} = J_{i+1,i} = \sqrt{i/2}$, $1 \le i \le m-1$. Then the quadrature point $\boldsymbol{\gamma}_i$ is calculated by $\boldsymbol{\gamma}_i = \sqrt{2}\boldsymbol{\varepsilon}_i$, where $\boldsymbol{\varepsilon}_i$ is the ith eigenvalue of J. The corresponding W_i is calculated by $W_i = (\mathbf{v}_i)_1^2$ where $(\mathbf{v}_i)_1$ is the first element of the ith normalized eigenvector of J. The univariate GHQ rule with m points is exact up to the $(2m-1)$th order of polynomials [94].

The multivariate GHQ rule extends the univariate m-point set to the n-dimensional point set by the tensor product rule [93, 94]. It is exact for all polynomials of the form $x_1^{i_1} x_2^{i_2} \cdots x_n^{i_n}$ with $1 \le i_j \le 2m-1$ [94]. However, the total number of points $N_p = m^n$ increases exponentially with the dimension n. Hence, it is hard to use for high dimensional problem. To alleviate this problem, the sparse Gauss-Hermite quadrature can

be used [96]. Conventional Gauss-Hermite quadrature is used here since the dimension of this problem is 3.

Since EKF uses first order Taylor expansion to approximate the non-linear function, the approximation can be accurate only to the first order. But the UKF approximation accuracy can be up to 3rd order polynomials because it uses Unscented Transformation. As a more advanced rule for approximation, the Gauss-Hermite quadrature rule used by GHQF can achieve even higher accuracy than UT.

8.4 Experimental results

The proposed on-line battery SOC estimation approach has been experimentally verified on the 6.8 Ah Ultralife UBBL10 lithium-ion battery module. For the model represented as (8.1) and (8.2), process noise and measurement noise are assumed to be white Gaussian noises and are added to the battery model. Thus for now the battery model with process noise and measurement noise are assumed to accurately represent the true system. To test the robustness of filters on starting from poor initial conditions, an initial value of 40% SOC was given to the models instead of the true value of 100%. The initial values for $\hat{V}_{c1,0}$ and $\hat{V}_{c2,0}$ are set to be 0.05 V, 0.05 V, instead of the true values 0 V, 0 V, respectively. The initial covariance is set to be $\mathbf{P}_0 = \mathrm{diag}\left(\left[0.01, 0.01, 0.1\right]\right)$. The process noise covariance is $Q = 1*10^{-8}$ and the measurement noise is $R = 1*10^{-4}$.

The SOC estimation results from one time running is shown in Fig. 8.2 with a detailed view in Fig. 8.3. The SOC estimation with the EKF diverged from the true SOC thus not plotted here. Fig. 8.4 shows the SOC estimation errors.

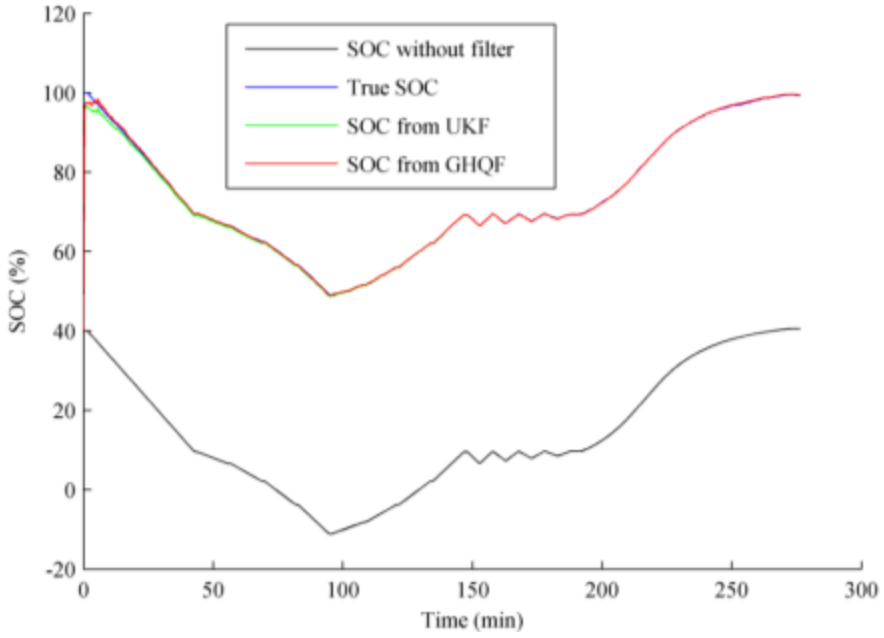

Figure 8.2 SOC estimation results from one time running

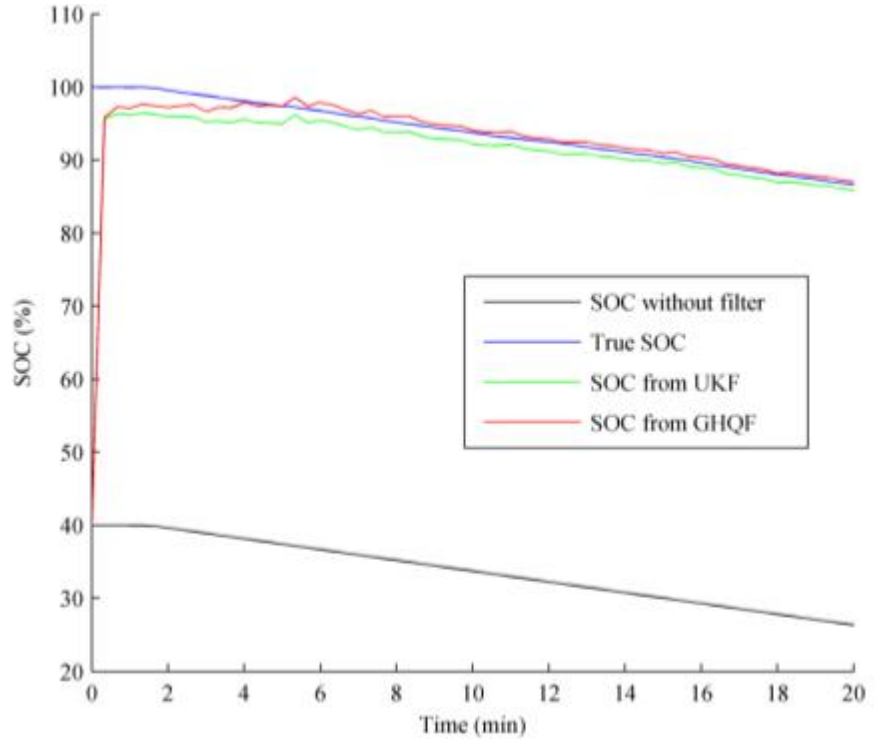

Figure 8.3 Detailed view of the SOC estimation in the first 20 min

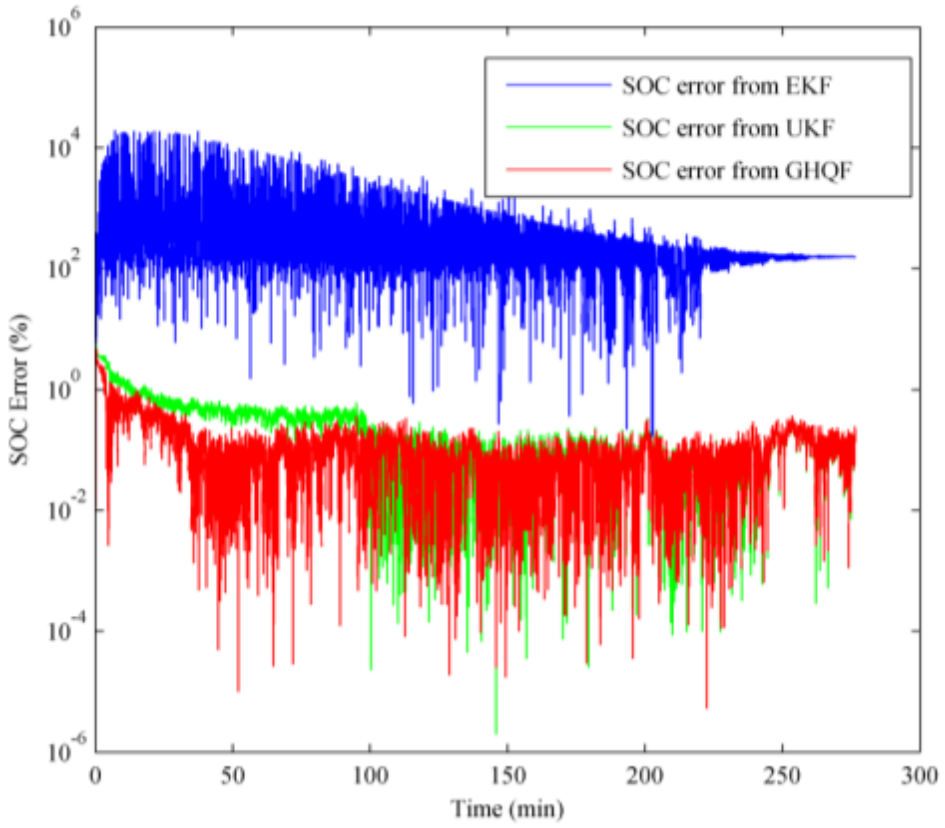

Figure 8.4 SOC estimation errors

The results shown in Fig. 8.5 are generated from a 50 time running, where the root mean square error (RMSE) is used as the criteria for comparison. From the SOC estimation results in Fig. 8.2 - 8.5, it can be observed that the estimated SOC quickly converges to the true SOC using the GHQF, and the SOC estimated using the UKF converges in a comparatively slower way. The errors from both GHQF and UKF quickly drops to 1% and stay below 0.2% in most parts.

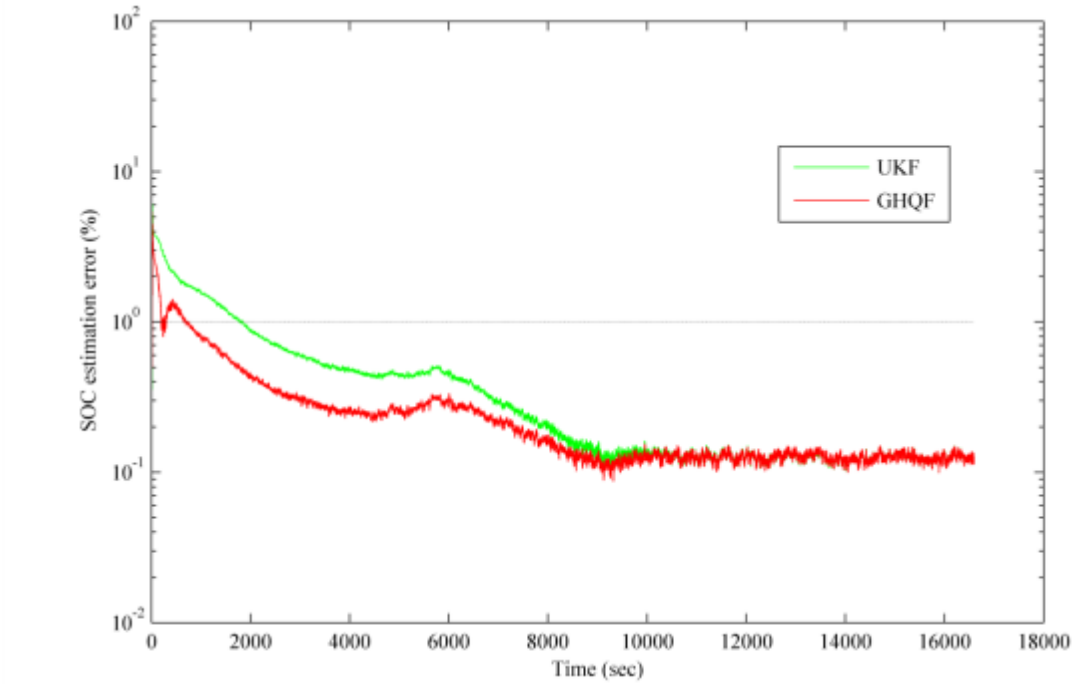

Figure 8.5 RMSE of SOC estimation from 50 times running

8.5 Discussions

The GHQF, EKF and UKF were introduced to the open-loop behavioral battery model to estimate battery SOC in realitme. The ability of the filter to self-start is tested by giving the model poor initial values. The results show that the GHQF is capable of starting with poor initial conditions and quickly converges to the true SOC. SOC estimations from the EKF diverged from the true SOC indicating that EKF is not capable of being used on the selected type of electrical analogue battery model with poor initial conditions. The UKF is able to start from poor initial conditions but it converges to the true SOC in a comparatively slower way than the GHQF. SOC estimation errors for GHQF and UKF remain between 0.13% - 1% of SOC in most parts, with the error from UKF slightly higher than that from GHQF. Therefore, when both the self-starting capability and estimation accuracy are considered, the GHQF excel in comparison to commonly reported EKF and UKF for realtime SOC estimation with the selected

electrical analogue battery model, because the GHQF is known to be more capable of handling high order polynomial based models [94, 96].

CHAPTER IX

CONCLUSIONS

An advanced battery modeling approach aimed at large format batteries is reported in this dissertation. The electric circuit components in the battery model are not physical but behavioral. They are used as a method for approximating the battery's dynamic response for use in system simulation or for embedded battery management systems. As a consequence, these components are convolved with the specific bandwidth of the data used to estimate the actual characteristics of the battery. Acknowledging the limited bandwidth characteristic of the model, the bandwidth related time constants of the RC networks in the model are determined according to the desired bandwidth of the battery application. Either SQP or GA can be employed to estimate the model parameters with the fixed time constants of the RC networks, and their performance were compared in the more demanding case of three RC networks.

The reported approach was experimentally verified on an Ultralife UBBL10 14.4 V, 6.8 Ah lithium-ion battery module with 0.41% terminal voltage estimation error. The robustness of the constructed battery model was verified on four battery modules of the same kind, with between 0.36% and 0.44% terminal voltage estimation error. When the modeling approach was used to model a 360 V, 21.3 kWh lithium-ion battery pack, the terminal voltage estimation error was observed as 1.11% under vehicle drive cycle tests, although this particular model did not include the benefit of the SOC-OCV profile correction procedure; if it had, it can be expected that less than 1% error would have been

observed. The battery model was scaled to 3-RC model from the 2-RC model with increased accuracy ranging from 0.24% to 0.38% terminal voltage estimation error, depending on the details of the parameter estimation algorithm used.

The above results proved that dramatically improved battery terminal voltage estimation accuracy is possible when the electrical analogue battery model is used off-line. The capability of the battery model to be used on-line for SOC estimation after the model parameters were extracted with the proposed method was also investigated with GHQF, EKF and UKF. Accurate SOC estimation results were observed when tested with an UBBL10 lithium-ion battery module.

Since electrical circuit components are used in the battery model, it is ideal for integration with Matlab/Simulink and circuit simulation software. The reported battery modeling approach is independent of battery chemistries, thus making it generically applicable to lithium-ion, NiMH, and lead-acid batteries, among others.

REFERENCES

[1] E. I. Administration, "Annual Energy Outlook 2007 With Projections to 2030," in *Outlook*, ed, 2007.

[2] U. S. E. I. Administration, "Annual Energy Outlook 2011," in *Outlook* vol. 0383, ed, 2011.

[3] I. E. Agency, "Key World Energy Statistics 2009," in *Statistics*, ed: OECD Publishing, 2010.

[4] C. C. Chan, "The state of the art of electric and hybrid vehicles," *Proceedings of the IEEE*, vol. 90, pp. 247-275, 2002.

[5] C. C. Chan, "The State of the Art of Electric, Hybrid, and Fuel Cell Vehicles," *Proceedings of the IEEE*, vol. 95, pp. 704-718, 2007.

[6] S. M. Lukic, *et al.*, "Energy Storage Systems for Automotive Applications," *IEEE Transactions on Industrial Electronics*, vol. 55, pp. 2258-2267, 2008.

[7] S. Vazquez, *et al.*, "Energy Storage Systems for Transport and Grid Applications," *IEEE Transactions on Industrial Electronics*, vol. 57, pp. 3881-3895, 2010.

[8] A. Khaligh and Z. Li, "Battery, Ultracapacitor, Fuel Cell, and Hybrid Energy Storage Systems for Electric, Hybrid Electric, Fuel Cell, and Plug-In Hybrid Electric Vehicles: State of the Art," *IEEE Transactions on Vehicular Technology*, vol. 59, pp. 2806-2814, 2010.

[9] (2010). *Green Chart of the Day: 6/16/10*. Available: http://www.emarketergreen.com/blog/index.php/green-chart-day-61610/

[10] S. Eaves and J. Eaves, "A cost comparison of fuel-cell and battery electric vehicles," *Journal of Power Sources*, vol. 130, pp. 208-212, 2004.

[11] C. Schweinsberg. (2011). *U.S. Hybrid Sales Hit 2 Million Mark*. Available: http://wardsauto.com/ar/hybrid_sales_million_110607/index.html

[12] J. Vanmierlo, *et al.*, "Which energy source for road transport in the future? A comparison of battery, hybrid and fuel cell vehicles," *Energy Conversion and Management*, vol. 47, pp. 2748-2760, 2006.

[13] R. T. Doucette and M. D. McCulloch, "A comparison of high-speed flywheels, batteries, and ultracapacitors on the bases of cost and fuel economy as the energy storage system in a fuel cell based hybrid electric vehicle," *Journal of Power Sources,* vol. 196, pp. 1163-1170, 2011.

[14] A. A. Pesaran, *et al.*, "Battery Requirements for Plug-In Hybrid Electric Vehicles – Analysis and Rationale," in *The 23rd International Electric Vehicle Symposium (EVS-23)*, 2007.

[15] T. Markel, *et al.*, "PHEV Energy Storage Performance / Life / Cost Trade-off Analysis," in *8th Advanced Automotive Battery Conference* vol. 43159, ed, 2008.

[16] A. A. Pesaran, "Choices and Requirements of Batteries for EVs , HEVs , PHEVs," 2011.

[17] K. Smith, *et al.*, "PHEV Battery Trade-Off Study and standby thermal control," in *NREL*, ed, 2009.

[18] E. Meissner and G. Richter, "The challenge to the automotive battery industry: the battery has to become an increasingly integrated component within the vehicle electric power system," *Journal of Power Sources,* vol. 144, pp. 438-460, 2005.

[19] K. Lahiri, *et al.*, "Battery-Driven System Design : A New Frontier in Low Power Design," 2002, pp. 261-267.

[20] S. Vrudhula and D. N. Rakhmatov, "Battery modeling for energy-aware system design," *Computer,* vol. 36, pp. 77-87, 2003.

[21] G. Plett, "Extended Kalman filtering for battery management systems of LiPB-based HEV battery packsPart 2. Modeling and identification," *Journal of Power Sources,* vol. 134, pp. 262-276, 2004.

[22] G. Plett, "Sigma-point Kalman filtering for battery management systems of LiPB-based HEV battery packsPart 2: Simultaneous state and parameter estimation," *Journal of Power Sources,* vol. 161, pp. 1369-1384, 2006.

[23] A. Vasebi, *et al.*, "A novel combined battery model for state-of-charge estimation in lead-acid batteries based on extended Kalman filter for hybrid electric vehicle applications," *Journal of Power Sources,* vol. 174, pp. 30-40, 2007.

[24] G. Plett, "Extended Kalman filtering for battery management systems of LiPB-based HEV battery packsPart 1. Background," *Journal of Power Sources,* vol. 134, pp. 252-261, 2004.

[25] G. L. Plett, "Extended Kalman filtering for battery management systems of LiPB-based HEV battery packs Part 3 . State and parameter estimation," *Journal of Power Sources,* vol. 134, pp. 277-292, 2004.

[26] K. Smith and Chao-YangWang, "Power and thermal characterization of a lithium-ion battery pack for hybrid-electric vehicles," *Journal of Power Sources,* vol. 160, pp. 662-673, 2006.

[27] C. Y. Wang and V. Srinivasan, "Computational battery dynamics (CBD)—electrochemical/thermal coupled modeling and multi-scale modeling," *Journal of Power Sources,* vol. 110, pp. 364-376, 2002.

[28] M. W. Verbrugge and P. Liu, "Electrochemical characterization of high-power lithium ion batteries using triangular voltage and current excitation sources," *Journal of Power Sources,* vol. 174, pp. 2-8, 2007.

[29] W. B. Gu, *et al.*, "Numerical Modeling of Coupled Electrochemical and Transport Processes in Lead-Acid Batteries," *Journal of Electrochemical Society,* vol. 144, pp. 2053-2061, 1997.

[30] D. W. Dees, *et al.*, "Electrochemical modeling of lithium polymer batteries," *Journal of Power Sources,* vol. 110, pp. 310-320, 2002.

[31] A. P. Schmidt, *et al.*, "Experiment-driven electrochemical modeling and systematic parameterization for a lithium-ion battery cell," *Journal of Power Sources,* vol. 195, pp. 5071-5080, 2010.

[32] M. Chen and G. A. Rincon-Mora, "Accurate Electrical Battery Model Capable of Predicting Runtime and I-V Performance," *IEEE Transactions on Energy Conversion,* vol. 21, pp. 504-511, 2006.

[33] L. Gao, *et al.*, "Dynamic Lithium-Ion Battery Model for System Simulation," *IEEE Transactions on Components and Packaging Technologies,* vol. 25, pp. 495-505, 2002.

[34] R. C. Kroeze and P. T. Krein, "Electrical Battery Model for Use in Dynamic Electric Vehicle Simulations," in *Power Electronics Specialists Conference*, 2008, pp. 1336-1342.

[35] Y. Hu, *et al.*, "A technique for dynamic battery model identification in automotive applications using linear parameter varying structures," *Control Engineering Practice,* vol. 17, pp. 1190-1201, 2009.

[36] O. Tremblay, *et al.*, "A Generic Battery Model for the Dynamic Simulation of Hybrid Electric Vehicles," in *Vehicle Power and Propulsion Conference*, 2007, pp. 284-289.

[37] M. Pedram, "An analytical model for predicting the remaining battery capacity of lithium-ion batteries," *IEEE Transactions on Very Large Scale Integration (VLSI) Systems,* vol. 14, pp. 441-451, 2006.

[38] J. Jang and J. Yoo, "Equivalent Circuit Evaluation Method of Lithium Polymer Battery Using Bode Plot and Numerical Analysis," *IEEE TRANSACTIONS ON ENERGY CONVERSION*, vol. 26, pp. 290-298, 2011.

[39] X. Hu, *et al.*, "A comparative study of equivalent circuit models for Li-ion batteries," *Journal of Power Sources*, vol. 198, pp. 359-367, 2012.

[40] K. M. Tsang, *et al.*, "Identification and modelling of Lithium ion battery," *Energy Conversion and Management*, vol. 51, pp. 2857-2862, 2010.

[41] N. K. Medora and A. Kusko, "An Enhanced Dynamic Battery Model of Lead-Acid Batteries Using Manufacturers ' Data," in *Telecommunications Energy Conference*, 2006, pp. 1-8.

[42] J. Zhang, *et al.*, "An enhanced circuit-based model for single-cell battery," in *Applied Power Electronics Conference and Exposition (APEC)*, 2010, pp. 672-675.

[43] J. Wang, *et al.*, "A high frequency battery model for current ripple analysis," in *Applied Power Electronics Conference and Exposition (APEC)*, 2010, pp. 676-680.

[44] A. A.-h. Hussein, *et al.*, "A Hysteresis Model for a Lithium Battery Cell with Improved Transient Response," in *Applied Power Electronics Conference and Exposition (APEC)*, 2011, pp. 1790-1794.

[45] M. Dubarry and B. Y. Liaw, "Development of a universal modeling tool for rechargeable lithium batteries," *Journal of Power Sources*, vol. 174, pp. 856-860, 2007.

[46] Y. Hu, *et al.*, "Electro-thermal battery model identification for automotive applications," *Journal of Power Sources*, vol. 196, pp. 449-457, 2011.

[47] L. W. Juang, *et al.*, "Improved Nonlinear Model for Electrode Voltage-Current Relationship for More Consistent Online Battery System Identification," in *Energy Conversion Congress and Exposition (ECCE)*, 2011, pp. 2628-2634.

[48] L. P. Mandal and R. W. Cox, "A Transient-Based Approach for Estimating the Electrical Parameters of a Lithium-ion Battery Model," in *Energy Conversion and Management*, 2011, pp. 2635-2640.

[49] M. A. Roscher and D. U. Sauer, "Dynamic electric behavior and open-circuit-voltage modeling of LiFePO4-based lithium ion secondary batteries," *Journal of Power Sources*, vol. 196, pp. 331-336, 2011.

[50] Y. Hu and S. Yurkovich, "Linear parameter varying battery model identification using subspace methods," *Journal of Power Sources*, vol. 196, pp. 2913-2923, 2011.

[51] M. C. Knauff, *et al.*, "Simulink Model for Hybrid Power System Test-bed," in *Electric Ship Technologies Symposium*, 2007, pp. 421-427.

[52] Y. Hu, *et al.*, "Model-Based Calibration for Battery Characterization in HEV Applications," in *American Control Conference*, 2008, pp. 318-325.

[53] G. Livint, *et al.*, "Estimation of Battery Paramieters Based on Continuous Time Model," in *International Symposium on Signals, Circuits and Systems*, 2007, pp. 1-4.

[54] M. Coleman, *et al.*, "An Improved Battery Characterization Method Using a Two-Pulse Load Test," *IEEE Transactions on Energy Conversion*, vol. 23, pp. 708-713, 2008.

[55] S. Abu-Sharkh and D. Doerffel, "Rapid test and non-linear model characterisation of solid-state lithium-ion batteries," *Journal of Power Sources*, vol. 130, pp. 266-274, 2004.

[56] B. Schweighofer, *et al.*, "Modeling of high power automotive batteries by the use of an automated test system," *IEEE Transactions on Instrumentation and Measurement*, vol. 52, pp. 1087 - 1091, 2003.

[57] I.-s. Kim, "The novel state of charge estimation method for lithium battery using sliding mode observer," *Journal of Power Sources*, vol. 163, pp. 584-590, 2006.

[58] S. Pang, *et al.*, "Battery State-of-Charge Estimation," in *Proceedings of the American Control Conference*, 2001, pp. 1644-1649.

[59] M. S. Mazzola, *et al.*, "Application of the singular valve decomposition–Prony method for analyzing deep-level transient spectroscopy capacitance transients," *Review of Scientific Instruments*, vol. 69, pp. 2459-2463, 1998.

[60] A. A. Istratov and O. F. Vyvenko, "Exponential analysis in physical phenomena," *Review of Scientific Instruments*, vol. 70, pp. 1233-1257, 1999.

[61] N. Watrin, *et al.*, "Multiphysical lithium-based battery pack modeling for simulation purposes," in *Vehicle Power and Propulsion Conference (VPPC)*, 2011, pp. 1-5.

[62] M. Zheng, *et al.*, "Dynamic Model for Characteristics of Li-ion Battery on Electric Vehicle," in *4th IEEE Conference on Industrial Electronics and Applications (ICIEA)*, 2009, pp. 2867 - 2871.

[63] G. Sarre, *et al.*, "Aging of lithium-ion batteries," *Journal of Power Sources*, vol. 127, pp. 65-71, 2004.

[64] L. Serrao, *et al.*, "An Aging Model of Ni-MH Batteries for Hybrid Electric Vehicles," in *IEEE Conference on Vehicle Power and Propulsion*, 2005, pp. 78-85.

[65] T. Matsushima, "Deterioration estimation of lithium-ion cells in direct current power supply systems and characteristics of 400-Ah lithium-ion cells," *Journal of Power Sources*, vol. 189, pp. 847-854, 2009.

[66] G. Ning, *et al.*, "A generalized cycle life model of rechargeable Li-ion batteries," *Electrochimica Acta*, vol. 51, pp. 2012-2022, 2006.

[67] T. Tsujikawa, *et al.*, "Estimation of the lifetimes of valve-regulated lead-acid batteries," *Journal of Power Sources*, vol. 187, pp. 613-619, 2009.

[68] J. Li, *et al.*, "A New Parameter Estimation Algorithm for an Electrical Analogue Battery Model," in *Applied Power Electronics Conference and Exposition (APEC)*, 2012, pp. 427-433.

[69] J. S. Arora, *Introduction to optimum design* McGraw-Hill, 1989.

[70] P. E. Gill, *Practical optimization* Academic Press, 1981.

[71] Agilent-Technologies, "Agilent 34970A/34972A Data Acquisition/Switch Unit User's Guide," ed, 2010.

[72] Ultralife, "UBI-2590 SMBus Technical Datasheet," ed, 2009, pp. 1-3.

[73] Panasonic, "Panasonic CGR18650DA Datasheet," ed, 2007, p. 1.

[74] Panasonic. (2007). *Overview of Lithium ion batteries*. Available: http://panasonic.com/industrial/includes/pdf/Panasonic_LiIon_Overview.pdf

[75] W. Zhang, *et al.*, "Lithium-based Energy Storage Management for Dc Distributed Renewable Energy System," in *Energy Conversion Congress and Exposition (ECCE)*, 2011, pp. 3270-3277.

[76] Y. Chen, *et al.*, "Simulation Study on Control Strategy for a Hybrid Electric Vehicle with Battery and Ultracapacitor," in *2011 International Conference on Electric Information and Control Engineering (ICEICE)*, 2011, pp. 2601 - 2604.

[77] L. Chen, *et al.*, "Development of a drive cycle based evaluation method for Variable Voltage Converter in vehicle electrification applications," in *2011 IEEE Energy Conversion Congress and Exposition*, 2011, pp. 254-259.

[78] A. Shafiei, *et al.*, "Battery Modeling Approaches and Management Techniques for Plug-in Hybrid Electric Vehicles," in *Vehicle Power and Propulsion Conference (VPPC)*, 2011, pp. 1-5.

[79] C. Sen, *et al.*, "Battery Pack Modeling for the Analysis of Battery Management System of a Hybrid Electric Vehicle," in *Vehicle Power and Propulsion Conference (VPPC)*, 2009, pp. 207-212.

[80] J. Kim, *et al.*, "Stable Configuration of a Li-Ion Series Battery Pack Based on a Screening Process for Improved Voltage / SOC Balancing," *IEEE Transactions on Power Electronics*, vol. 27, pp. 411-424, 2012.

[81] M. Dubarry, *et al.*, "From single cell model to battery pack simulation for Li-ion batteries," *Journal of Power Sources*, vol. 186, pp. 500-507, 2009.

[82] U. S. Kim, *et al.*, "Modeling for the scale-up of a lithium-ion polymer battery," *Journal of Power Sources*, vol. 189, pp. 841-846, 2009.

[83] R. Carter, *et al.*, "An Improved Lead – Acid Battery Pack Model for Use in Power Simulations of Electric Vehicles," *IEEE Transactions on Energy Conversion*, vol. 27, pp. 21 - 28, 2012.

[84] S. Lajeunesse, "Building a better automotive battery pack," presented at the The applied power electronis conference and exposition (APEC), 2012.

[85] A123-Systems, "Introducing a New Module for the EcoCAR Battery Packs," 2009.

[86] F. B. Hildebrand, *Introduction to Numerical Analysis*. New York: McGraw-Hill, 1956.

[87] J. N. Holt and R. J. Antill, "Determining the Number of Terms in a Prony Algorithm Exponential Fit," *Mathematical Biosciences*, vol. 36, pp. 319-332, 1977.

[88] D. W. Tufts and R. Kumaresan, "Singular value decomposition and improved frequency estimation using linear prediction," *IEEE transactions on acoustics, speech, and signal processing*, vol. 30, pp. 671-675, 1982.

[89] K. Holmström and J. Petersson, "A review of the parameter estimation problem of fitting positive exponential sums to empirical data," *Applied Mathematics and Computation*, vol. 126, pp. 31-61, 2002.

[90] J. Li, *et al.*, "On-line Battery State of Charge Estimation using Gauss-Hermite Quadrature Filter," in *Applied Power Electronics Conference and Exposition (APEC)*, 2012, pp. 434-438.

[91] S. Piller, *et al.*, "Methods for state-of-charge determination and their applications," *Journal of Power Sources,* vol. 96, pp. 113-120, 2001.

[92] G. Plett, "Sigma-point Kalman filtering for battery management systems of LiPB-based HEV battery packsPart 1: Introduction and state estimation," *Journal of Power Sources,* vol. 161, pp. 1356-1368, 2006.

[93] I. Arasaratnam, *et al.*, "Discrete-Time Nonlinear Filtering Algorithms Using Gauss–Hermite Quadrature," *Proceedings of the IEEE,* vol. 95, pp. 953-977, 2007.

[94] K. Ito and K. Xiong, "Gaussian filters for nonlinear filtering problems," *IEEE Transactions on Automatic Control,* vol. 45, pp. 910-927, 2000.

[95] S. Julier, *et al.*, "A New Method for the Nonlinear Transformation of Means and Covariances in Filters and Estimators," *IEEE Transactions on Automatic Control,* vol. 45, pp. 477-482, 2000.

[96] B. Jia, *et al.*, "Sparse Gauss-Hermite Quadrature Filter with an Application to Spacecraft Attitude Estimation," *Journal of Guidance, Control, and Dynamics,* vol. 34, pp. 367-379, March-April 2011.